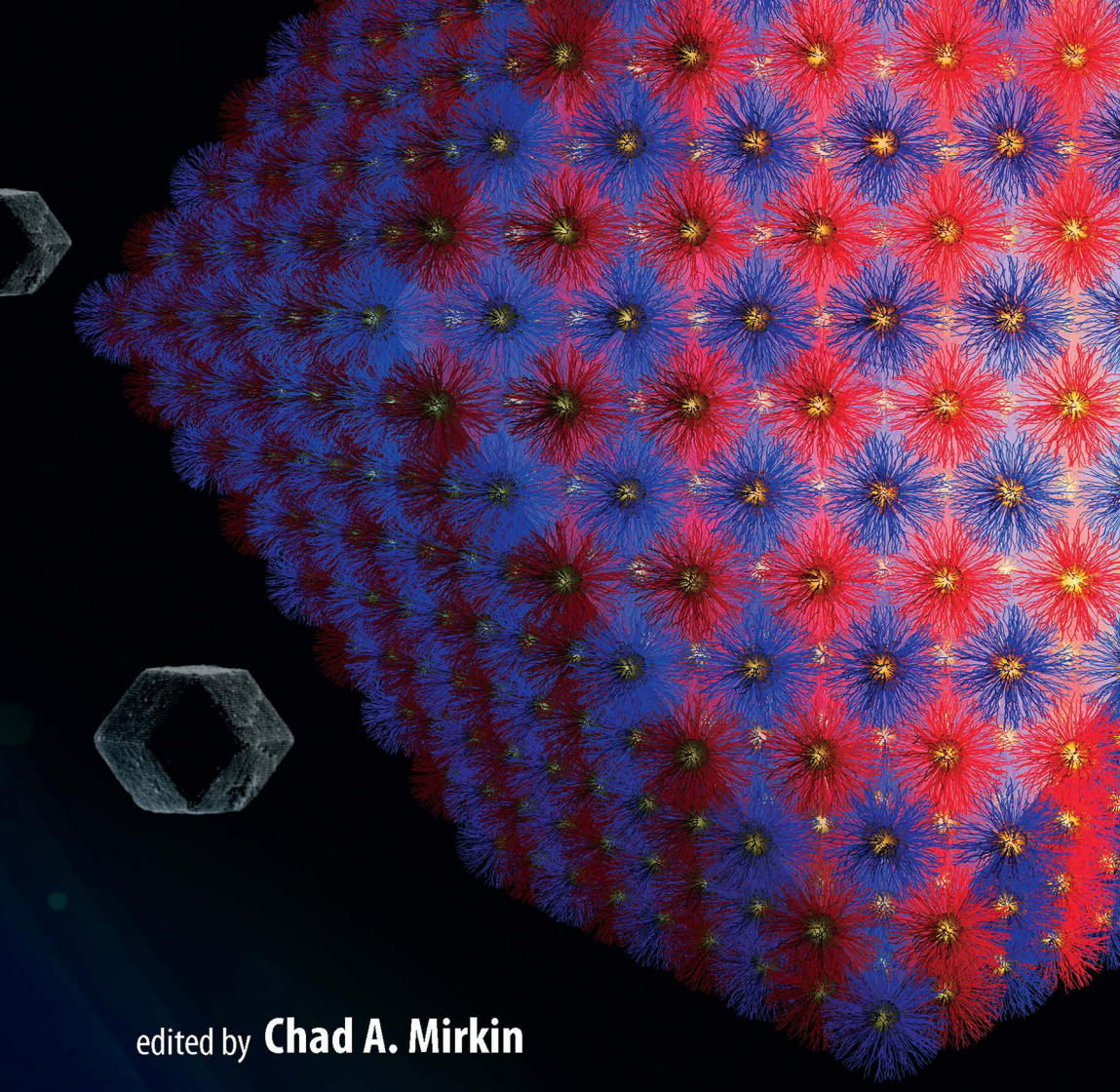

edited by **Chad A. Mirkin**

Spherical Nucleic Acids

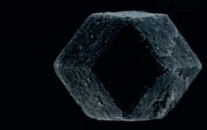

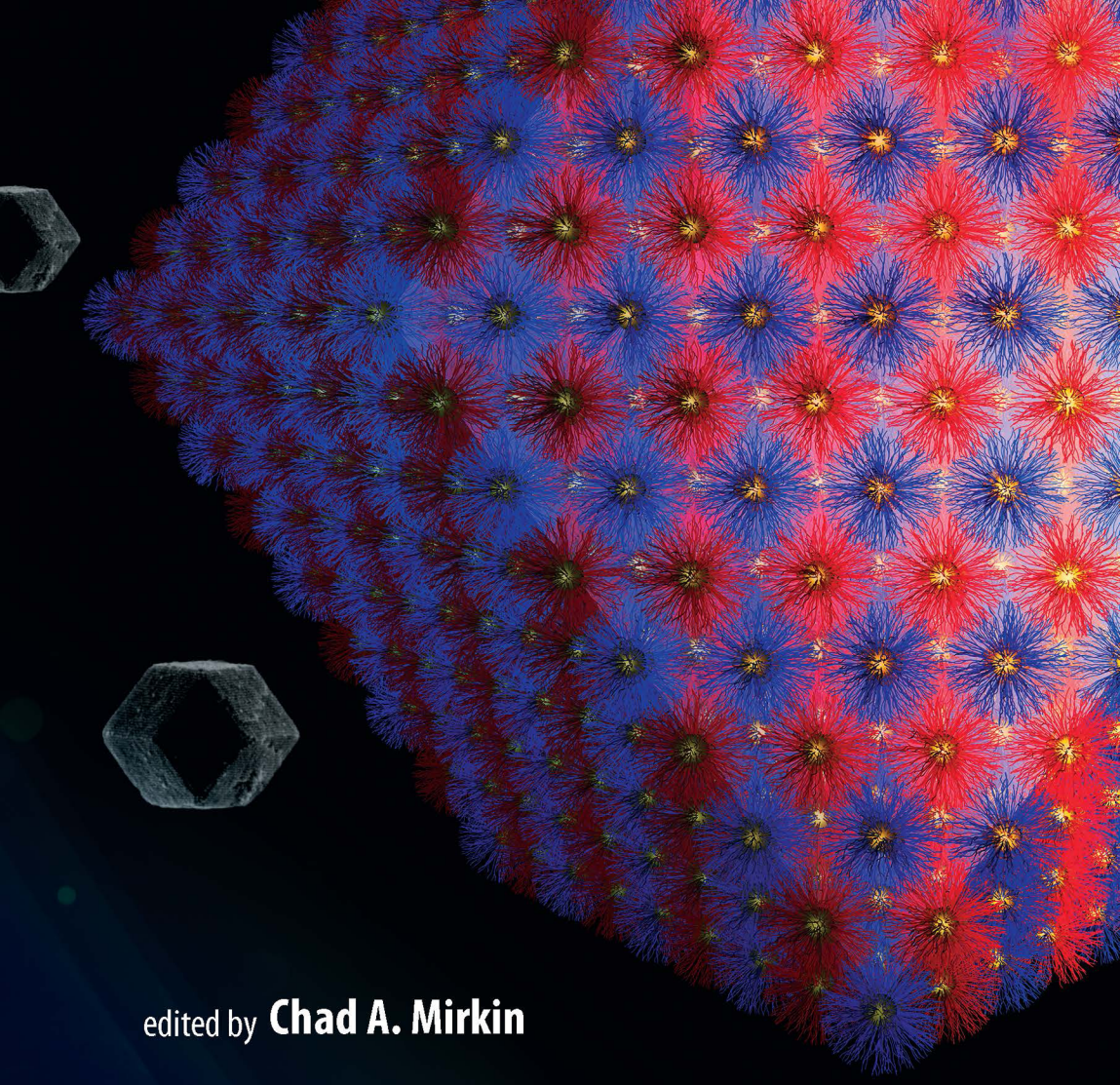

edited by **Chad A. Mirkin**

Spherical Nucleic Acids

Volume 1

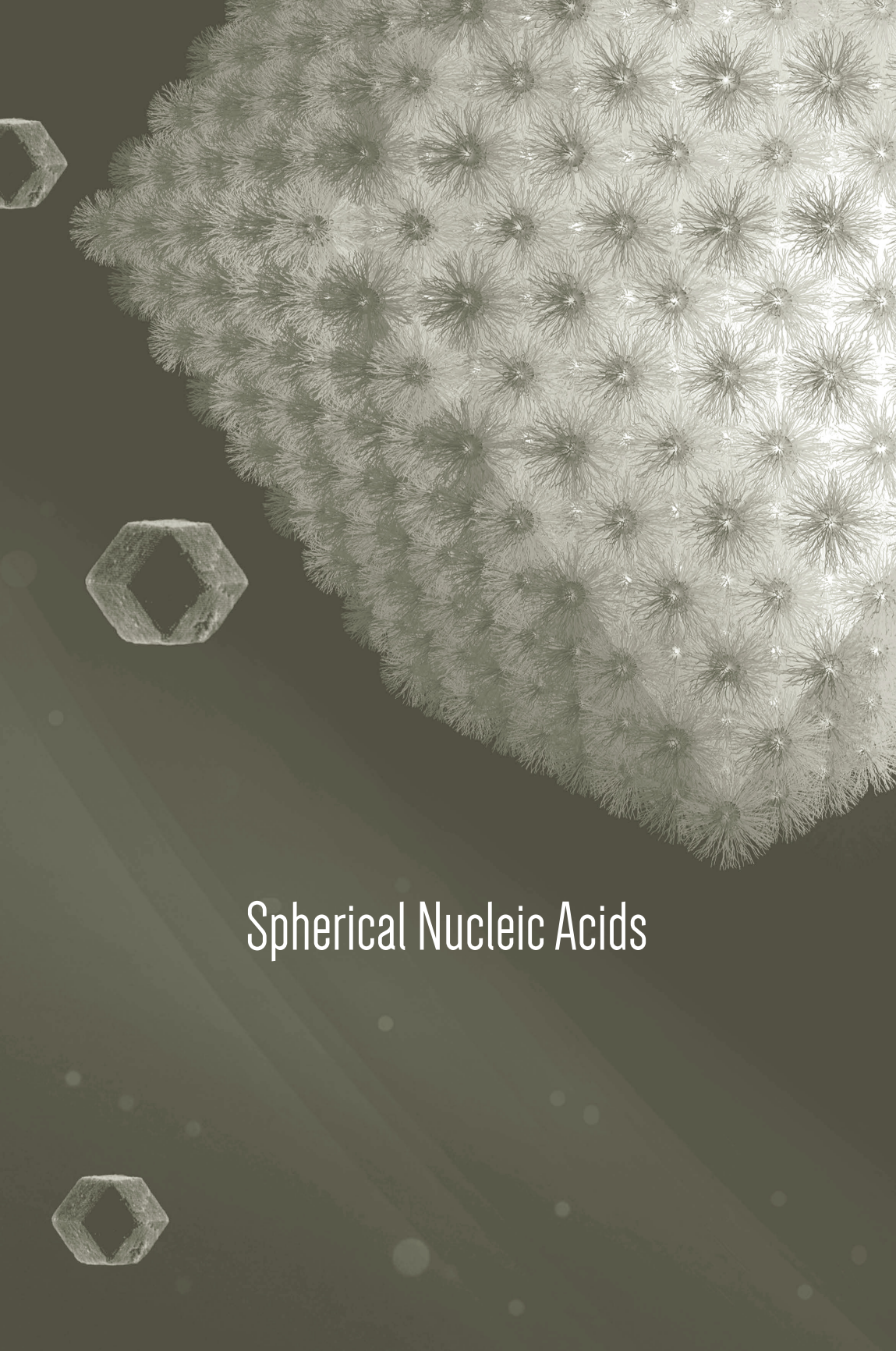
Spherical Nucleic Acids

Spherical Nucleic Acids

Volume 1

edited by

Chad A. Mirkin

JENNY STANFORD
PUBLISHING

Published by

Jenny Stanford Publishing Pte. Ltd.
Level 34, Centennial Tower
3 Temasek Avenue
Singapore 039190

Email: editorial@jennystanford.com
Web: www.jennystanford.com

British Library Cataloguing-in-Publication Data
A catalogue record for this book is available from the British Library.

Spherical Nucleic Acids, Volume 1

ISBN 978-981-4800-35-8 (Hardcover)
ISBN 978-0-429-20015-1 (eBook)

Contents

Preface xv

Part 1 Overview

1. A DNA-Based Method for Rationally Assembling Nanoparticles into Macroscopic Materials **3**
Chad A. Mirkin, Robert L. Letsinger, Robert C. Mucic, and James J. Storhoff

2. Nanostructures in Biodiagnostics **13**
Nathaniel L. Rosi and Chad A. Mirkin

2.1 Introduction 13
2.1.1 Background and Perspectives 14
2.1.2 Why Nanomaterials? 15
2.2 Nanoparticle-Based Detection Methods 17
2.2.1 Optical Detection 17
2.2.1.1 Nucleic acids 17
2.2.1.2 Proteins and biologically relevant small molecules 28
2.2.1.3 Metal ions 31
2.2.2 Electrical and Electrochemical Detection 32
2.2.2.1 Nucleic acids 32
2.2.3 Magnetic Relaxation Detection 34
2.2.3.1 Nucleic acids 34
2.2.3.2 Proteins and viruses 35
2.3 Nanowire- and Nanotube-Based Detection Methods 36
2.3.1 Electrical Detection 36
2.3.1.1 Nucleic acids 36
2.3.1.2 Proteins, viruses, and biologically relevant small molecules 37
2.4 Nanofabrication 38
2.4.1 Nanopatterning 38

2.4.2 Nanoelectromechanical Devices 40
2.5 Conclusions and Outlook 41

3. Gold Nanoparticles for Biology and Medicine 55

David A. Giljohann, Dwight S. Seferos, Weston L. Daniel, Matthew D. Massich, Pinal C. Patel, and Chad A. Mirkin

3.1 Introduction 56
3.2 Citrate and Transferrin 58
3.3 Amines 59
3.3.1 Gene Transfection 60
3.3.2 Drug Delivery 61
3.3.3 Stability 63
3.4 Oligonucleotides 63
3.4.1 Synthesis 64
3.4.2 Properties 65
3.4.3 Cellular Uptake 66
3.4.4 Applications in Cells 68
3.4.4.1 Antisense gene control 69
3.4.4.2 Intracellular detection and imaging 71
3.4.4.3 RNA interference 72
3.4.4.4 Cellular detection 73
3.5 Peptides 73
3.5.1 Peptide Nanoconjugates 74
3.5.2 Peptide/DNA-Gold Nanoparticle Conjugates 75
3.5.3 Multifunctional and Multicomponent DNA Nanoconjugates 75
3.6 Antibodies 76
3.6.1 Imaging 76
3.6.2 Photothermal Therapy 77
3.7 Lipids 77
3.7.1 Therapeutics 77
3.7.2 Imaging 78
3.8 Summary and Outlook 79
3.8.1 Mechanism of Uptake in Cells 79
3.8.2 Targeting 79
3.8.3 Toxicity 80
3.8.4 Conclusion 82

4. Spherical Nucleic Acids **91**

Joshua I. Cutler, Evelyn Auyeung, and Chad A. Mirkin

4.1 Introduction 92
4.2 The Emergence of DNA as a Surface Ligand for Nanoparticles 94
4.3 Structural Considerations for SNA and SNA–NP Conjugates 95
4.4 Controlling the Density of SNA Conjugates 100
4.5 Cooperative Binding with High-Density SNA Conjugates 103
4.6 Nanoparticle Assembly and Crystallization Programmed with Spherical and Other 3D Nucleic Acid Nanostructures 107
4.7 Moving beyond Spherical Conjugates to Other Forms of 3D Nucleic Acids 112
4.8 Diagnostics 114
4.9 Spherical Nucleic Acids as Single-Entity Gene Regulation Constructs 118
4.10 Combined Intracellular Diagnostics and Imaging 124
4.11 Conclusions and Outlook 126

5. Nucleic Acid-Modified Nanostructures as Programmable Atom Equivalents: Forging a New "Table of Elements" **137**

Robert J. Macfarlane, Matthew N. O'Brien, Sarah Hurst Petrosko, and Chad A. Mirkin

5.1 Introduction 137
5.2 Discussion 143
5.3 Outlook 154

6. Programmable Materials and the Nature of the DNA Bond **167**

Matthew R. Jones, Nadrian C. Seeman, and Chad A. Mirkin

6.1 Introduction 168
6.2 Background 173
6.3 Advances 173
6.4 Outlook 174

6.5 Hybridization-Based DNA Bonds: Tiles 174
6.6 Hybridization-Based DNA Bonds: Origami 179
6.7 Nanoparticle-Templated DNA Bonds 183
6.8 Conclusions 190

7. The Nature and Implications of Uniformity in the Hierarchical Organization of Nanomaterials 199

Matthew N. O'Brien, Matthew R. Jones, and Chad A. Mirkin

7.1 Hierarchical Organization 200
7.2 From Atoms to Crystalline Nanoparticles 202
7.2.1 What Does It Mean to Be Uniform at This Length Scale? 202
7.2.2 Successful Approaches to Control Uniformity at This Scale 205
7.3 Ligands Arranged on Nanoparticle Surfaces 207
7.3.1 What Does It Mean to Be Uniform at This Length Scale? 208
7.3.2 Successful Approaches to Control Uniformity at This Scale 211
7.4 From Nanoparticles to Colloidal Crystals 213
7.4.1 What Does It Mean to Be Uniform at This Length Scale? 214
7.4.2 Successful Approaches to Control Uniformity at This Scale 217
7.5 Beyond Colloidal Crystals 221

8. Crystal Engineering with DNA 227

Christine R. Laramy, Matthew N. O'Brien, and Chad A. Mirkin

8.1 Introduction 228
8.2 DNA Design Elements 230
8.2.1 The Anatomy of a Building Block 230
8.2.2 Primarily Double-Stranded with Linkers (DNA Design 1) 233
8.2.3 Single-Stranded with No Linkers (DNA Design 2) 237
8.2.4 Single-Stranded with Linkers (DNA Design 3) 239

8.2.5 DNA Surface Density 240
8.2.6 Temperature Control 242
8.3 Crystal Symmetry and Habit Engineering 243
8.3.1 Isotropic Building Blocks 245
8.3.2 Building Blocks with Anisotropic Particle Cores 252
8.3.3 Chemically Anisotropic Building Blocks 259
8.3.4 Template-Directed Crystallization 262
8.4 Functional Consequences 267
8.4.1 Functional Behavior Driven by DNA 267
8.4.2 Functional Behavior Driven by Particle Core 270
8.5 Outlook 275

Part 2 Enabling Features of Nucleic Acid-Functionalized Nanomaterials

9. What Controls the Optical Properties of DNA-Linked Gold Nanoparticle Assemblies? 293

James J. Storhoff, Anne A. Lazarides, Robert C. Mucic, Chad A. Mirkin, Robert L. Letsinger, and George C. Schatz

9.1 Introduction 294
9.2 Experimental Section 296
9.2.1 Reagents 296
9.2.2 Instrumentation 296
9.2.3 Preparation of 3′- or 5′-(Alkanethiol) Oligonucleotide-Modified Au Nanoparticles 297
9.2.4 Preparation and Characterization of Linker DNA 297
9.2.5 Preparation and Characterization of DNA-Linked Au Nanoparticle Aggregates 299
9.2.6 Dynamic Light Scattering 300
9.2.7 Transmission Electron Microscopy 300
9.2.8 Small-Angle X-ray Scattering 300
9.3 Calculations of UV-Visible Extinction Spectra 301
9.4 Results and Discussion 301

9.4.1 DNA-Linked Au Nanoparticle Assemblies from 24-, 48-, and 72-Base-Pair Linkers 301
9.4.2 Melting Analyses 305
9.4.3 Annealing Studies of the 24-, 48-, and 72-Base Linked Aggregates 307
9.4.4 Theoretical Studies of the Dependence of the UV-Visible Spectra upon Aggregate Size and Volume Fraction 310
9.4.5 Small-Angle X-ray Scattering 312
9.4.6 Dynamic Light Scattering of DNA-Linked Aggregates 313
9.4.7 Sedimentation Rates of the DNA-Linked Aggregates before and after Annealing 315
9.4.8 TEM of the DNA-Linked Aggregates before and after Annealing 316
9.4.9 Ostwald Ripening of DNA-Linked Aggregates 319
9.5 Conclusions 321

10. What Controls the Melting Properties of DNA-Linked Gold Nanoparticle Assemblies? 325

Rongchao Jin, Guosheng Wu, Zhi Li, Chad A. Mirkin, and George C. Schatz

10.1 Introduction 326
10.2 Results 328
10.2.1 Assay Formats 328
10.2.2 Effect of Probe Oligonucleotide Density on the Au Nanoparticle Surface 330
10.2.3 Effect of Au Nanoparticle Size 332
10.2.4 Effect of Salt Concentration 333
10.2.5 Effect of Interparticle Distance 336
10.2.6 Mechanistic Studies of DNA Melting in the Presence of Nanoparticles 339
10.3 Thermodynamic Melting Model 341
10.3.1 The Model 341

10.3.2 Extensions and Limitations of the Model 345
10.4 Model Results and Discussion 345
10.4.1 Fitting the Experimental Data 345
10.4.2 Effect of Nanoparticle Size 347
10.4.3 Salt-Induced Melting 348
10.4.4 Effect of Probe DNA Density 349
10.4.5 Effect of Interparticle Distance 350
10.5 Conclusions 350
10.6 Experimental Section 352
10.6.1 Synthesis of DNA 352
10.6.2 Functionalization of Au Nanoparticles 353
10.6.3 Functionalization of Glass Substrates 354
10.6.4 Hybridization of Nanoparticles with Targets in the Solution System 355
10.6.5 Hybridization of Nanoparticles on Oligonucleotide-Modified Glass Surfaces 356
10.6.6 Melting Analyses 356
10.6.7 Transmission Electron Microscopy 357
10.6.8 Circular Dichroism 357

11. Thermodynamic Investigation into the Binding Properties of DNA Functionalized Gold Nanoparticle Probes and Molecular Fluorophore Probes 363

Abigail K. R. Lytton-Jean and Chad A. Mirkin

11.1 Introduction 363
11.2 Results and Discussion 364
11.3 Conclusion 369

12. What Controls the Hybridization Thermodynamics of Spherical Nucleic Acids? 371

Pratik S. Randeria, Matthew R. Jones, Kevin L. Kohlstedt, Resham J. Banga, Monica Olvera de la Cruz, George C. Schatz, and Chad A. Mirkin

12.1 Introduction 372
12.2 Methods 375
12.3 Results and Discussion 376
12.4 Conclusion 380

13. The Role of Structural Enthalpy in Spherical Nucleic Acid Hybridization **385**

Lam-Kiu Fong, Ziwei Wang, George C. Schatz, Erik Luijten, and Chad A. Mirkin

13.1 Introduction 386
13.2 Results and Discussion 387
13.3 Conclusion 394

14. Nanoparticle Shape Anisotropy Dictates the Collective Behavior of Surface-Bound Ligands **399**

Matthew R. Jones, Robert J. Macfarlane, Andrew E. Prigodich, Pinal C. Patel, and Chad A. Mirkin

14.1 Introduction 400
14.2 Results and Discussion 402
14.3 Conclusions 409

15. Oligonucleotide Loading Determines Cellular Uptake of DNA-Modified Gold Nanoparticles **413**

David A. Giljohann, Dwight S. Seferos, Pinal C. Patel, Jill E. Millstone, Nathaniel L. Rosi, and Chad A. Mirkin

15.1 Introduction 414
15.2 Results and Discussion 415

16. Polyvalent DNA-Nanoparticle Conjugates Stabilize Nucleic Acids **425**

Dwight S. Seferos, Andrew E. Prigodich, David A. Giljohann, Pinal C. Patel, and Chad A. Mirkin

16.1 Introduction 426
16.2 Results and Discussion 426

17. Cellular Response of Polyvalent Oligonucleotide–Gold Nanoparticle Conjugates **437**

Matthew D. Massich, David A. Giljohann, Abrin L. Schmucker, Pinal C. Patel, and Chad A. Mirkin

17.1 Introduction 438
17.2 Results and Discussion 439
17.3 Conclusions 445
17.4 Methods 446

17.4.1 Nucleic Acid Synthesis 446
17.4.2 Nanoparticle Synthesis and Functionalization 446
17.4.3 Cell Culture and Transfection 447
17.4.4 Gene Expression Analysis 447
17.4.5 Cellular Assays 447
17.4.6 Nanoparticle Uptake 448

18. Strategy for Increasing Drug Solubility and Efficacy through Covalent Attachment to Polyvalent DNA-Nanoparticle Conjugates 451

Xue-Qing Zhang, Xiaoyang Xu, Robert Lam, David Giljohann, Dean Ho, and Chad A. Mirkin

18.1 Introduction 452
18.2 Results and Discussion 455
18.3 Conclusion 464
18.4 Materials and Methods 465
18.4.1 Synthesis of Paclitaxel–Oligonucleotide Conjugate 2 465
18.4.2 Preparation of PTX–DNA@AuNPs and Fluorescein–PTX–DNA@AuNPs 3 466
18.4.3 Quantification of Alkanethiol Oligonucleotides Loaded on Gold Nanoparticles 466
18.4.4 Dynamic Light Scattering (DLS) and Transmission Electron Microscopy (TEM) 467
18.4.5 General Cell Culture 468
18.4.6 Fluorescence Imaging 468
18.4.7 TUNEL Assay 468
18.4.8 MTT Assay 469

19. Mechanism for the Endocytosis of Spherical Nucleic Acid Nanoparticle Conjugates 475

Chung Hang J. Choi, Liangliang Hao, Suguna P. Narayan, Evelyn Auyeung, and Chad A. Mirkin

19.1 Introduction 476
19.2 Results and Discussion 478

19.2.1 Cellular Uptake Kinetics and Intracellular Transport 478
19.2.2 Caveolae/Lipid-Raft as the Major Pathway of Endocytosis 480
19.2.3 Endocytosis via Class A Scavenger Receptors 483
19.2.4 Collective Involvement of SR-A and Lipid-Raft Proteins 485
19.2.5 Effect of CAV-1 and SR-A on Endocytosis of SNAs in Multiple Cell Types 487
19.3 Conclusions 488
19.4 Materials and Methods 489
19.4.1 Synthesis of Oligonucleotides 489
19.4.2 Preparation of SNA Nanoconjugates 489
19.4.3 Generation of Stably Transfected Deficient Cells 489
19.4.4 Uptake Kinetics and Binding Assays 490
19.4.5 ICP-MS 490
19.4.6 TEM 490
19.4.7 Confocal Microscopy and Immunofluorescence 491
19.4.8 Chemical Blocking Studies 491
19.4.9 Western Blotting 492
19.4.10 Protein Precipitation Assay 492

Part 1
OVERVIEW

Chapter 1

A DNA-Based Method for Rationally Assembling Nanoparticles into Macroscopic Materials*

Chad A. Mirkin, Robert L. Letsinger, Robert C. Mucic, and James J. Storhoff
Department of Chemistry, Northwestern University, 2145 Sheridan Road, Evanston, IL 60208, USA
chadnano@northwestern.edu

Colloidal particles of metals and semiconductors have potentially useful optical, optoelectronic and material properties [1–4] that derive from their small (nanoscopic) size. These properties might lead to applications including chemical sensors, spectroscopic enhancers, quantum dot and nanostructure fabrication, and microimaging methods [2–4]. A great deal of control can now be exercised over the chemical composition, size and polydispersity [1, 2] of colloidal particles, and many methods have been developed

*Reprinted from Mirkin, C. A., Letsinger, R. L., Mucic, R. C. and Storhoff, J. J. (1996). A DNA-based method for rationally assembling nanoparticles into macroscopic materials, *Nature*. **382**, 607–609, Copyright © 1996, Springer Nature.

Spherical Nucleic Acids, Volume 1
Edited by Chad A. Mirkin

ISBN 978-981-4800-35-8 (Hardcover), 978-0-429-20015-1 (eBook)
www.jennystanford.com

for assembling them into useful aggregates and materials. Here we describe a method for assembling colloidal gold nanoparticles rationally and reversibly into macroscopic aggregates. The method involves attaching to the surfaces of two batches of 13-nm gold particles non-complementary DNA oligonucleotides capped with thiol groups, which bind to gold. When we add to the solution an oligonucleotide duplex with "sticky ends" that are complementary to the two grafted sequences, the nanoparticles self-assemble into aggregates. This assembly process can be reversed by thermal denaturation. This strategy should now make it possible to tailor the optical, electronic and structural properties of the colloidal aggregates by using the specificity of DNA interactions to direct the interactions between particles of different size and composition.

Previous assembly methods have focused on the use of covalent 'linker' molecules that possess functionalities at opposing ends with chemical affinities for the colloids of interest. One of the most successful approaches to date [5] has involved the use of gold colloids and well established thiol adsorption chemistry [6, 7]. In this approach, linear alkanedithiols were used as the particle linker molecules. The thiol groups at each end of the linker molecule covalently attach themselves to the colloidal particles to form aggregate structures. The drawbacks of this method are that the process is difficult to control and the assemblies are formed irreversibly. Methods for systematically controlling the assembly process are needed if the materials properties of these unusual structures are to be exploited fully.

Our oligonucleotide-based method allows the controlled and reversible assembly of gold nanoparticles into supramolecular structures. Oligonucleotides offer several advantages over non-biological-based linker molecules. For example, discrete sequences of controlled length and with the appropriate surface binding functionality may be prepared in an automated fashion with a DNA synthesizer. In this way, the molecular recognition properties of the oligonucleotides may be used to trigger the colloidal self-assembly process. The interparticle distances and stabilities of the supramolecular structures generated by this method can be controlled through the choice of oligonucleotide sequence and length, solvent, temperature and supporting electrolyte concentration.

Others also have recognized the utility of DNA for the preparation of new biomaterials and nanofabrication methods. Previous

researchers have focused on using the sequence-specific molecular-recognition properties of oligonucleotides to design impressive structures with well defined geometric shapes and sizes [8–18]. The chemistry proposed here focuses on merging the chemistry of DNA with the chemistry of inorganic colloidal materials. In addition to generating materials with properties that are hybrids of their DNA and colloidal precursors, the union of metal-colloid and DNA chemistry offers significant opportunities relative to the construction of pure DNA materials. As noted by Seeman [19], 'the theory of producing DNA [structures] is well ahead of experimental confirmation. It is much easier to design a [structure] than it is to prove its synthesis.' An advantage of the DNA/colloid hybrid materials reported herein is that the assemblies can be characterized easily by transmission electron microscopy (TEM) and/or atomic force microscopy (AFM) as well as spectroscopic methods conventionally used with DNA.

Our approach to using oligonucleotides for the controlled assembly of gold nanoparticles into aggregate macroscopic structures is outlined in Fig. 1.1. First, 13-nm-diameter Au particles are prepared [2, 20]. These particles form a dark red suspension in water, and like thin-film Au substrates [21], they are easily modified with oligonucleotides, which are functionalized with alkane thiols at their 3′ termini. In a typical experiment, one solution of 17 nM (150 μl) Au colloids is treated for 24 h with 3.75 μM (46 μl) 3′-thiol-TTTGCTGA, and a second solution of colloids is treated with 3.75 μM (46 μl) 3′-thiol-TACCGTTG. Note that these oligonucleotides are non-complementary. After treatment with the thiol-capped oligonucleotides, the two colloidal Au solutions are combined, and because of the non-complementary nature of the oligonucleotides, no reaction takes place. A beneficial consequence of capping the colloids with these oligonucleotides is that they are much more stable than bare Au colloids to increased salt concentration and temperature. When heated or in a solution of high salt concentration (0.1 M NaCl), bare colloids undergo irreversible particle-growth reactions that result in their precipitation. In contrast, the DNA-modified Au nanoparticles reported here are stable at elevated temperatures (80°C) and in aqueous 0.1 M NaCl solutions for days, presumably because their DNA-modified surfaces prohibit them from getting close enough to undergo particle growth. This is

important because high salt concentrations are needed for the DNA hybridization events depicted in Fig. 1.1.

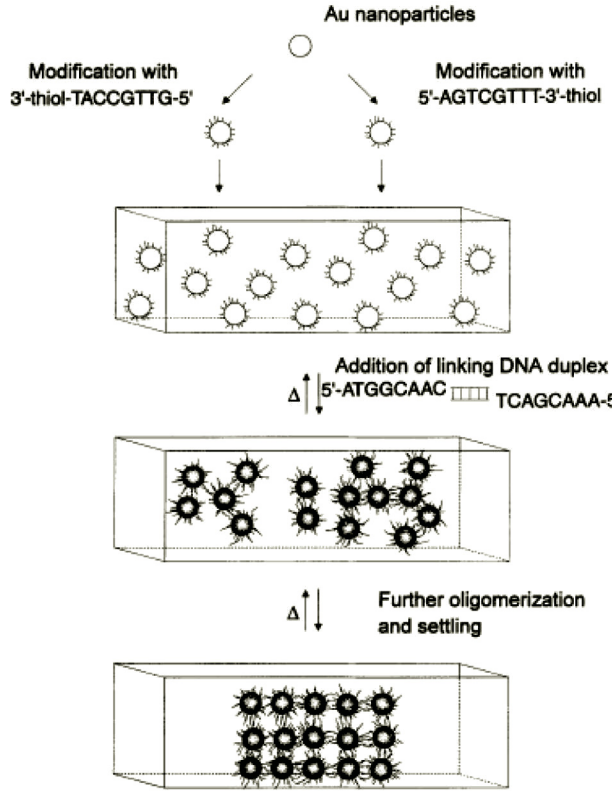

Figure 1.1 Scheme showing the DNA-based colloidal nanoparticle assembly strategy (the hybridized 12-base-pair portion of the linking duplex is abbreviated as ⊏⊐). If a duplex with a 12-base-pair overlap but with "sticky ends" with four base mismatches (5′-AAGTCAGTTATACGCGCTAG and 3′-ATATGCGCGATCAAATCACA) is used in the second step, no reversible particle aggregation is observed. The scheme is not meant to imply the formation of a crystalline lattice but rather an aggregate structure that can be reversibly annealed. Δ is the heating above the dissociation temperature of the duplex.

In the next step of the assembly scheme, a duplex consisting of 5′-ATGGCAACTATACGCGCTAG and 3′-ATATGCGCGATCTCAGCAAA (the duplex has a 12-base-pair overlap (underlined), containing 8-base-pair sticky ends, which are complementary to the 8-base-pair oligonucleotides that are covalently attached to the Au colloids;

Fig. 1.1) is added to the dark red solution. The solution is then diluted with aqueous NaCl (to 1 M) and buffered at pH 7 with 10 mM phosphate, conditions which are suitable for hybridization of the oligonucleotides. Significantly, an immediate colour change from red to purple is observed and a precipitation reaction ensues. Over the course of several hours, the solution becomes clear and a pinkish-gray precipitate settles to the bottom of the reaction vessel (Fig. 1.2). Presumably, the free ends of the 'linking' duplex bind to the complementary oligomers anchored to the gold, thereby crosslinking the colloids, which ultimately results in the formation of the pinkish-gray polymeric DNA–colloid precipitate. To verify that this process involved both the DNA and colloids, the precipitate was collected and resuspended (by shaking) in 1 M aqueous NaCl buffered at pH 7. Then, a temperature/time dissociation experiment was performed by monitoring both an optical absorption dependent on hybridization of DNA (260 nm) and one dependent on the degree of colloid aggregation (700 nm), Fig. 1.3a. As the temperature is cycled between 0 and 80°C, which is 38°C above the dissociation temperature (T_m) for the DNA-duplex (T_m = 42°C), there is an excellent correlation between the optical signatures for both the colloids and DNA. In the absence of DNA, the ultraviolet–visible

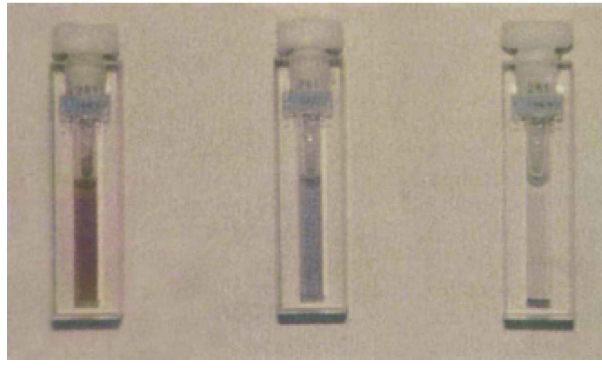

Figure 1.2 Cuvettes with the Au colloids and the four DNA strands responsible for the assembly process. Left cuvette, at 80°C with DNA-modified colloids in the unhybridized state; centre, after cooling to room temperature but before the precipitate settles; and right, after the polymeric precipitate settles to the bottom of the cuvette. Heating either of these cool solutions results in the reformation of the DNA-modified colloids in the unhybridized state (shown in the left cuvette).

spectrum for the naked Au colloids is much less temperature-dependent (Fig. 1.3b). There is a substantial optical change when the polymeric DNA–colloid precipitate is heated above its melting point. The clear solution turns dark red as the polymeric biomaterial dehybridizes to generate the unlinked colloids which are soluble in the aqueous solution. This process is very reversible as evidenced by the temperature traces in Fig. 1.3a. In a control experiment designed to verify that this process was due to oligonucleotide hybridization, a duplex with four base-pair mismatches in each of the "sticky" ends of the linkers (step 2 in Fig. 1.1) did not induce the reversible particle aggregation process.

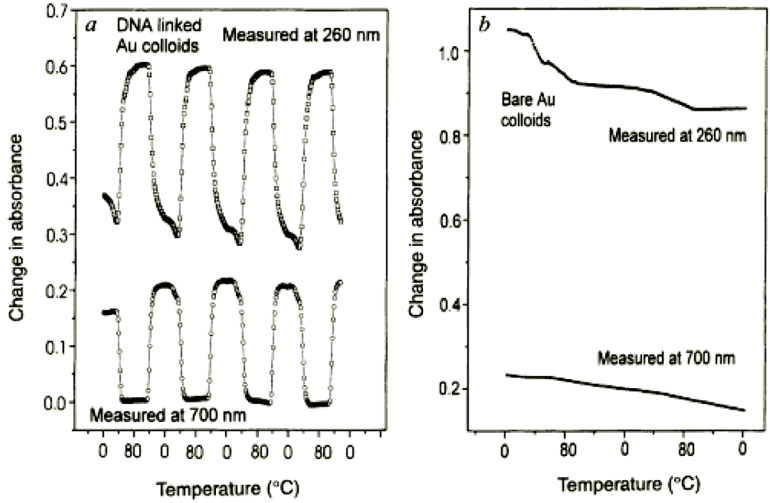

Figure 1.3 (a) Absorbance versus temperature/time profile for DNA/colloid hybridized materials. At low temperatures the Au colloids aggregate owing to the hybridization of 'linking' DNA. At high temperature (80°C), the colloids dehybridize and form a dark red solution (see Fig. 1.1 and Fig. 1.2). The temperature versus time profile shows that this is a reversible process. (b) Results of same procedure shown in (a), but applied to an aqueous solution of unmodified Au colloids (5.1 nM, same concentration as in (a)).

Further evidence of the polymerization/assembly process comes from TEM studies of the polymeric precipitate (Fig. 1.4). TEM images of the colloids linked with hybridized DNA show large assembled networks of the Au colloids (Fig. 1.4a). Naked Au colloids do not aggregate in this manner under comparable conditions, but

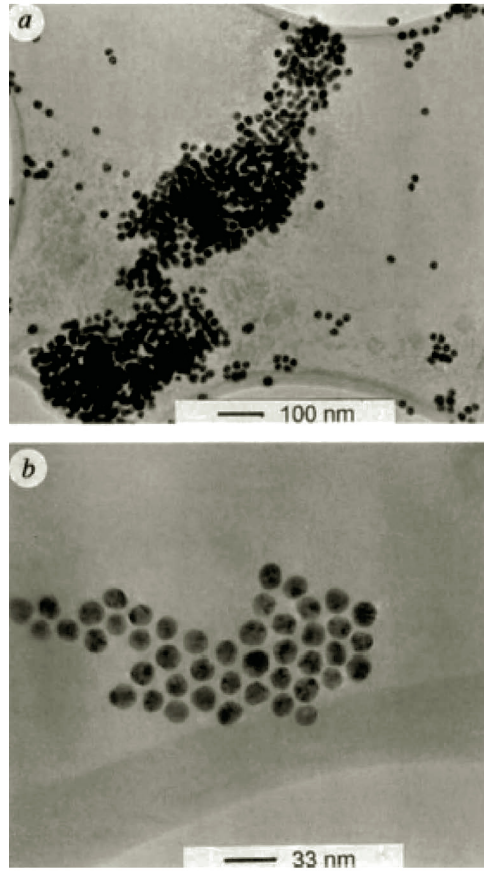

Figure 1.4 TEM images of: (a) an aggregated DNA/colloid hybrid material; (b) a two-dimensional colloidal aggregate showing the ordering of the DNA-linked Au nanoparticles. Images were taken with a Hitachi 8100 Transmission Electron Microscope.

rather undergo particle-growth reactions [2]. Note that there is no evidence of colloid particle growth as the hybridized colloids seem to be remarkably regular in size with an average diameter of 13 nm. With TEM, because of the superposition of layers, it is difficult to assess the degree of order for three-dimensional aggregates. But smaller-scale images of single-layer, two-dimensional aggregates provide more compelling evidence of the self-assembly process (Fig. 1.4b). This figure shows close-packed assemblies of the

aggregates with uniform particle separations ~60 Å. This distance is somewhat shorter than the maximum spacing (95 Å) expected for colloids connected by rigid DNA hybrids with the selected sequences. But because of the nicks in the DNA duplex, these are not rigid hybrids and are quite flexible. It should be noted that, in principle, this is a variable that can be controlled by reducing the system from four overlapping strands to three (thereby reducing the number of nicks) or by using triplexes instead of duplexes.

This work gives entry into a new class of DNA/nanoparticle hybrid materials and assemblies, which might have useful electrical, optical and structural properties that should be controllable through choice of nanoparticle size and chemical composition, and oligonucleotide sequence and length. We note that it should be possible to extend this strategy easily to other noble-metal (for example, Ag, Pt) [22] and semiconductor (for example, CdSe and CdS) [23, 24] colloidal nanoparticles with well established surface coordination chemistry. Our initial results bode well for the utility of this strategy for developing new types of biosensing and sequencing schemes for DNA. The Au colloidal particles have large extinction coefficients for the bands that give rise to their colours (Fig. 1.2). These intense colours, which depend on particle size and concentration and interparticle distance, make these materials particularly attractive for new colorimetric sensing and sequencing strategies for DNA.

Acknowledgments

We thank I. M. Klotz for discussions, and V. Dravid for assistance with the TEM experiments. C.A.M. was seed-supported by an ONR Young Investigator award, an A. P. Sloan Foundation fellowship, a DuPont Young Professor award, an NSF Young Investigator award and a Cammille Dreyfus Teacher-Scholar Award; C.A.M. thanks the Materials Research Center of Northwestern University for the use of a TEM, which was purchased by the MRSEC Program of the National Science Foundation; R.L.L. was supported by the NIGMS.

References

1. Schmid, G. (ed.) (1994). *Clusters and Colloids* (VCH, Weinheim).
2. Hayat, M. A. (ed.) (1991). *Colloidal Gold: Principles, Methods, and Applications* (Academic, San Diego).

3. Bassell, G. J., Powers, C. M., Taneja, K. L. and Singer, R. H. (1994). *J. Cell Biol*. **126**, 863–876.
4. Creighton, J. A., Blatchford, C. G. and Albrecht, M. G. (1979). *J. Chem. Soc. Faraday II* **75**, 790–798.
5. Brust, M., Bethell, D., Schiffrin, D. J. and Kiely, C. J. (1995). *Adv. Mater*. **7**, 795–797.
6. Dubois, L. H. and Nuzzo, R. G. (1992). *Annu. Rev. Phys. Chem*. **43**, 437–463.
7. Bain, C. D. and Whitesides, G. M. (1989). *Angew. Chem. Int. Ed. Engl*. **28**, 506–512.
8. Shekhtman, E. M., Wasserman, S. A., Cozzarelli, N. R. and Solomon, M. J. (1993). *New J. Chem*. **17**, 757–763.
9. Shaw, S. Y. and Wang, J. C. (1993). *Science* **260**, 533–536.
10. Herrlein, M. K., Nelson, J. S. and Letsinger, R. L. (1995). *J. Am. Chem. Soc*. **117**, 10151–10152.
11. Chen, J. H. and Seeman, N. C. (1991). *Nature* **350**, 631–633.
12. Smith, F. W. and Feigon, J. (1992). *Nature* **356**, 164–168.
13. Wang, K. Y., McCurdy, S., Shea, R. G., Swaminathan, S. and Bolton, P. H. (1993). *Biochemistry* **32**, 1899–1904.
14. Chen, L. Q., Cai, L., Zhang, X. H. and Rich, A. (1994). *Biochemistry* **33**, 13540–13546.
15. Marsh, T. C., Vesenka, J. and Henderson, E. (1995). *Nucleic Acids Res*. **23**, 696–700.
16. Mirkin, S. M. and Frankkamenetskii, M. D. (1994). *Annu. Rev. Biophys. Biomol. Struct*. **23**, 541–576.
17. Wells, R. D. (1988). *J. Biol. Chem*. **263**, 1095–1098.
18. Wang, Y., Mueller, J. E., Kemper, B. and Seeman, N. C. (1991). *Biochemistry* **30**, 5667–5674.
19. Seeman, N. C., et al. (1993). *New J. Chem*. **17**, 739–755.
20. Grabar, K. C., Freeman, R. G., Hommer, M. B. and Natan, M. J. (1995). *Analyt. Chem*. **67**, 735–743.
21. Mucic, R. C., Herrlein, M. K., Mirkin, C. A. and Letsinger, R. L. (1996). *J. Chem. Soc., Chem. Commun*. 555–557.
22. Linnert, T., Mulvaney, P. and Henglein, A. (1993). *J. Phys. Chem*. **97**, 679–682.
23. Herron, N., Wang, Y. and Eckert, H. (1990). *J. Am. Chem. Soc*. **112**, 1322–1326.
24. Colvin, V. L., Goldstein, A. N. and Alivisatos, A. P. (1992). *J. Am. Chem. Soc*. **114**, 5221–5230.

Chapter 2

Nanostructures in Biodiagnostics*

Nathaniel L. Rosi and Chad A. Mirkin
Department of Chemistry, Northwestern University, 2145 Sheridan Road, Evanston, IL 60208, USA
chadnano@northwestern.edu

2.1 Introduction

In the last 10 years the field of molecular diagnostics has witnessed an explosion of interest in the use of nanomaterials in assays for gases, metal ions, and DNA and protein markers for many diseases. Intense research has been fueled by the need for practical, robust, and highly sensitive and selective detection agents that can address the deficiencies of conventional technologies. Chemists are playing an important role in designing and fabricating new materials for application in diagnostic assays. In certain cases assays based upon

*Reprinted with permission from Rosi, N. L. and Mirkin, C. A. (2005). Nanostructures in biodiagnostics, *Chem. Rev.* **105**, 1547–1562. Copyright (2005) American Chemical Society.

Spherical Nucleic Acids, Volume 1
Edited by Chad A. Mirkin

ISBN 978-981-4800-35-8 (Hardcover), 978-0-429-20015-1 (eBook)
www.jennystanford.com

nanomaterials have offered significant advantages over conventional diagnostic systems with regard to assay sensitivity, selectivity, and practicality. Some of these new methods have recently been reviewed elsewhere with a focus on the materials themselves or as subclassifications in more generalized overviews of biological applications of nanomaterials [1–7]. We intend to review some of the major advances and milestones in the field of detection systems based upon nanomaterials and their roles in biodiagnostic screening for nucleic acids, proteins, and some biologically relevant small molecules and metal ions. Moreover, we focus on some of the key fundamental properties of certain nanostructures that make them ideal for specific diagnostic applications.

2.1.1 Background and Perspectives

Nucleic acid sequences unique to every living organism and every bacterium, virus, or pathogen provide practical targets for the identification and diagnosis of various diseases. With the advent of rapid sequencing capabilities, sequence information is now available for many diseases, including those associated with bioterrorism and warfare. To more effectively combat these diseases in the medical arena and accelerate response to bioterrorism threats, early and accurate detection of DNA markers is crucial. In this area, multidisciplinary teams of researchers including chemists, biochemists, and physicists have been evaluating the prospect of using assays based upon nanomaterials to compete effectively with the polymerase chain reaction (PCR) coupled with molecular fluorophore assays [8–11]. PCR, a technology that allows duplication of portions of prospective targets, represents the ultimate in terms of sensitivity [12] but has significant drawbacks including complexity, sensitivity to contamination, cost, and lack of portability and major challenges with respect to multiplexing (detecting multiple targets in a single assay) [13]. Many researchers view these limitations as some of the biggest impediments to moving nucleic-acid-based detection to point-of-care settings, including the doctor's office, the battlefield, the third world, and first responder sites in the case of bioterrorism defense. These settings require straightforward, inexpensive, and

disposable detection formats that have rapid and accurate readouts and require limited processing and user expertise. For nanomaterials to compete in the area of nucleic-acid detection, they have to make a compelling case, with PCR and molecular fluorophore technology setting the benchmarks for comparison.

Abnormal concentrations of certain proteins often signal the presence of various cancers and diseases. However, current protein detection methods only allow detection after protein levels reach critical threshold concentrations. At these concentrations the cancer or disease is often significantly advanced. More sensitive methods that allow for early detection of protein markers could potentially revolutionize physician treatment of various cancers and diseases and increase patient survival rates. In the area of protein diagnostics, the current gold standard is the enzyme-linked immunosorbent assay (ELISA) (~pM detection limits [14]), which also relies on fluorophore labeling and is extraordinarily general. An equivalent to PCR in the protein detection arena does not exist; therefore, there is greater room with which to compete with respect to sensitivity. It is important to note, however, that molecular fluorophores have many significant drawbacks, including susceptibility to photobleaching, broad absorption and emission bands, and a reliance on relatively expensive equipment to probe their presence in an assay. Again, these properties limit their use in point-of-care settings, so less expensive and more portable detection systems would be beneficial. For nanomaterials to compete in the area of protein detection, they must address one or more of the limitations imposed by the use of molecular fluorophores.

2.1.2 Why Nanomaterials?

Not all molecular fluorophores make for suitable probes in biodiagnostic assays nor do all nanomaterials offer advantages in biodetection. Certain nanomaterials are attractive probe candidates because of their (1) small size (1–100 nm) and correspondingly large surface-to-volume ratio, (2) chemically tailorable physical properties, which directly relate to size, composition, and shape

(Fig. 2.1), (3) unusual target binding properties, and (4) overall structural robustness. The size of a nanomaterial can be an advantage over a bulk structure, simply because a target binding event involving the nanomaterial can have a significant effect on its physical and chemical properties, thereby providing a mode of signal transduction not necessarily available with a bulk structure made of the same material. Tailorable physical properties are a very important aspect of nanomaterials. Indeed, in this regard, nanomaterials and biology have a long history as nanoparticles have been used in bioconjugation and as cellular labeling agents for the past four decades [15]. However, new synthesis, fabrication, and characterization methods for nanomaterials have evolved to the point that deliberate modulation of their size, shape, and composition is possible, thereby allowing exquisite control of their properties. The ability to carefully tailor the physical properties of nanomaterials is essential for their application in biodetection [1]. Specifically, the sizes, shapes, and compositions of metal nanoparticles and quantum dots can now be systematically varied to produce materials with specific emissive, absorptive, and light-scattering properties (Fig. 2.1), which make these materials ideal for multiplexed analyte detection [1, 16–19]; the composition of nanowires and nanotubes also can be controlled, thus allowing for measurement and variation of their conductive properties in the presence of target analytes [20]. Additionally, tools and techniques for surface modification and patterning have advanced to a point that now allows generation of nanoscale arrays of biomacromolecules and small molecules on surfaces [21–24]. Along with synthetic advances for varying the size, shape, and composition of nanostructured materials has come the ability to tailor their binding affinities for various biomolecules through surface modification and engineering [25–28]. Each of these capabilities allows researchers to design materials that can potentially be implemented into new assays having improved modes of signal transduction that can compete favorably with the molecular fluorophore-dominated methods of PCR and ELISA.

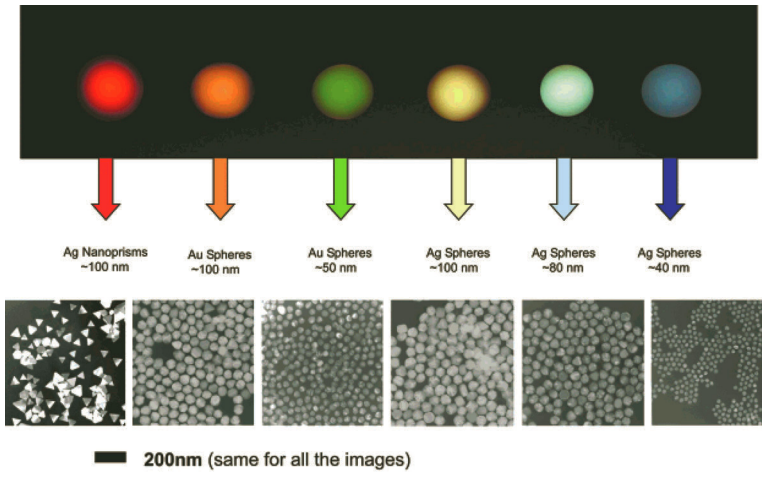

Figure 2.1 Sizes, shapes, and compositions of metal nanoparticles can be systematically varied to produce materials with distinct light-scattering properties.

2.2 Nanoparticle-Based Detection Methods

2.2.1 Optical Detection

2.2.1.1 Nucleic acids

An early indication of the potential of nanomaterials as biodetection agents, beyond conventional histochemical staining, was reported in 1996 with the observation that oligonucleotide-modified nanoparticles and sequence-specific particle assembly events, induced by target DNA, could be used to generate materials with unusual optical and melting properties [25]. Specifically, when 13-nm gold particles were used in the assay, the color of the solution changed from red to blue upon the analyte-directed aggregation of gold nanoparticles, a consequence of interacting particle surface plasmons and aggregate scattering properties. This simple phenomenon pointed toward the use of nanoparticles as DNA detection agents in a type of "litmus test" for nucleic acid targets, and indeed, it was found that spotting the solution onto a white support enhanced the colorimetric change and provided a permanent record for each test (Fig. 2.2) [29, 30]. Further studies indicated that the melting profiles of the nanoparticle-labeled DNA

aggregates were extraordinarily sharp, occurring over a temperature range much more narrow than the transition for unlabeled or conventional fluorophore-labeled DNA (Fig. 2.2) [29–32]. These two observations, both consequences of the high surface area and unique optical activity of the gold nanoparticles, created worldwide interest in exploring the potential for designer nanomaterials in biodiagnostic applications. The colorimetric change pointed to a simple and inexpensive way of diagnosing disease, and the unanticipated sharp melting profile suggested that assays based upon such nanostructures should have higher selectivities than the conventional molecular fluorophore-labeled structures that exhibit broad melting profiles when hybridized with complementary DNA. The sharp melting transitions associated with these nanoparticle probes derive from the dense loading of oligonucleotides on their surfaces and their ability to bind to complementary DNA in a highly cooperative manner [32]. These properties have not been observed with microparticle probes, partly because the loading efficiency of oligonucleotides does not compare with the gold nanoparticle—thiol system. It is worth noting that colorimetric responses have been utilized in viral detection systems based upon supramolecular polydiacetylene liposomes [33].

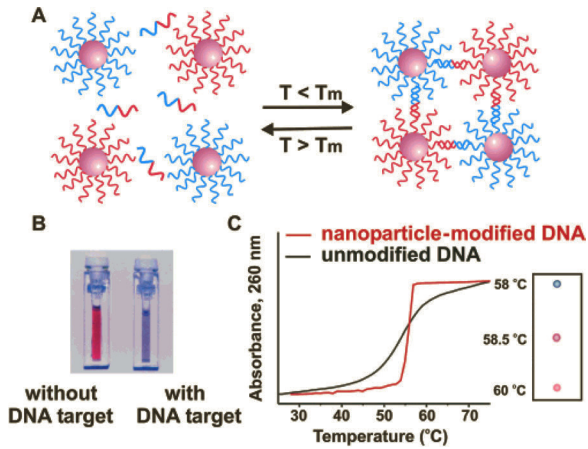

Figure 2.2 In the presence of complementary target DNA, oligonucleotide-functionalized gold nanoparticles will aggregate (A), resulting in a change of solution color from red to blue (B). The aggregation process can be monitored using UV–vis spectroscopy or simply by spotting the solution on a silica support (C). From Ref. [29]. Reprinted with permission from AAAS.

Further exploration of the potential of these materials in DNA detection showed that by virtue of these sharp melting transitions target DNA could be differentiated from DNA with single base-pair mismatches simply by measuring absorbance (or looking at color) as a function of temperature [29, 30]. This technique offered several advantages over other techniques such as arrays probed by fluorescence in that (1) it exhibited a high degree of discrimination between perfectly matched target oligonucleotides and targets with single base-pair mismatches, (2) it was "quick and easy," and (3) its optical read-out did not require expensive, sophisticated instrumentation. It should be further noted that this assay had the potential for modest multiplexing simply by synthetically tuning the composition of the nanoparticles to yield particles with different surface plasmon resonances [34]. At least two color pairs are available via this approach (red and blue for gold particles; yellow and black for core–shell, gold-coated silver particles). A limitation of this approach involved its sensitivity, which in the unoptimized format was in the 1–10 nM range. Modest improvements to this assay were made when larger nanoparticles (50 or 100 nm probes) were employed. Specifically, in using 50 nm probes target could be quantitatively detected between 5 nM and 50 pM [31]. However, these values are still not as good as the best results from fluorophore-based assays (typically in picomolar range; best reported ~600 fM) [35], thus limiting its application to assays that require preamplification of target through methods such as PCR.

In addition to DNA hybridization-promoted nanoparticle aggregation, others demonstrated that hybridization reactions involving oligonucleotide-modified gold nanoparticles that do not result in aggregate assembly can result in measurable optical changes that correlate with target concentration [36]. The authors contend that in these systems the aggregation is promoted by a reduction of the repulsive interactions between nanoparticles upon formation of duplex DNA on the surface of the nanoparticles. Specifically, they postulate that the stiffening of the DNA upon formation of duplex raises the binding constant with counterions, which can serve to better shield the negative charges. While an interesting phenomenon, this assay is even less sensitive (detection limit = 60–500 nM range) than the assay involving particles cross-linked through hybridization [29] because it requires more DNA to effect the optical changes. Another

DNA detection format involves nanocrystals modified with peptide nucleic acids (PNAs) and hybridized with target DNA [37]. This method relies on the increased salt stability of PNA-functionalized particles in the presence of hybridized target oligonucleotides. By slowly increasing the salt concentration of a suspension of PNA-functionalized particles hybridized with target DNA while also monitoring the colloidal stability, the extent of binding of the target oligonucleotide can be determined. If the target has a mutation, the colloid will aggregate at lower salt concentrations.

Very recently, the interactions between citrate-coated gold nanoparticles and short single-strand DNA were exploited to detect sequences in PCR-amplified genomic DNA [38, 39]. Researchers found that short single-strand DNA oligomers stabilize citrate-coated gold nanoparticles and prevent salt-induced aggregation [39]. Thus, exposure of citrate-coated gold nanoparticles to a saline mixture containing amplified, dehybridized genomic DNA and short oligomers that are complementary to regions along the genomic DNA results in particle aggregation (color change from red to blue) because the oligomers hybridize to the target genomic DNA and are therefore not available to stabilize the particles. If the oligomers are not complementary to regions along the genomic DNA, they can then stabilize the gold nanoparticles, resulting in no color change and signaling the absence of target DNA.

Introduction of nanoparticles into some well-studied DNA assays results in improved sensitivity. For example, surface plasmon resonance (SPR) is used to detect and probe real-time DNA hybridization on surfaces with detection limits of ~150 nM target [40]. However, when targets are hybridized in a sandwich format between surface-capture strands and oligonucleotide-functionalized nanoparticle labels, the detection limit improves approximately 1000-fold to less than 10 pM target concentration [41]. Another real-time detection method that utilizes oligonucleotide-labeled gold nanoparticles was recently developed [42]. This method involves the immobilization of capture oligonucleotide strands onto chemoresponsive diffraction gratings followed by capture of target DNA and finally labeling of targets with oligonucleotide-functionalized nanoparticle probes. Monitoring target hybridization in real-time using laser diffraction results in femtomolar concentration detection limits.

Molecular beacons are commonly used for nucleic acid detection [10, 11]. A drawback of molecular beacons is the quenching efficiency of the molecular quencher [43]. When the molecular quencher is replaced with a gold nanoparticle, the quenching is much more efficient, resulting in a more sensitive probe [43]. Moreover, these probes have higher single base mismatch selectivity (25:1) compared to conventional molecular beacons (4:1). Nie and coworkers also used gold nanoparticles as quenchers in a molecular fluorophore nucleic acid probe [44]. Their design, however, does not incorporate the DNA hairpin structure used in molecular beacons. Rather, they modify gold nanoparticles with oligonucleotides functionalized on one end with a thiol and the other end with a molecular fluorophore. The thiol end binds to the gold particle surface, and the fluorophore nonspecifically binds to the gold surface, resulting in a "loop" structure in which the gold nanoparticle quenches the emission from the fluorophore. Target binding breaks the "loop" structure, thus distancing the fluorophore from the nanoparticle quencher, resulting in measurable fluorescence [44].

Tan and coworkers developed fluorescent dye-doped silica nanoparticles functionalized with oligonucleotides as labels for chip-based sandwich DNA assays [45]. The nanoparticles are composed of a silica matrix that encapsulates large numbers of fluorophores. Not only does this increase the fluorescent signal associated with each target recognition event, but the silica matrix also acts as a protective barrier against fluorophore bleaching. This method results in an impressive detection limit of ~1 fM target and provides ~14:1 differentiation between target DNA and DNA with only one base mismatch. Tan's group used similar particles to detect single bacterium cells [46]. Here, they modify the fluorescent nanoparticles with monoclonal antibodies specific for the O-antigen of *E. coli* O157:H7. When mixed with 100 μL samples containing single bacterium cells, the fluorescent particles densely coat the cell walls, allowing detection with typical fluorescent plate readers. These methods improve upon typical molecular fluorophore-based assays, but they remain somewhat limited by the fundamental drawbacks of molecular fluorophores including broad adsorption and emission profiles, which reduces multiplexing capabilities.

Quantum dots, with their broad excitation spectra, sharp emission spectra, and easily tunable emission properties, are potential candidates for replacing conventional fluorescent markers

in biodetection assays. Having already shown considerable promise as intracellular imaging and tracking agents [47–51], quantum dots made of CdSe and ZnS, with few exceptions [52–56], have not been widely investigated as materials for biodetection assays. The first example of chemically modifying CdSe quantum dots with DNA involved ligand exchange coupled with particle surface engineering [53]. Recent studies employed quantum dots as labels imbedded in polymeric structures [54]. Using this strategy, Nie and coworkers provided a proof-of-concept study to display the potential of quantum dots as tags for multiplexed DNA detection (Fig. 2.3). In this work they labeled the target DNA with a fluorophore and oligonucleotide-functionalized polymeric microbeads with quantum dots designed to emit at various specified wavelengths other than that of the target DNA. Microbeads with different ratios of quantum dots exhibited different signature fluorescence spectra. After capture of target DNA by the microbead/quantum dot assembly, single-bead spectroscopy studies revealed both the presence and the identity of the target DNA. In essence, this work demonstrates that quantum dot labels can be "mixed and matched" to produce emission signals with variable intensities. This results in a palette of quench-resistant labels for biomolecule detection that compare favorably with molecular fluorophores.

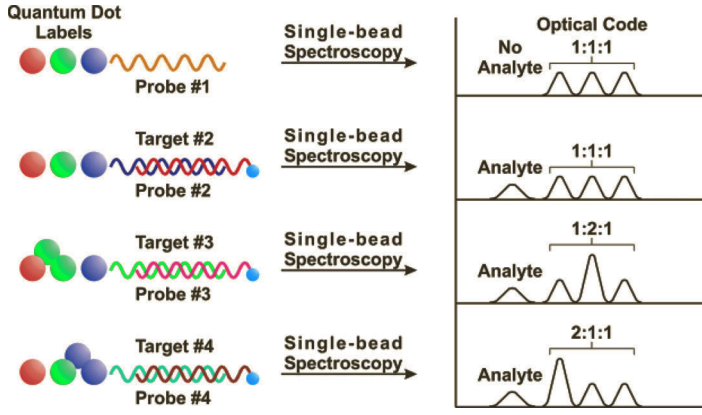

Figure 2.3 Quantum dots can be employed for detecting multiple targets in a single assay. Specifically, varying the numbers and ratios of different quantum dots per target results in a unique fluorescent signal for each individual target. Reprinted by permission from Springer Nature Customer Service Centre GmbH: Springer Nature, *Nature Biotechnology*, Ref. [54], Copyright (2001).

Alivisatos and coworkers recently reported studies using CdSe/ZnS quantum dots in chip-based assays to detect single base-pair mutations in DNA [56]. They detect perfectly complementary target DNA at concentrations as low as ~2 nM in the presence of background oligonucleotides containing various sequence mismatches. Since individual quantum dots have previously been used to detect single molecules under ideal conditions using fluorescence microscopy [57], it is likely that the sensitivity of these assays can be improved with proper surface modification processes and engineering. However, as for any assay, the ultimate sensitivity of techniques based upon these materials will not be based upon how few quantum dots can be detected but rather the target binding constant for the particles and their selectivity in complex media. They will undoubtedly be used extensively for research applications, but their use in the medical diagnostic arena will be determined by the advances made over the next few years in increasing sensitivity and selectivity and the movement toward materials less toxic than CdSe [58].

The unique light-scattering properties of nanoparticles (Fig. 2.1) have prompted interest in their potential application as labels for multiplexed analyte detection [59–65]. In 1995 Stimpson and coworkers incorporated light-scattering selenium nanoparticles into a simple proof-of-concept chip-based DNA assay [59]. Since that initial report Yguerabide and Yguerabide demonstrated that light-scattering particles favorably compete with conventional fluorophores as diagnostic labels [60–62]. For example, they showed that a single 80 nm gold particle has a light-scattering power equivalent to the signal generated from ~10^6 fluorescein molecules [60], and unlike molecular fluorophores, the light-scattering signal from metal nanoparticles is quench resistant. Given these properties, they replaced molecular fluorophores with resonance light-scattering (RLS) particles (essentially 40–120 nm metal nanoparticles) in typical cDNA microarrays [9] to evaluate their potential as labeling agents. In these experiments biotinylated probe DNA binds to specific regions in the cDNA microarrays. Then, anti-biotin-labeled RLS particles signal the presence of these specific regions by binding to the biotinylated probe sequences. In comparing this approach to molecular fluorophore-based approaches, they

found that at low probe DNA concentrations (16.7 pg/μL) RLS particles detected ~300 times more genes than Cy3, a commonly used molecular fluorophore [60]. The drawback of light scattering based on nanoparticles is that the signal depends on not only the size and shape of each particle, which is difficult to control on a large scale, but also the orientation of the particles on the surface and their interactions with other particles. This makes response calibration very difficult. More recently, researchers used the colorimetric light scattering of nanoparticles to detect synthetic DNA and genomic DNA at concentrations of 333 and 33 fM, respectively [65]. This assay involves pairs of 50-nm diameter gold probes, each modified with oligonucleotides that are complementary to neighboring regions on the target DNA. In the presence of target, the nanoparticle probes scatter orange light as a result of a plasmon band red shift; if the target is absent, the probes scatter green light.

One of the most important advantages offered by the colorimetric nanoparticle approach to DNA detection is the exquisite selectivity that results from the sharp melting transitions of nanoparticle-labeled DNA (Fig. 2.2) [29–32]. This advantage has been realized in a chip-based system that relies on a sandwich assay involving an oligonucleotide-modified glass slide, a nanoparticle probe, and target [66]. The assay consists of a capture DNA strand immobilized on a glass chip that recognizes the DNA of interest. A separate sequence on the captured target strand is then labeled with an oligonucleotide-functionalized nanoparticle probe. At this point, a thermal stringency wash removes nonspecifically bound target strands, allowing for over 10:1 selectivity for single base-pair mutations. After catalytic reduction of silver onto the gold nanoparticle surfaces to amplify the target signal (Fig. 2.4), the capture-strand/target/nanoparticle sandwich can be visualized with a flatbed scanner (hence the term “scanometric” is used to describe the approach) at target concentrations as low as 50 fM, a nearly 100-fold increase in sensitivity over traditional fluorescence-based assays. Since the original study the technique has been significantly refined and new research shows that 250 base-pair PCR amplicons of the Factor V Leiden gene can be distinguished from strands containing a single base-pair mismatch at concentrations as low as 100 aM [35]. Moreover, researchers unambiguously detected

the MTHFR gene from a 20 μg sample of human genomic DNA (~200 fM in target) without prior PCR amplification [67]. This was a major advance, demonstrating the ability to use nanostructures to detect genomic DNA in samples without PCR at concentrations relevant to real medical diagnostic applications. The use of nanoparticles is the key to these advances. Indeed, the selectivity of this method is a consequence of the sharp melting transitions of DNA-modified gold nanoparticles, and its sensitivity derives from the catalytic properties of the gold nanoparticles and their ability to effect the reduction of silver ions to amplify the detection signal.

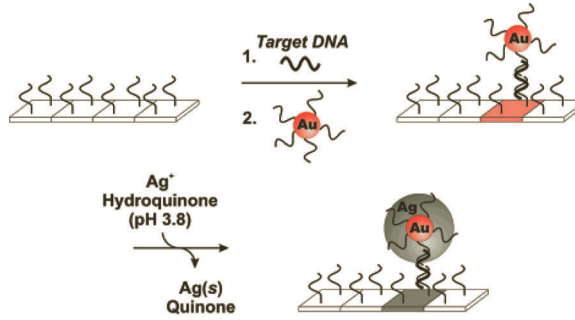

Figure 2.4 Scanometric DNA assay. In this assay a surface-bound capture oligonucleotide binds one-half of the target of interest, and an oligonucleotide-functionalized gold nanoparticle probe binds to the other half. Catalytic reduction of silver onto the capture/target/probe sandwich results in a signal that can be detected scanometrically. From Ref. [66]. Reprinted with permission from AAAS.

Attaching Raman-dye-labeled oligonucleotides to the gold nanoparticle probes generates spectroscopic codes for individual targets of interest, thus permitting multiplexed detection of analytes [68, 69]. Specifically, the presence of the target is confirmed by silver staining, and the identity of the target is revealed by detecting the surface-enhanced Raman scattering (SERS) of the Raman dye near the nanoparticle surface (Fig. 2.5). The silver coating enables detection of the signal from the dye-labeled particle (~1 fM) [68]. SERS is one of the most sensitive diagnostic approaches available to the analytical chemist [70]. This approach is similar to that which employs multiple fluorophores as labels; however, the spectroscopic lines in Raman spectroscopy are not as broad as the bands in fluorescence

spectroscopy, and the spectral window is much broader. This, in principle, will allow a greater degree of multiplexing. Indeed, target DNA sequences specific to multiple different bioterrorism agents have been identified using this approach with spectroscopically distinguishable nanoparticle probes (Fig. 2.5). Furthermore, only single-wavelength laser radiation is needed to scan a highly multiplexed array with numerous target-specific Raman dyes. This is in contrast to array-based detection of molecular fluorophore probes, where different excitation frequencies are needed for each fluorophore.

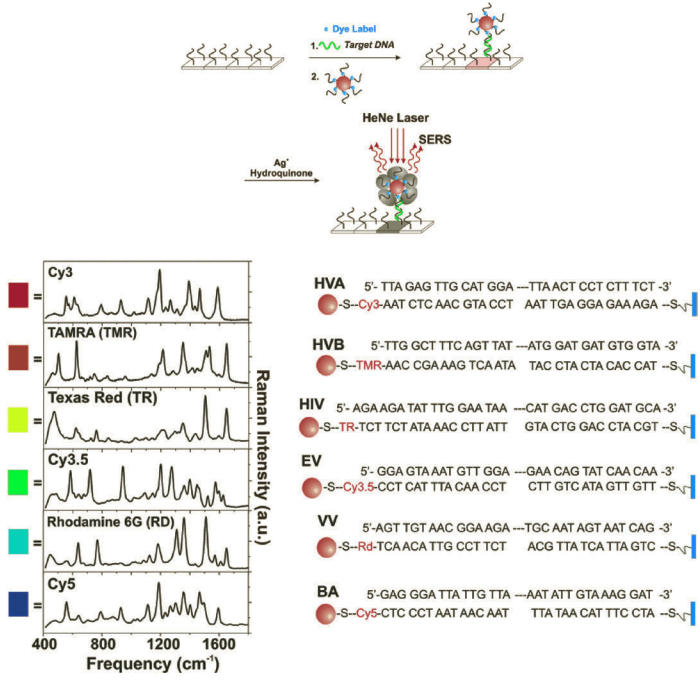

Figure 2.5 If Raman dyes (blue spheres) are attached to the labeling probe in the scanometric assay, the targets can be encoded and detected via the Raman signal of their labels. From Ref. [68]. Reprinted with permission from AAAS.

The catalytic deposition of metals onto gold nanoparticles allowed for signal amplification in the scanometric detection of DNA [66, 67]. Indeed, silver enhancement resulted in 100 aM detection limits [35], nearly a 5 orders of magnitude increase over solution-phase, unamplified colorimetric detection. Even with signal amplification,

however, most of the reported assays still require enzymatic-based target amplification steps such as PCR prior to detection steps. A new assay, which couples silver enhancement with an additional indirect target amplification method, pushes nanoparticle-based detection limits to values previously approached only by using PCR. This assay, called bio-barcode amplification (BCA) [71], employs oligonucleotides that act as barcodes for target DNA (Fig. 2.6). There are two components to the assay: magnetic microparticles functionalized with target capture strands and gold nanoparticles functionalized with both target capture and hundreds of barcode capture oligonucleotides that are hybridized to barcode DNA. In the presence of target DNA, the magnetic microparticles and the gold nanoparticles form sandwich structures that are magnetically separated from solution and washed with water to remove the hybridized barcode DNA. The barcodes (hundreds to thousands per target) are detected using the scanometric approach, resulting in detection limits as low as 500 zM (10 strands in solution) [71].

This method obviates the need for PCR in DNA detection and is fast, regardless of target concentration since the kinetics of the target binding process can be controlled by adjusting probe concentrations. Additionally, it is well suited for multiplexing as barcodes can be synthesized for virtually any target of interest.

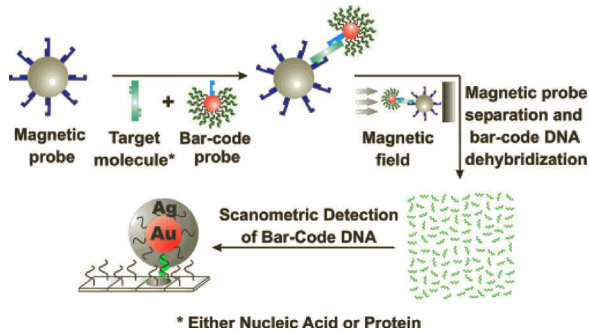

Figure 2.6 Nanostructure-based bio-barcode amplification scheme. In this assay magnetic microparticles capture either the target DNA or the protein. Gold nanoparticles loaded with barcode oligonucleotides and target capture molecules are added to the assay to form a sandwich system. The sandwich complexes are magnetically separated from the assay mixture and then washed with water to remove the barcode DNA that code for the target DNA or protein of interest. The barcodes are detected using the scanometric approach.

2.2.1.2 Proteins and biologically relevant small molecules

Protein and small molecule detection strategies that incorporate nanoparticles typically rely on the specific interactions between nanoparticle-bound antibodies with the target protein and the resulting effects these interactions have on the optical signature of the nanoparticles. The versatile surface chemistry of nanoparticles is important for these applications in that there are numerous straightforward methods of conjugating antibodies to various types of nanoparticles. One approach, pioneered by Halas, West, and coworkers, uses antibodies conjugated to the surface of gold nanoshells to detect proteins in saline, serum, and whole blood [72]. Upon interaction with the target protein, the antibody-functionalized nanoshells aggregate, resulting in a corresponding broadening of the nanoshell extinction peak at 720 nm. This assay is simple, fast (10 min), and detects target proteins in the range of 88–0.88 ng/mL, which is within the range of ELISA. An important aspect of this assay that should not be overlooked is its ability to detect proteins in serum and whole blood, which is important for any assay designed to function in nonlaboratory sites where sample preparation and purification is limited. Similar assays involve monitoring the light-scattering properties of gold colloids before and after avidin–biotin-induced particle aggregation [73]. As the concentration of avidin decreases, the light-scattering intensity of the gold colloids also decreases. However, this assay is only sensitive down to 1 nM avidin concentrations.

Another route involves tagging protein recognition molecules with oligonucleotides that are complementary to oligonucleotides coating the surfaces of Au nanoparticles [74]. These molecules are then recognized by specific proteins in solution, resulting in aggregation of the nanoparticle system. This assay has the potential for massive multiplexing as different protein targets can be tagged with specific oligonucleotides. As proof-of-concept, it was shown that both IgG1 (anti-biotin) and IgE (anti-dinitrophenyl) could be detected simultaneously by labeling the small molecules, biotin and dinitrophenyl, with oligonucleotides of different sequence and then hybridizing these moieties to nanoparticles functionalized with the appropriate strands of complementary oligonucleotides. To detect both IgG1 and IgE the nanoparticles were added to a solution

containing the two proteins, and then the melting profile of the resulting aggregate was examined. In solutions where both IgG1 and IgE were present there was evidence of melting for both the biotin-labeled oligonucleotide and the dinitrophenyl oligonucleotide. An alternative approach requires isolation and separation of the protein–DNA–nanoparticle aggregate followed by dehybridization of the DNA that tags the individual proteins. This DNA can then be detected using the scanometric approach. Both assays, melting and scanometric, exhibit optimal detection limits in the nanomolar range, 3 orders of magnitude lower in sensitivity than ELISA, thus necessitating optimization and improvement in order to compete. To this end, this methodology has recently evolved into the bio-barcode amplification (BCA) method used for DNA (vide supra) and protein detection, which is unparalleled in terms of assay sensitivity, especially with respect to protein markers.

Specifically, BCA for proteins involves scanometric detection of DNA barcodes that code for target proteins instead of DNA (Fig. 2.6) [75]. As before, there are two components in this assay: magnetic microparticles functionalized with monoclonal antibodies for the target protein and gold nanoparticles coated with both polyclonal antibodies for the target protein and also oligonucleotides hybridized to barcode strands that code for the target protein. In this method the magnetic microparticles first capture target proteins in solution, and addition of the gold nanoparticles results in the formation of sandwich structures. Following the same procedure in the DNA-BCA assay, protein targets can be detected at attomolar concentrations. While PCR amplification enhances DNA detection limits, protein detection has not benefited from a similar target amplification strategy [76, 77]. The BCA assay is impressive in this regard, providing a PCR-less method of amplifying protein concentrations by coding for protein targets with hundreds of barcode oligonucleotides. With this advance, protein markers that flag the presence of diseases such as prostate and breast cancer, Alzheimer's disease [78], and AIDS can be detected at levels unachievable with current techniques, thus potentially allowing for earlier detection and perhaps more effective treatment protocols for these ailments.

Heterogeneous chip-based systems also have been explored for protein detection. Niemeyer and colleagues used the scanometric approach as a method for detecting proteins [79]. In this procedure

capture antibodies specific for target proteins are immobilized on a surface. After the target proteins bind to the capture antibodies, antibody-labeled gold nanoparticles bind to the proteins to generate a sandwich system. Silver amplification is used to detect protein binding either spectrophotometrically or using a flatbed scanner, resulting in a detection limit of ~200 pM which is comparable with ELISA. A Raman-based approach that relies on many of the principles used in DNA detection (vide supra) provides a method for detecting protein–protein and protein–small molecule interactions [80]. In this approach protein microarrays [81] are screened with gold nanoparticles functionalized with specific antibodies or small molecules in addition to a Raman dye to code for the antibody or small molecule. After the functionalized gold nanoparticles interact with the surface-bound proteins, the arrays are amplified with silver to elucidate particle binding, and then SERS is employed to determine the type of protein–protein or protein–small molecule interactions. In a similar approach Porter and coworkers sandwiched target proteins between an antibody-coated gold substrate and gold nanoparticles coated with both antibody and Raman labels [82]. The resulting Raman signal indicated the presence of target protein, and the intensity of the signal correlated with target concentration. Using this method they detected ~1 pg/mL (~30 fM) prostate-specific antigen in human serum and ~4 pg/ mL (~120 fM) in bovine serum albumin.

Many solution-based nanoparticle assays take advantage of analyte-induced aggregation events that result in measurable changes and shifts of nanoparticle surface plasmon absorption bands. Van Duyne and coworkers demonstrated that surface nanostructures can be used to detect proteins by monitoring shifts in their surface plasmon resonance after binding of target proteins [83, 84]. In their system triangular silver nanoparticles are generated on surfaces using nanosphere lithography, and then biotin is immobilized on the surfaces of the particles. After adding streptavidin to the system a shift in the surface plasmon resonance of the silver triangles is observed which results from changes in the refractive index near the nanoparticle surfaces. This method allows detection of streptavidin at concentrations as low as ~0.1–1 pM [83]. Because streptavidin has a total of four biotin binding sites, biotinylated gold nanoparticles can be added to the assay after the detection step to

amplify the surface plasmon signal shift. In further studies using the same approach it was shown that anti-biotin, instead of streptavidin, could be detected at ~100 pM concentrations [84]. Most recently, this technique has been used to detect nanomolar amounts of amyloid β-derived diffusible ligands (ADDLs), potential molecular markers for Alzheimer's disease [85].

2.2.1.3 Metal ions

The simplicity of the colorimetric detection format pointed toward its use as a general method to detect wide varieties of analytes. Lu and coworkers provided a particularly elegant example of colorimetric detection by implementing an oligonucleotide-assembled nanoparticle network to detect Pb(II) ions in aqueous media and lead-containing paint samples at concentrations as low as 100 nM [86]. In this assay the nanoparticle network was assembled using a linking strand with 3′ and 5′ ends that were complementary to strands on the Au nanoparticles. The middle region of the linking strand was complementary to a DNAzyme with a high affinity for Pb(II). In the presence of Pb(II), the DNAzyme hydrolyzes the linking strand, causing the nanoparticle aggregate to disassemble, thus resulting in a color change from violet to red.

Spectroscopically silent metal ions such as Hg(I) can induce the aggregation of nanoparticles functionalized with appropriately designed chelating groups such as mercaptocarboxylic acids. Here, metal ions bridge the carboxylate moieties of different gold nanoparticles, resulting in a concomitant colloidal color change from red to blue [87]. Using this technique Pb was detected at concentrations as low as 400 μm. Another approach uses gold nanoparticles functionalized with a phenanthroline ligand designed to bind Li^+ ions in a 2:1 fashion. In the presence of Li^+ ions, the particles aggregate, allowing detection of Li^+ in the 10–100 mM range [88]. Last, gold nanoparticle systems are also useful for selectively detecting K^+ ions versus Na^+ ions in water [89]. When millimolar solutions of K^+ ions are exposed to solutions of 15-crown-5-modified gold nanoparticles that also contain Na^+ ions, the particles aggregate as a result of sandwich complex formation between two 15-crown-5 (from neighboring nanoparticles) and one K^+. In the case of Na^+, there is no sandwich formation and thus no particle aggregation. This technique could provide a useful method of detecting K^+ ions in

serum samples that typically have a high background concentration of Na^+ [89]. Continued improvement of ligand design that allows for highly specific metal coordination will result in even more selective metal ion detection assays that implement nanostructured probes.

Detection and tracking of metal ions in vivo necessitates the use of robust and highly specific detection agents that can withstand intracellular environments. Nanoparticle-based methods have proven to be viable tools for these tasks in certain cases. In particular, different nanoparticle probes that consist of fluorescent dyes encapsulated in a biocompatible polymer matrix can be designed to detect a wide variety of intracellular cations including calcium [90], zinc [91], and magnesium [92]. These probes, called PEBBLEs (probes encapsulated by biologically localized embedding), are advantageous in that the polymer matrix can both reduce the amount of dye photobleaching and nonspecific binding and protect the cell from potential toxic side effects of certain dyes. Variation of the polymer matrixes enables encapsulation of both hydrophilic and hydrophobic dyes. Moreover, multiple different dyes can be encapsulated in one particle, thus allowing signal ratioing for quantification purposes.

2.2.2 Electrical and Electrochemical Detection

2.2.2.1 Nucleic acids

Electrical detection methods offer the possibility of portable assays that could be used in a variety of point-of-care environments. Nanoparticle sandwich assays combined with silver amplification can be used for the electrical detection of DNA in a handheld format (Fig. 2.7) [93]. If oligonucleotide capture strands are immobilized in the gap between two electrodes and a sandwich assay analogous to the one used in the scanometric approach is performed, DNA can be detected as a measure of the change in electrical current or resistance between the two electrodes. In the absence of target DNA, there is no current flow across the electrode gap, but in the presence of target DNA, the associated nanoparticle probes, and catalytically deposited silver, current can flow between the electrodes. This method registers an unoptimized detection limit of 500 fM, but more importantly, when coupled with a salt-concentration-based

stringency wash, it exhibits a selectivity factor of 10 000:1, which is impressive when compared to the analogous array experiment carried out with a molecular fluorophore probe using identical chip and probe sequences (2.6:1) or even the scanometric approach with a thermal stringency (10:1) [66]. This potentially eliminates the need for on-chip temperature control, dramatically reducing the complexity of a hand-held device for DNA detection.

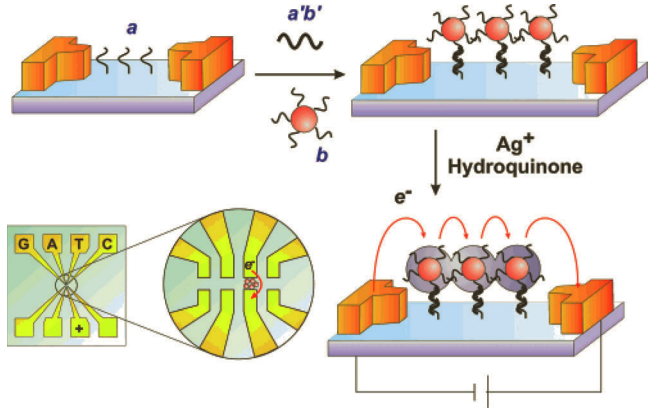

Figure 2.7 When the capture/target/probe sandwich is positioned in the gap between two electrodes, catalytic reduction of silver onto the sandwich system results in a signal that can be detected electrically. From Ref. [93]. Reprinted with permission from AAAS.

The detection of DNA using a quartz crystal microbalance (QCM) can be amplified using gold nanoparticle probes [6, 94]. Here, a DNA capture strand is immobilized on a gold/quartz piezoelectric crystal. After hybridization of the capture strand to one-half of the target, a gold nanoparticle-modified oligonucleotide hybridizes to the second half of the target strand, thus enhancing the signal output of the QCM device. Gold is then electrochemically reduced onto the surface of the gold nanoparticle to provide further signal enhancement. Using this method 1 fM concentrations of target DNA can be detected [94].

Coupling DNA detection with electrochemical readout has been widely studied [5]. Redox-active nanoparticle probes are attractive because their electrochemical signal can be systematically tuned by changing their compositions and their binding properties to various biomolecules can be controlled. Recently, new assays were developed that involve electrochemical stripping of the

nanoparticle portion of DNA-nanoparticle conjugates [95, 96]. These systems employ a sandwich assay in which target capture strands are attached to magnetic beads (Fig. 2.8) [96]. Once the target oligonucleotide hybridizes to the capture strand, it is then labeled with an oligonucleotide-functionalized inorganic nanoparticle probe that codes for the target strand of interest. The sandwich system can be magnetically separated and transferred to an electrochemical cell where the nanoparticles are dissolved and detected electrochemically. Different nanoparticles yield different voltammetric signals, depending upon their composition. The magnitude of the recorded signal corresponds to the concentration of target DNA, thus making this method amenable to multiplexing and quantification. However, the optimized detection limit of this assay is at 270 pM target concentration, still necessitating target amplification with PCR.

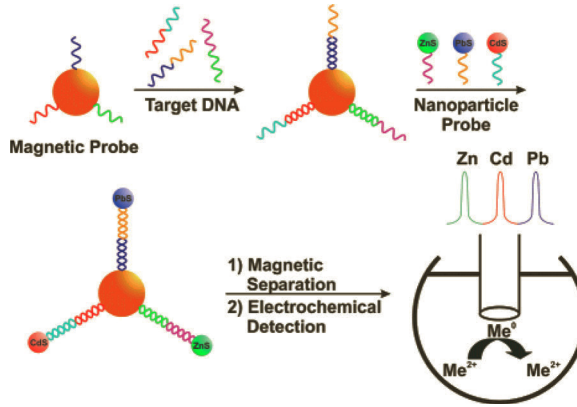

Figure 2.8 Magnetic microparticles (large brown spheres) labeled with DNA capture strands can bind target DNA, and then oligonucleotide-functionalized nanoparticle labels (small spheres) with different electrochemical signatures can be used to code for the specific target DNA of interest.

2.2.3 Magnetic Relaxation Detection

2.2.3.1 Nucleic acids

Magnetic nanoparticles also have shown promise in solution-based assays for DNA. Upon aggregation, magnetic nanoparticles can act as magnetic relaxation switches (MRS) by dephasing

the spins of the protons in the surrounding water, resulting in an enhancement of the T_2 relaxation times. Weissleder, Perez, and colleagues exploited this phenomenon for use in biodetection [97]. For example, oligonucleotide-functionalized iron oxide particles aggregate in the presence of target oligonucleotides (20 pM limit), resulting in a measurable increase (30 ms) in the T_2 relaxation times of the surrounding water. It was further discovered that base-pair insertions in the target strand resulted in only 2–5 ms increases in the relaxation times, while single base-pair mismatches resulted in 1–21 ms increases in T_2, suggesting that these systems could potentially be used to selectively detect DNA mutations.

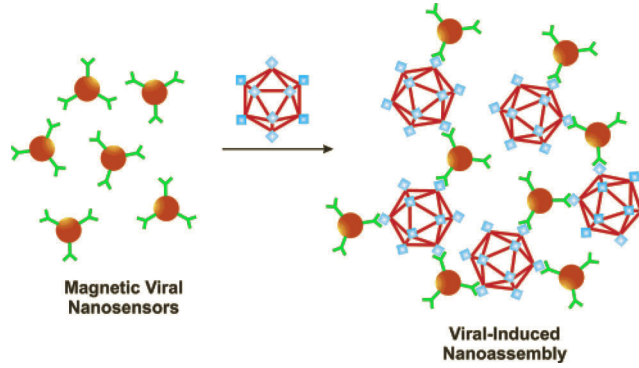

Figure 2.9 Superparamagnetic iron oxide nanoparticles (brown spheres) labeled with antibodies (green) specific to antigens (blue) presented on viral capsids (red) will form aggregates in the presence of target viruses, which result in detectable perturbations of the T_2 magnetic relaxation times of protons in the surrounding media.

2.2.3.2 Proteins and viruses

The magnetic relaxation phenomenon exhibited by magnetic nanoparticles also has been exploited for the detection of proteins and viruses (Fig. 2.9) [97, 98]. To detect viruses in solution and in serum, Perez and Weissleder's team immobilized antibodies specific to surface antigens present on the herpes simplex virus capsid to the surfaces of magnetic nanoparticles and then incubated the particles in the presence of solutions and serum containing the virus. They observed that the virus promotes formation of virus–particle aggregates, and they could therefore measure the concomitant increase in the relaxation time of the surrounding media. As the

concentration of virus particles increased, the relaxation time also increased, allowing for quantitative determination of viral concentrations. Given the magnetic basis of this detection method, it might be well suited for in vivo and patient sample diagnostics because the magnetic signal is not affected by the turbidity of the analyte medium.

2.3 Nanowire- and Nanotube-Based Detection Methods

2.3.1 Electrical Detection

2.3.1.1 Nucleic acids

Nanotubes and nanowires are being explored as new signal transduction motifs in the electrical detection of DNA [99–103] as they have for the detection of gases [104–107], small molecules [108], and proteins (vide infra) [20, 103, 109, 110]. For example, Lieber and colleagues demonstrated that silicon nanowires functionalized with PNA can be used for real-time, label-free detection of DNA [99]. In their assay the conductance of a PNA-functionalized silicon nanowire bridging two electrodes is measured in the presence of target DNA and mutant DNA with three consecutive base deletions. Introduction of target DNA into the assay caused a rapid and immediate change in conductance, while the effect of mutant DNA was negligible. Furthermore, the conductance changes scale with target concentration, and target DNA can be detected at concentrations as low as 10 fM. In the case of nanotubes, Lieber and colleagues showed that specific sequences of kilobase-size DNA can be detected using single-walled carbon nanotube (SWNT) atomic force microscopy (AFM) probes [100]. Specifically, they marked particular sequences along the DNA strand with streptavidin-labeled complementary DNA probes and then used AFM to identify the streptavidin and thus the location of the target sequences. This technique enabled the detection of specific haplotypes that code for genetic disorders.

Glassy carbon electrodes modified with carbon nanotubes can amplify the electrochemical signal of guanine bases. Wang and

coworkers exploited this phenomenon by showing that label-free electrochemical detection of DNA can be performed by carbon nanotube-modified electrodes at nanomolar concentrations [101]. In similar studies carbon nanotube arrays [102] and gold nanoelectrode arrays [111] were used to detect DNA hybridization. Here, the nanotubes or nanoelectrodes in the array are functionalized with a capture oligonucleotide strand. Upon target capture in the nanotube system $Ru(bpy)_3^{2+}$ is introduced to mediate guanine base oxidation, which can then be detected by the carbon nanotube nanoelectrodes [102]. In the case of the gold nanoelectrodes, target capture is monitored by measuring Ru(III)/Fe(III) electrocatalysis at the gold electrodes before and after hybridization [111].

Recent work utilized carbon nanotubes coated with alkaline phosphatase enzymes as labels in an assay for amplified DNA detection [103]. This assay employs a magnetic microparticle modified with oligonucleotides that are complementary to one-half of the target DNA sequence and carbon nanotubes coated with alkaline phosphatase enzymes and modified with oligonucleotides that are complementary to the other half of the target DNA sequence. Target DNA promotes the formation of a magnetic microparticle–target–carbon nanotube sandwich system that can be magnetically separated from the assay medium. After separation, α-naphthyl phosphate substrate is added to the mixture, resulting in formation of α-naphthol product that is ultimately detected at a carbon nanotube-modified electrode via chronopotentiometric stripping. This method can detect target DNA at concentrations as low as 54 aM [103].

2.3.1.2 Proteins, viruses, and biologically relevant small molecules

Nanoscale conducting materials such as nanowires and nanotubes also have been used for protein detection. Lieber and coworkers used boron-doped silicon nanowires modified with biotin to detect picomolar concentrations of streptavidin [20]. Specifically, they showed that the conductivity of the silicon nanowire increased in the presence of streptavidin and that the magnitude of the conductivity change depended on the concentration of analyte. Lieber's group also interfaced nanowires functionalized with antibodies specific for influenza A virus particles with a microfluidic sampling system to

demonstrate that single virus/nanowire recognition events can be detected by measuring real-time changes in nanowire conductivity [109].

Similar studies have been performed with carbon nanotubes. Dai's team has shown that poly(ethylene oxide) (PEO) coated carbon nanotubes resist nonspecific adsorption of proteins onto the nanotube surface [110]. At the same time, the PEO coating can be selectively functionalized with antibodies specific to target proteins of interest. In the presence of ~1 nM concentrations of target protein, the conductance of the nanotube decreases. No change in conductance is observed in the presence of structurally similar proteins. While carbon nanotubes and nanowires currently are not as easily functionalized as quantum dots or spherical nanoparticles, they offer the distinct advantage of rapid, real-time detection. With continued research into methods of surface modification, nanotube/nanowire alignment, and integration with microelectrode devices, nanowire and nanotube systems may become viable options as nanostructured biodiagnostic devices.

2.4 Nanofabrication

2.4.1 Nanopatterning

In current chip-based biodiagnostic detection formats (nanomaterial-based or otherwise) the capture molecules on chip surfaces are patterned on the microscale. This format allows for massive parallel screening of various analytes in a small area, a feature that has proven invaluable in genomics and proteomics research. Moreover, microarrays provide a platform for multiplexed DNA and protein detection in small areas [81]. Further miniaturization in the form of nanoarrays would allow for orders of magnitude more massively paralleled multiplexed detection in the same array area as a microarray and potentially improved detection limits resulting from the smaller analyte capture area (Fig. 2.10A) [112]. Various methods including dip-pen nanolithography (DPN) [21, 113–118], nanografting [22–24, 119], and finely focused ion beam lithography [120], among others [121–123], have been developed to fabricate nanoscale patterns of biomolecules such as DNA and proteins on

surfaces. DPN can be used to both directly and indirectly pattern reactive protein features and directly pattern reactive DNA features onto various surfaces (Au, silica, Ni) with nanoscale resolution. Nanografting and ion-beam methods rely on indirect deposition processes.

The potential of nanoarrays for detection purposes hinges on their reactivity with targets and the ability to effectively screen for targets using conventional techniques. To this end, it was shown that DNA nanoarrays fabricated using DPN can recognize complementary target DNA labeled with either molecular fluorophores [114] or oligonucleotide-functionalized gold nanoparticles (Fig. 2.10B) [113, 114]. In the case of molecular fluorophore labeling, the presence of target can be detected with a fluorescence microscope, and for nanoparticle labeling, target presence is assessed using AFM, which measures the change in height profile after nanoparticle probe binding events. For slightly larger spots with nanoparticle probes, light scattering can be used to measure and probe target binding events. The reactivity of protein nanoarrays is determined by rinsing the substrates with antibodies specific to the patterned proteins. The antibodies, tagged with either a molecular fluorophore or a nanoparticle probe, can be detected using either fluorescence microscopy [117, 118] or AFM [115, 116]. Lithographic techniques also can be used to fabricate nanoscopic wells [124, 125] and channels [126] on surfaces. Such features could be used as nanoconfinement vessels for recognition events between probes and target analytes, allowing for significant reduction in sample volume and possibly lower detection limits. While these nanopatterning techniques are still in their infancy, they represent the next step toward further miniaturization of biodetection assays. In principle, they will require smaller sample volumes and thus may result in higher sensitivities than is achieved with microarrays. Recently, DPN was used to fabricate nanoarrays of monoclonal antibodies against HIV-1 p24 [127]. These arrays were used to capture HIV p24 proteins from human plasma samples. After capture, the presence of p24 was determined using AFM. To amplify the signal, the nanoarray was rinsed with anti-p24-modified gold nanoparticles, which bind to the spots only when p24 is present and increase the height of the spots. Importantly, only 1 μL of sample is required for this assay, which is critical in cases where sample volumes are small and limited. The

detection limit for p24 using this assay is 0.025 pg/mL, which is much better than conventional ELISAs (5 pg/mL).

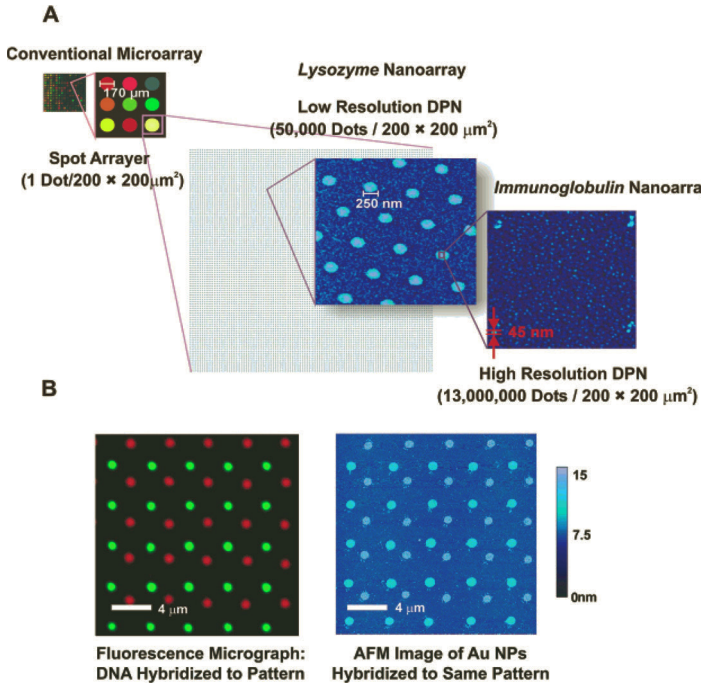

Figure 2.10 In a conventional microarray spot sizes are typically 200 × 200 μm^2. Using low-resolution dip-pen nanolithography (DPN), 50 000 250-nm protein spots can be spotted in an equivalent area. Patterns can be further miniaturized using high-resolution DPN to generate a total of 13 000 000 spots in a 200 × 200 μm^2 area (A). Similarly, DPN can be used to construct nanopatterns of oligonucleotides on SiO_x surfaces. The reactivity of the patterns can be interrogated using either fluorescence microscopy or atomic force microscopy (AFM) (B). From Ref. [114]. Reprinted with permission from AAAS.

2.4.2 Nanoelectromechanical Devices

Advances in photo- and e-beam lithographic techniques continue to enable the fabrication of complex devices on the micrometer and nanometer scale. Microcantilevers with nanoscale thickness allow detection of important biomolecules and microorganisms through measurement of their frequency as a function of target binding.

Functionalizing microcantilevers with target capture DNA [128, 129], for example, provides a platform for formation of a sandwich assay between target capture DNA, target DNA, and DNA-modified gold nanoparticle labels. The gold labels provide a site for silver ion reduction, which increases the mass on the cantilever and results in a detectable frequency shift that can be correlated with target detection [129]. The detection of viruses and bacteria is also possible using nanoelectromechanical devices [130–133]. In particular, Craighead and coworkers modified microcantilevers with antibodies for either specific viruses [131] or bacteria [133]. Upon exposure to solutions containing these species, they recorded measurable frequency changes associated with target binding events.

2.5 Conclusions and Outlook

Throughout this review the promise of nanostructure-based biodiagnostic assays has been assessed with respect to how they compare with the PCR/molecular fluorophore approach for DNA (Table 2.1) or ELISAs for proteins (Table 2.2). However, the merit of nanostructure-based assays must also be gauged in light of other assays that have been developed to compete with the conventional approaches. Dendrimers [134, 135] (nanostructures in their own right) and molecular electrochemical tags [5] have been successfully incorporated into DNA assays in efforts to improve upon or replace the molecular fluorophore-based assay. Specifically, dendrimers have primarily been used as a means to increase the number of labels associated with each target binding event. Using a dendrimer probe that contains approximately 250 fluorophores instead of a conventional molecular fluorophore probe, the fluorescent assay sensitivity increases by a factor of ~16 [134]. However, the dendrimer introduces an additional level of synthetic complexity to the assay, which might negate the improvement in sensitivity. Electrochemical assays based upon molecular probes are attractive because of their low cost and simplicity [5]. An electrochemical DNA assay in which each target recognition event is indirectly amplified by detecting the electrochemical signal from a microbead imbedded with electroactive molecules exhibits ~100 aM sensitivity [136]. This represents the lowest detection limit reported to date

for an electrochemical assay and one that competes favorably with molecular fluorophore-based assays; however, it is still higher than the best reported for a nanostructure-based assay (500 zM) [71]. Indirect protein amplification schemes also have received much attention for the sensitive detection of proteins. Immuno-PCR, which involves tagging antibodies specific to target proteins with DNA oligomers followed by PCR amplification after the detection step, offers significantly higher sensitivities than ELISA [76, 77]. However, PCR introduces complications [13], thus making immuno-PCR less favorable than the simpler and more user-friendly ELISAs. The nanoparticle-based bio-barcode approach for detecting proteins eliminates the need for PCR amplification and is approximately 6 orders of magnitude more sensitive than ELISAs [75]. Very recently, Wang and coworkers adopted a method similar to the bio-barcode approach for protein detection, but instead of scanometrically detecting barcode DNA, they fragmented the barcodes and then detected the bases electrochemically, resulting in a detection limit of ~13 fM [137].

Table 2.1 Detection limits of nucleic acid assays[a]

	Assay	ssDNA	PCR products	Genomic DNA
Nanostructure-based methods	Colorimetric[29] (cross-linked Au nanoparticles)	~4210 nM		
	Colorimetric[36] (non-cross-linked Au nanoparticles)	60 nM		
	Magnetic relaxation[97] (iron oxide nanoparticles)	20 pM		
	Electrochemical[96] (nanoparticles)	270 pM		
	Scanometric[35,66,67] (Au nanoparticles with Ag amplification)	50 fM	100 aM[b]	200 fM

	Assay	ssDNA	PCR products	Genomic DNA
	Raman spectroscopy[68] (Au nanoparticles with Ag amplification)	431 fM		
	Electrical[93] (Au nanoparticles with Ag amplification)	500 fM		
	Electrical[99] (Si nanowire)	10 fM		
	Electrical[103] (carbon nanotube)	54 aM		
	Resonant light-scattering[61-66] (metal nanoparticles)	170 fM[b]		33 fM
	Fluorescence[56] (ZnS and CdSe quantum dots)	2 nM		
	Surface plasmon resonance[41] (Au nanoparticles)	10 pM		
	Quartz crystal microbalance[94] (Au nanoparticles)	431 fM		
	Laser diffraction[42] (Au nanoparticles)	4350 fM		
	Fluorescence[45] (fluorescent nanoparticles)	431 fM		
	Bio-barcode amplification[71] (Au nanoparticles with Ag amplification)	500 zM		
Other non-enzymatic based methods	Fluorescence[35] (molecular fluorophores)		~600 fM[b]	

(*Continued*)

Table 2.1 (*Continued*)

Assay	ssDNA	PCR products	Genomic DNA
Fuorescence (dendrimer amplification)[134]		2.5 mg	
Electrochemical amplification[136] (electroactive reporter molecules)	100 aM		

[a]Detection limits can vary based on target length and sequence; therefore, it is difficult to compare assays without testing them using identical targets and conditions. [b]Values taken from Ref. [34].

Indeed, some nanostructure-based assays outperform conventional assays in terms of sensitivity, selectivity, and practicality. Continued optimization of these parameters will be necessary to determine the applicability of these assays in point-of-care settings. In particular, many of the assays reviewed herein have only been tested using synthetic single-strand DNA oligomers or commercially available protein samples, but some have proven effective for detecting genomic DNA (Table 2.1) and proteins from patient serum (Table 2.2). The ability of an assay to detect analytes in complex environments with high background and competing targets requires exquisite selectivity and sensitivity and will ultimately serve as a yardstick for determining its applicability in laboratory, clinical, and point-of-care settings. In this regard, diagnostic systems based upon many of the aforementioned nanomaterials look promising; however, most have not been studied in real-world settings. The transition to such settings often results in added complexity and affects ultimate assay performance. In most cases, these assays will need to be merged with simple and convenient sample handling systems in a way that does not make them prohibitively complicated or costly. Important advances in microfluidics will certainly complement these systems, but much work needs to be done before their full potential can be realized [138]. Future advances will require continued innovations by chemists in close collaboration with experts in medical and biological fields.

Table 2.2 Detection limits of protein assays

	Assay	Target	Protein in saline	Protein in serum
Nanostructure-based methods	Optical[72] (Au nanoshells)	Rabbit IgG	0.88 ng/mL (~4.4 pM)[a]	0.88 ng/mL (~4.4 pM)[a]
	Optical[74] (Au nanoparticles)	IgE and IgG1	~20 nM	
	Magnetic relaxation[98] (iron oxide nanoparticles)	Adenovirus (ADV) and herpes simplex virus (HSV)	100 ADV/ 100μL	50 HSV/ 100 μL
	Scanometric[79] (Au nanoparticles with Ag amplification)	Mouse IgG	200 pM	
	Raman[82] (Au nanoparticles with Raman labels)	Prostate-specific antigen		30 fM
	Surface plasmon resonance[83,84] (triangular Ag particles on surfaces)	Streptavidin(S A) and anti-biotin (AB)	~1 pM SA and ~700 pM AB	
	Electrical[110] (single-walled carbon nanotubes)	10E3 antibody to U1A RNA splicing factor	~1 nM	
	Electrical[20] (Si nanowires)	Streptavidin	10 pM	

(*Continued*)

Table 2.2 (*Continued*)

	Assay	Target	Protein in saline	Protein in serum
	Bio-barcode amplification[75] (Au nanoparticles with Ag amplification)	Prostate-specific antigen	30 aM (3 aM)[b]	(30 aM)[b]
Molecular fluorophore methods	Enzyme-linked immunosorbent assay	Various	pM range	pM range
Electrochemical methods	Electrochemical amplification[137] (oligonucleotide reporter molecules)	IgG	13 fM	
Enzyme-based amplification methods	Immuno-PCR[76]	Bovine serum albumin	2 fM	
	Rolling circle amplification[77]	Prostate-specific antigen	3 fM	

[a]Reported in ng/mL; authors converted to molar concentration for ease of comparison. [b]These values are the lower limits when PCR is used to amplify the barcode DNA prior to scanometric detection of barcodes.

Acknowledgments

C.A.M thanks and acknowledges the AFOSR, NSF, and DARPA for supporting this work.

References

1. Alivisatos, P. (2004). *Nat. Biotechnol.* **22**, 47.
2. West, J. L. and Halas, N. J. (2000). *Curr. Opin. Biotechnol.* **11**, 215.
3. Parak, W. J., Gerion, D., Pellegrino, T., Zanchet, D., Micheel, C., Williams, S. C., Boudreau, R., Le Gros, M. A., Larabell, C. A. and Alivisatos, A. P. (2003). *Nanotechnology* **14**, R15.
4. Chan, W. C. W., Maxwell, D. J., Gao, X., Bailey, R. E., Han, M. and Nie, S. (2002). *Curr. Opin. Biotechnol.* **13**, 40.
5. Drummund, T. G., Hill, M. G. and Barton, J. K. (2003). *Nat. Biotechnol.* **21**, 1192.
6. Willner, I., Patolsky, F., Weizmann, Y. and Willner, B. (2002). *Talanta* **56**, 847.
7. Niemeyer, C. M. (2001). *Angew. Chem. Int. Ed.* **40**, 4128.
8. Lander, E. S. (1999). *Nat. Biotechnol.* **21**, 3.
9. Duggan, D. J., Bitttner, M., Chen, Y., Meltzer, P. and Trent, J. M. (1999). *Nat. Genet. Suppl.* **21**, 10.
10. Tyagi, S. and Kramer, F. R. (1996). *Nat. Biotechnol.* **14**, 303.
11. Fang, X., Liu, X., Schuster, S. and Tan, W. (1999). *J. Am. Chem. Soc.* **121**, 2921.
12. Saiki, R. K., Scharf, S., Faloona, F., Mullis, K. B., Horn, G. T., Erlich, H. A. and Arnheim, N. (1985). *Science* **230**, 1350.
13. Kirk, B. W., Feinsod, M., Favis, R., Kliman, R. M. and Barany, F. (2002). *Nucleic Acids Res.* **30**, 3295.
14. Detectable concentration varies with target protein, but they are typically in the pM range.
15. Baudhuin, P., van der Smissen, P., Beavois, S. and Courtoy, J. (1989). *Colloidal Gold: Principles, Methods, and Applications*, Vol. 2 (Academic Press), pp. 1–17.
16. Jin, R., Cao, Y., Mirkin, C. A., Kelly, K. L., Schatz, G. C. and Zheng, J. (2001). *Science* **294**, 1901.

17. Jin, R., Cao, Y. C., Hao, E., Metraux, G. S., Schatz, G. C. (2003). Mirkin, C. A. *Nature* **425**, 487.
18. Sun, Y. G. and Xia, T. N. (2002). *Science* **298**, 2176.
19. Sau, T. K. and Murphy, C. J. (2004). *J. Am. Chem. Soc.* **126**, 8648.
20. Cui, Y., Wei, Q., Park, H. and Lieber, C. M. (2003). *Science* **293**, 1289.
21. Ginger, D. S., Zhang, H. and Mirkin, C. A. (2004). *Angew. Chem. Int. Ed.* **43**, 30.
22. Wadu-Mesthrige, K., Xu, S., Amro, N. A. and Liu, G.-Y. (1999). *Langmuir* **15**, 8580.
23. Liu, M., Amro, N. A., Chow, C. S. and Liu, G.-Y. (2002). *Nano Lett.* **2**, 863.
24. Kenseth, J. R., Harnisch, J. A., Jones, V. W. and Porter, M. D. (2001). *Langmuir* **17**, 4105.
25. Mirkin, C. A., Letsinger, R. L., Mucic, R. C. and Storhoff, J. J. (1996). *Nature* **382**, 607.
26. Alivisatos, A. P., Johnsson, K. P., Peng, X. G., Wilson, T. E., Loweth, C. G., Bruchez, M. P. and Schultz, P. G. (1996). *Nature* **382**, 609.
27. Chen, R. J., Zhang, Y., Wang, D. and Dai, H. (2001). *J. Am. Chem. Soc.* **123**, 3838.
28. Mbindyo, J. K. N., Reiss, B. D., Martin, B. R., Keating, C. D., Natan, M. J. and Mallouk, T. E. (2001). *Adv. Mater.* **13**, 249.
29. Elghanian, R., Storhoff, J. J., Mucic, R. C., Letsinger, R. L. and Mirkin, C. A. (1997). *Science* **277**, 1078.
30. Storhoff, J. J., Elghanian, R., Mucic, R. C., Mirkin, C. A. and Letsinger, R. L. (1998). *J. Am. Chem. Soc.* **120**, 1959.
31. Reynolds, R. A., Mirkin, C. A. and Letsinger, R. L. (2000). *J. Am. Chem. Soc.* **122,** 3705.
32. Jin, R. C., Wu, G., Li, Z., Mirkin, C. A. and Schatz, G. C. (2003). *J. Am. Chem. Soc.* **125**, 1643.
33. Reichert, A., Nagy, J. O., Spevak, W. and Charych, D. (1995). *J. Am. Chem. Soc.* **117**, 829.
34. Cao, Y. W., Jin, R. C. and Mirkin, C. A. (2001). *J. Am. Chem. Soc.* **123**, 7961.
35. Storhoff, J. J., Marla, S. S., Garimella, V. and Mirkin, C. A. (2004). Labels and Detection Methods. In *Microarray Technology and Its Applications* (Springer), pp. 147–174.
36. Sato, K., Hosokawa, K. and Maeda, M. (2003). *J. Am. Chem. Soc.* **125**, 8102.

37. Chakrabarti, R. and Klibanov, A. M. (2003). *J. Am. Chem. Soc.* **125**, 12531.

38. Li, H. and Rothberg, L. (2004). *Proc. Natl. Acad. Sci. U.S.A.* **101**, 14036.

39. Li, H. and Rothberg, L. J. (2004). *J. Am. Chem. Soc.* **126**, 10958.

40. Kai, E., Sawata, S., Ikebukuro, K., Iida, T., Honda, T. and Karube, I. (1999). *Anal. Chem.* **71**, 796.

41. He, L., Musick, M. D., Nicewarner, S. R., Salinas, F. G., Benkovic, S. J., Natan, M. J. and Keating, C. D. (2000). *J. Am. Chem. Soc.* **122**, 9071.

42. Bailey, R. C., Nam, J.-M., Mirkin, C. A. and Hupp, J. T. (2003). *J. Am. Chem. Soc.* **125**, 13541.

43. Dubertret, B., Calame, M. and Libchaber, A. J. (2001). *Nat. Biotechnol.* **19**, 365.

44. Maxwell, D. J., Taylor, J. R. and Nie, S. (2002). *J. Am. Chem. Soc.* **124**, 9606.

45. Zhao, X., Tapec-Dytioco, R. and Tan, W. (2003). *J. Am. Chem. Soc.* **125**, 11474.

46. Zhao, X., Hilliard, L. R., Mechery, S. J., Wang, Y., Bagwe, R. P., Jin, S. and Tan, W. (2004). *Proc. Natl. Acad. Sci. U.S.A.* **101**, 15027.

47. Dubertret, B., Skourides, P., Norris, D. J., Noireaux, V., Brivanlou, A. H. and Libchaber, A. (2002). *Science* **298**, 1759.

48. Chan, W. C. W. and Nie, S. (1998). *Science* **281**, 2016.

49. Dahan, M., Levi, S., Luccardini, C., Rostaing, P., Riveau, B. and Triller, A. (2003). *Science* **302**, 442.

50. Bruchez, M., Moronne, M., Gin, P., Weiss, S. and Alivisatos, A. P. (1998). *Science* **281**, 2013.

51. Gao, X., Cui, Y., Levenson, R. M., Chung, L. W. K. and Nie, S. (2004). *Nat. Biotechnol.* **22**, 969.

52. Pathak, S., Choi, S.-K., Arnheim, N. and Thompson, M. E. (2001). *J. Am. Chem. Soc.* **123**, 4103.

53. Mitchell, G. P., Mirkin, C. A. and Letsinger, R. L. (1999). *J. Am. Chem. Soc.* **121**, 8122.

54. Han, M., Gao, X., Su, J. Z. and Nie, S. (2001). *Nat. Biotechnol.* **19**, 631.

55. Gerion, D., Parak, W. J., Williams, S. C., Zanchet, D., Micheel, C. M. and Alivisatos, A. P. (2002). *J. Am. Chem. Soc.* **124**, 7070.

56. Gerion, D., Chen, F. Q., Kannan, B., Fu, A. H., Parak, W. J., Chen, D. J., Majumdar, A. and Alivisatos, A. P. (2003). *Anal. Chem.* **75**, 4766.

57. Empedocles, S. and Bawendi, M. (1999). *Acc. Chem. Res.* **32**, 389.

58. Derfus, A. M., Chan, W. C. W. and Bhatia, S. N. (2004). *Nano Lett.* **4**, 11.
59. Stimpson, D. I., Hoijer, J. V., Hsieh, W., Jou, C., Gordon, J., Theriault, T., Gamble, R. and Baldeschwieler, J. D. (1995). *Proc. Natl. Acad. Sci. U.S.A.* **92**, 6379.
60. Yguerabide, J. and Yguerabide, E. E. (2001). *J. Cell. Biochem.* **37**, 71.
61. Yguerabide, J. and Yguerabide, E. E. (1998). *Anal. Biochem.* **262**, 137.
62. Yguerabide, J. and Yguerabide, E. E. (1998). *Anal. Biochem.* **262**, 157.
63. Bao, P., Frutos, A. G., Greef, C., Lahiri, J., Muller, U., Peterson, T. C., Warden, L. and Xie, X. Y. (2002). *Anal. Chem.* **74**, 1792.
64. Taton, T. A., Lu, G. and Mirkin, C. A. (2001). *J. Am. Chem. Soc.* **123**, 5164.
65. Storhoff, J. J., Lucas, A. D., Garimella, V., Bao, Y. P. and Muller, U. R. (2004). *Nat. Biotechnol.* **22**, 883.
66. Taton, T. A., Mirkin, C. A. and Letsinger, R. L. (2000). *Science* **289**, 1757.
67. Storhoff, J. J., Marla, S. S., Bao, P., Hagenow, S., Mehta, H., Lucas, A., Garimella, V., Patno, T., Buckingham, W., Cork, W. and Muller, U. R. (2004). *Biosens. Bioelectron.* **19**, 875.
68. Cao, Y. W. C., Jin, R. C. and Mirkin, C. A. (2002). *Science* **297**, 1536.
69. Faulds, K., Smith, W. E. and Graham, D. (2004). *Anal. Chem.* **76**, 412.
70. Petry, R., Schmitt, M. and Popp, J. (2003). *ChemPhysChem* **4**, 14.
71. Nam, J.-M., Stoeva, S. and Mirkin, C. A. (2004). *J. Am. Chem. Soc.* **126**, 5932.
72. Hirsch, L. R., Jackson, J. B., Lee, A., Halas, N. J. and West, J. (2003). *Anal. Chem.* **75**, 2377.
73. Roll, D., Malicka, J., Gryczynski, I., Gryczynski, Z. and Lakowicz, J. R. (2003). *Anal. Chem.* **75**, 3440.
74. Nam, J.-M., Park, S.-J. and Mirkin, C. A. (2002). *J. Am. Chem. Soc.* **124**, 3820.
75. Nam, J.-M., Thaxton, C. S. and Mirkin, C. A. (2003). *Science* **301**, 1884.
76. Sano, T., Smith, C. L. and Cantor, C. R. (1992). *Science* **258**, 120.
77. Schweitzer, B., Wiltshire, S., Lambert, J., O'Malley, S., Kukanskis, K., Zhu, Z. R., Kingsmore, S. F., Lizardi, P. M. and Ward, D. C. (2000). *Proc. Natl. Acad. Sci. U.S.A.* **97**, 10113.
78. Georganopoulou, D. G., Chang, L., Nam, J.-M., Thaxton, C. S., Mufson, E. J., Klain, W. L. and Mirkin, C. A. (2005). *Proc. Nat. Acad. Sci. U.S.A.* **102**, 2273–2276.
79. Niemeyer, C. M. and Ceyhan, B. (2001). *Angew. Chem. Int. Ed.* **40**, 3685.

80. Cao, Y. C., Jin, R. C., Nam, J-.M., Thaxton, C. S. and Mirkin, C. A. (2003). *J. Am. Chem. Soc.* **125**, 14676.
81. MacBeath, G. and Schreiber, S. L. (2000). *Science* **289**, 1760.
82. Grubisha, D. S., Lipert, R. J., Park, H.-Y., Driskell, J. and Porter, M. D. (2003). *Anal. Chem.* **75**, 5936.
83. Haes, A. J. and Van Duyne, R. P. (2002). *J. Am. Chem. Soc.* **124**, 10596.
84. Riboh, J. C., Haes, A. J., McFarland, A. D., Yonzon, C. R. and Van Duyne, R. P. (2003). *J. Phys. Chem. B* **107**, 1772.
85. Haes, A. J., Hall, W. P., Chang, L., Klein, W. L. and Van Duyne, R. P. (2004). *Nano Lett.* **4**, 1029.
86. Liu, J. and Lu, Y. (2003). *J. Am. Chem. Soc.* **125**, 6642.
87. Kim, Y., Johnson, R. C. and Hupp, J. T. (2001). *Nano Lett.* **1**, 165.
88. Obare, S. O., Hollowell, R. E. and Murphy, C. J. (2002). *Langmuir* **18**, 10407.
89. Lin, S-.Y., Liu, S-.W., Lin, C-.M. and Chen, C-.H. (2002). *Anal. Chem.* **74**, 330.
90. Clark, H. A., Kopelman, R., Tjalkens, R. and Philbert, M. A. (1999). *Anal. Chem.* **71**, 4837.
91. Sumner, J. P., Aylott, J. W., Monson, E. and Kopelman, R. (2002). *Analyst* **127**, 11.
92. Park, E. J., Brasuel, M., Behrend, C., Philbert, M. A. and Kopelman, R. (2003). *Anal. Chem.* **75**, 3784.
93. Park, S.-J., Taton, T. A. and Mirkin, C. A. (2002). *Science* **295**, 1503.
94. Weizmann, Y., Patolsky, F. and Willner, I. (2001). *Analyst* **126**, 1502.
95. Wang, J., Xu, D., Kawde, A-.N. and Polsky, R. (2001). *Anal. Chem.* **73**, 5576.
96. Wang, J., Liu, G. and Merkoci, A. (2003). *J. Am. Chem. Soc.* **125**, 3214.
97. Perez, J. M., Josephson, L., O'Loughlin, T., Hogemann, D. and Weissleder, R. (2002). *Nat. Biotechnol.* **20**, 816.
98. Perez, J. M., Simeone, F. J., Saeki, Y., Josephson, L. and Weissleder, R. (2003). *J. Am. Chem. Soc.* **125**, 10192.
99. Hahm, J.-I. and Lieber, C. M. (2004). *Nano Lett.* **4**, 51.
100. Woolley, A. T. Guillemette, C., Cheung, C. L., Housman, D. E. and Lieber, C. M. (2000). *Nat. Biotechnol.* **18**, 760.
101. Wang, J., Kawde, A.-N. and Musameh, M. (2003). *Analyst* **128**, 912.
102. Li, J., Ng, H. T., Cassell, A., Fan, W., Chen, H., Ye, Q., Koehne, J., Han, J. and Meyyappan, M. (2003). *Nano Lett.* **3**, 597.

103. Wang, J., Liu, G. and Jan, M. R. (2004). *J. Am. Chem. Soc.* **126**, 3010.

104. Kong, J., Franklin, N. R., Zhou, C. W., Chapline, M. G., Peng, S., Cho, K. J. and Dai, H. J. (2000). *Science* **287**, 622.

105. Qi, P. F., Vermesh, O., Grecu, M., Javey, A., Wang, O., Dai, H. J., Peng, S. and Cho, K. J. (2003). *Nano Lett.* **3**, 347.

106. Modl, A., Koratkar, N., Lass, E., Wei, B. Q. and Ajayan, P. M. (2003). *Nature* **424**, 171.

107. Li, J., Lu, Y. J., Ye, Q., Cinke, M., Han, J. and Meyyappan, M. (2003). *Nano Lett.* **3**, 929.

108. Wang, J. and Musameh, M. (2003). *Analyst* **128**, 1382.

109. Patolsky, F., Zheng, G., Hayden, O., Lakadamyali, M., Zhuang, X. and Lieber, C. M. (2004). *Proc. Natl. Acad. Sci. U.S.A.* **101**, 14017.

110. Chen, R. J., Bangsaruntip, S., Drouvalakis, K. A., Kam, N. W. S., Shim, M., Li, Y. M., Kim, W., Utz, P. J. and Dai, H. J. (2003). *Proc. Natl. Acad. Sci. U.S.A.* **100**, 4984.

111. Gasparac, R., Taft, B. J., Lapierre-Devlin, M. A., Lazareck, A. D., Xu, J. M. and Kelley, S. O. (2004). *J. Am. Chem. Soc.* **126**, 12270.

112. Ekins, R. P. (1998). *Clin. Chem.* **44**, 2015.

113. Demers, L. M., Park, S. J., Taton, T. A., Li, Z. and Mirkin, C. A. (2001). *Angew. Chem. Int. Ed.* **40**, 3071.

114. Demers, L. M., Ginger, D. S., Park, S. J., Li, Z., Chung, S. W. and Mirkin, C. A. (2002). *Science* **296**, 1836.

115. Lee, K.-B., Park, S. J., Mirkin, C. A., Smith, J. C. and Mrksich, M. (2002). *Science* **295**, 1702.

116. Lee, K.-B., Lim, J.-H. and Mirkin, C. A. (2003). *J. Am. Chem. Soc.* **125**, 5588.

117. Lim, J.-H., Ginger, D. S., Lee, K. B., Heo, J., Nam, J-.M. and Mirkin, C. A. (2003). *Angew. Chem. Int. Ed.* **42**, 2309.

118. Nam, J.-M., Han, S. W., Lee, K. B., Liu, X. G., Ratner, M. A. and Mirkin, C. A. (2004). *Angew. Chem. Int. Ed.* **43**, 1246.

119. Schwartz, P. V. (2001). *Langmuir* **17**, 5971.

120. Bergman, A. A., Buijs, J., Herbig, J., Mathes, D. T., Demarest, J. J., Wilson, C. D., Reimann, C. T., Baragiola, R. A., Hu, R. and Oscarsson, S. O. (1998). *Langmuir* **14**, 6785.

121. Bruckbauer, A., Zhou, D., Ying, L., Korchev, Y. E., Abell, C. and Klenerman, D. (2003). *J. Am. Chem. Soc.* **125**, 9834.

122. Gu, J., Yam, C. M., Li, S. and Cai, C. (2004). *J. Am. Chem. Soc.* **126**, 8098.

123. Kramer, S., Fuierer, R. R. and Gorman, C. B. (2003). *Chem. Rev.* **103**, 4367.

124. Evans, U., Colavita, P. E., Doescher, M. S., Schiza, M. and Myrick, M. L. (2002). *Nano Lett.* **2**, 641.

125. Chen, X., Chen, Z. M., Fu, N., Lu, G. and Yang, B. (2003). *Adv. Mater.* **15**, 1413.

126. Czaplewski, D. A., Kameoka, J., Mathers, R., Coates, G. W. and Craighead, H. G. (2003). *Appl. Phys. Lett.* **83**, 4836.

127. Lee, K.-B., Kim, E-.Y., Mirkin, C. A. and Wolinsky, S. M. (2004). *Nano Lett.* **4**, 1869.

128. Hagan, M. F., Majumdar, A. and Chakraborty, A. K. (2002). *J. Phys. Chem. B*, **106**, 10163.

129. Su, M., Li, S. and Dravid, V. P. (2003). *Appl. Phys. Lett.* **82**, 20.

130. Gupta, A., Akin, D. and Bashir, R. (2004). *Appl. Phys. Lett.* **84**, 1976.

131. Ilic, B., Yang, Y. and Craighead, H. G. (2004). *Appl. Phys. Lett.* **85**, 2604.

132. Weeks, B. L., Camarero, J., Noy, A., Miller, A. E., Stanker, L. and De Yoreo, J. J. (2003). *Scanning* **25**, 297.

133. Ilic, B., Czaplewski, D., Zalalutdinov, M., Craighead, H. G., Neuzil, P., Campagnolo, C. and Batt, C. (2001). *J. Vac. Sci. Technol.* **19**, 2825.

134. Stears, R. L., Getts, R. C. and Gullans, S. R. (2000). *Physiol. Genomics* **3**, 93.

135. Wang, J. and Jiang, M. (1999). *J. Am. Chem. Soc.* **120**, 8281.

136. Wang, J., Polsky, R., Merkoci, A. and Turner, K. L. (2003). *Langmuir* **19**, 989.

137. Wang, J., Liu, G., Munge, B., Lin, L. and Zhu, Q. (2004). *Angew. Chem. Int. Ed.* **43**, 2158.

138. Sia, S. K., Linder, V., Parviz, B. A., Siegel, A. and Whitesides, G. M. (2004). *Angew. Chem. Int. Ed.* **43**, 498.

Chapter 3

Gold Nanoparticles for Biology and Medicine*

David A. Giljohann,[a,b] Dwight S. Seferos,[c] Weston L. Daniel,[a,b] Matthew D. Massich,[a,b] Pinal C. Patel,[a,b] and Chad A. Mirkin[a,b]

[a]*Department of Chemistry, Northwestern University, 2145 Sheridan Road, Evanston, IL 60208, USA*

[b]*International Institute for Nanotechnology, Northwestern University, 2145 Sheridan Road, Evanston, IL 60208, USA*

[c]*Department of Chemistry, University of Toronto, 80 St. George Street, Toronto, Ontario M5S 3H6, Canada*

chadnano@northwestern.edu

Gold colloids have fascinated scientists for over a century and are now heavily utilized in chemistry, biology, engineering, and medicine. Today these materials can be synthesized reproducibly, modified with seemingly limitless chemical functional groups, and, in certain cases, characterized with atomic-level precision. This review highlights recent advances in the synthesis, bioconjugation, and cellular uses of gold nanoconjugates. There are now many examples of highly sensitive and selective assays based upon gold

*Reprinted with permission from Giljohann, D. A., Seferos, D. S., Daniel, W. L., Massich, M. D., Patel, P. C. and Mirkin, C. A. (2010). Gold nanoparticles for biology and medicine, *Angew. Chem. Int. Ed.* **49**, 3280–3294. Copyright © 2010, John Wiley and Sons.

Spherical Nucleic Acids, Volume 1
Edited by Chad A. Mirkin

ISBN 978-981-4800-35-8 (Hardcover), 978-0-429-20015-1 (eBook)
www.jennystanford.com

nanoconjugates. In recent years, focus has turned to therapeutic possibilities for such materials. Structures which behave as gene-regulating agents, drug carriers, imaging agents, and photoresponsive therapeutics have been developed and studied in the context of cells and many debilitating diseases. These structures are not simply chosen as alternatives to molecule-based systems, but rather for their new physical and chemical properties, which confer substantive advantages in cellular and medical applications.

3.1 Introduction

Gold nanoparticles (AuNPs) have a rich history in chemistry, dating back to ancient Roman times where they were used to stain glasses for decorative purposes. The modern era of AuNP synthesis began over 150 years ago with the work of Michael Faraday, who was possibly the first to observe that colloidal gold solutions have properties that differ from bulk gold [1, 2]. Reliable and high-yielding methods for the synthesis of AuNPs, including those with spherical and nonspherical shapes, have been developed over the last half-century [3]. The resulting AuNPs have unique properties, such as size- and shape-dependent optical and electronic features, a high surface area to volume ratio, and surfaces that can be readily modified with ligands containing functional groups such as thiols, phosphines, and amines, which exhibit affinity for gold surfaces [3]. By using these functional groups to anchor the ligands, additional moieties such as oligonucleotides, proteins, and antibodies can be used to impart even greater functionality. The realization of such gold nanoconjugates has enabled a broad range of investigations, including programmed assembly and crystallization of materials [4, 5], arrangement of nanoparticles into dimers and trimers onto DNA templates [6], bioelectronics [7–9], and detection methods [10, 11]. The application of gold nanoconjugates for biodetection and biodiagnostics have been reviewed elsewhere [12–14].

In recent years, gold nanoconjugates and their properties have led to new and exciting developments with enormous potential in biology and medicine. These investigations represent a new direction that greatly deviates from the more established use of gold nanoconjugates as labels for electron microscopy [15]. Our recent studies, as well as those of several other research groups,

have shown that gold nanoconjugates, when functionalized with appropriate surface moieties, can readily enter living cells. These developments have forged a new frontier in nanoparticle research, including the broader use of gold nanoconjugates in cellular biology and the promise for their eventual use as therapeutic agents.

In this review we describe the current status of gold nanoconjugates for cellular and therapeutic uses. As surface chemistry is one of the key features that controls the properties and functionality, we have divided this review into sections based on the type of surface functionalization, including citrate, amine, nucleic acid, peptide, antibody, and lipid ligands (Table 3.1). In each section, our discussion focuses on chemical synthesis, physical and chemical properties, as well as investigations and applications in cells. In Section 3.8, we also propose key opportunities and open questions that have yet to be addressed by the scientific community. These questions should inspire future investigations and lead to discoveries that continue the development of the rich chemistry of gold nanoparticles.

Table 3.1 AuNP surface functionalities

Surface functionality	Application	Reference
Citrate	Cell uptake	[18, 19]
Transferrin	Cell uptake	[20, 21]
CTAB	Cell uptake	[14, 94]
Amine	Gene transfection	[26, 30, 31]
	Antiviral activity	[34]
	Drug delivery	[34]
	Oligonucleotide transfection	[36]
Oligonucleotide	Antisense gene regulation	[25, 77, 88, 102]
	mRNA detection	[87, 88]
	Small-molecule detection	[89]
	RNA interference	[90]
	Cancer cell detection	[93]
Peptide	Nuclear translocation	[23, 100]
	Antisense gene regulation	[102]
Antibody	Imaging	[15, 106, 107, 110]
	Photothermal therapy	[108, 109, 110]
Lipid	Imaging	[112]
	Cholesterol binding	[111]

3.2 Citrate and Transferrin

Citrate-functionalized gold nanoparticles can be prepared on a relatively large scale and with a high degree of monodispersity by using the methods of Frens [16] as well as Enustun and Turkevich [17]. These methods allow for the synthesis of citrate-capped spherical nanoparticles with diameters ranging from 5 to 250 nm [16, 17]. This well-established synthesis and the ability to finely control size has contributed to citrate-functionalized nanoconjugates forming the basis of recent investigations of the uptake of gold nanoparticles by cells [18]. In one such study, Chan and coworkers determined how the size and shape of the particles influence their ability to be internalized by cells [19]. Their study demonstrates that, in a HeLa cell model, the amount of time that the citrate particles remain internalized is independent of the particle size when they have diameters between 14 and 74 nm. However, the size does affect the total number of nanoparticle conjugates internalized during the experiment. By using inductively coupled plasma atomic emission spectroscopy (ICP-AES) to determine the intracellular gold content, these researchers determined that citrate-capped gold nanoconjugates with diameters of 50 nm are most readily internalized by HeLa cells (Fig. 3.1). They found that the maximum number of citrate-stabilized gold nanoconjugates taken up by a HeLa cell is 3000, 6160, and 2988 for gold nanoconjugates with diameters of 14, 50, and 74 nm, respectively.

The mechanism by which the citrate-capped gold nanoconjugates enter cells has been the subject of investigation. Chan and coworkers recorded transmission electron microscopy images of internalized "bare" citrate nanoconjugates and showed that the particles were mainly localized within vesicles inside of the cells [19]. They correlated cell uptake with the nonspecific adsorption of proteins to the citrate-capped nanoparticle surfaces.

The negatively charged citrate surface provides a convenient scaffold to attach positively charged proteins such as transferrin, which is expected to facilitate and improve entry into cells. In one study, atomic force microscopy was used to image transferrin-coated citrate-functionalized gold nanoconjugates on the cell surface [20]. The images obtained suggest vesicle formation at the cell surface and nanoconjugate internalization through endocytosis. A series of experiments by Chithrani and Chan further determined that

transferrin-coated citrate-functionalized gold nanoconjugates enter cells through the clathrin-mediated endocytosis pathway [21].

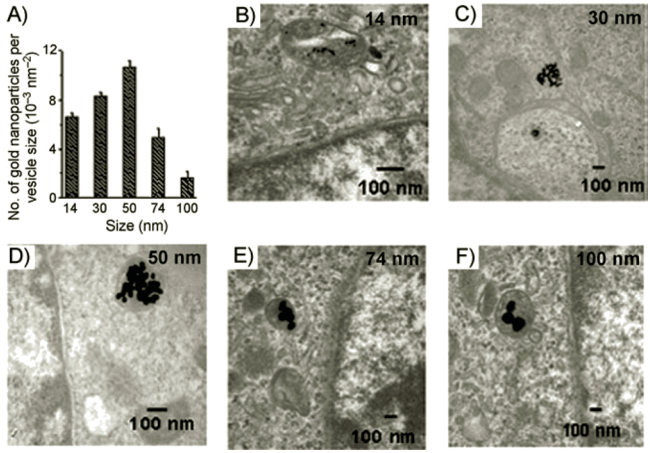

Figure 3.1 Transmission electron microscopy imaging and measurements of gold nanoparticles in cells. (A) Graph of number of gold nanoparticles per vesicle diameter for various nanoparticle sizes. (B–F) TEM images of gold nanoparticles with sizes of 14, 30, 50, 74, and 100 nm, respectively, trapped inside vesicles of a HeLa cell. Adapted with permission from Ref. [19]. Copyright (2006) American Chemical Society.

Many investigations in cells use citrate-capped AuNPs as important precursors of covalent conjugates with additional functionality, because further derivatization has been shown to increase uptake ability [22], alter intracellular localization [23, 24], or impart functionality that can be used to affect a cellular response [25, 26]. Indeed, citrate-coated particles are generally not ideal structures for investigations and internalization studies on cells. They are susceptible to environmentally induced aggregation and can be quite difficult to work with. In the next sections we describe the major classes of gold nanoconjugates that are functionalized with designer ligands, which have been developed and used for experiments on cells.

3.3 Amines

In addition to the methods of Enustun and Turkevich and of Frens, alternative methods for the synthesis of gold nanoparticles

have been developed. The Brust–Schiffrin method allows for the synthesis of monodisperse gold nanoparticles ranging from 1 to 3 nm in diameter [27]. The resultant nanoparticles are stabilized by a monolayer of alkanethiolates. The composition of the monolayer can be changed through a substitution reaction to include specific functionalities, depending on the intended use of the nanoparticles [28]. Accordingly, gold nanoconjugates functionalized with a monolayer of amine-terminated alkanethiolates (hereafter referred to as amine-functionalized) have been prepared for various biological applications.

3.3.1 Gene Transfection

The ability to induce control over biological systems at the genetic level is a fundamental concept in experimental biology, and holds great promise for developing new treatments of disease [29]. The search for the best method for controlling gene expression is ongoing. Their straightforward synthesis and high-degree of chemical tunability has resulted in amine-functionalized nanoparticles having been developed as a means to transfer genetic material into cell models [26, 30].

Amine surface groups are positively charged at physiological pH values, and thus amine-functionalized nanoconjugates electrostatically interact with negatively charged nucleic acids. Studies by Rotello and coworkers have demonstrated that 2 nm gold nanoparticles functionalized with a mixed monolayer containing quaternary amines and uncharged surface groups are able to bind DNA plasmids and deliver them efficiently to 293T cells [26]. In fact, these nanoconjugates are able to transfect these cells with a greater efficiency than the commonly used cationic polymer transfection agent polyethylenimine (PEI, 60 kDa). These researchers also found that the efficiency of the nanoparticle-mediated gene transfection was affected by the ratio of positively charged quaternary amines to negatively charged phosphate groups on the DNA, as well as the relative amount and length of the surface-bound uncharged thiol chain. Building on these observations, these researchers have recently shown that gold nanoparticles functionalized with lysine moieties are highly efficacious at delivering DNA plasmids, and outperform a commercial vector by a factor of 28 [31].

The utility of amine-functionalized nanoconjugates for gene delivery was also demonstrated by Thomas and Klibanov [30]. In this study, combinations of thiol-modified PEI (2 kDa) and dodecyl-PEI (2 kDa) were used as surfactants or complexing agents during AuNP synthesis. The concentration of PEI was used to control the size of the functionalized nanoparticles from 2.3 to 4.1 nm in diameter. The resultant nanoconjugates deliver plasmid DNA to COS-7 cells more efficiently than PEI alone.

3.3.2 Drug Delivery

Site-specific delivery, stability, and the programmed release of the drugs to physiological targets have been major challenges for molecular and macromolecular therapeutics [32]. The highly tunable and multivalent surface architecture of gold nanoconjugates offers the potential to incorporate multiple therapeutic agents as well as to target and protect molecules on the surface of a single nanoparticle, and thus are expected to improve the delivery and efficacy of therapeutic payloads. New generations of novel nanoconjugates with AuNPs as their cores have been designed and synthesized [33]. A recent study by Feldheim and coworkers has shown how multivalent AuNPs functionalized with derivatives of an important HIV antagonist are highly effective at silencing viral production in a cell model [34].

Rotello and coworkers have developed a cationic 2 nm gold nanoconjugate functionalized with thiol-modified alkyl amines that possess photoactive *o*-nitrobenzyl ester linkages, which can be cleaved with near-UV irradiation (Fig. 3.2) [35]. Irradiation releases the positively charged alkyl amine from the particle, thereby resulting in a net negatively charged carboxylate-functionalized nanoparticle. The reversal in charge provides an effective means of releasing a negatively charged payload such as an oligonucleotide from the nanoparticle surface. These cationic nanoparticles with photocleavable ligands were shown to inhibit transcription of the bound oligonucleotide; however, the transcription activity can be recovered following the cleavage reaction. Intracellular delivery of the bound oligonucleotide was also demonstrated in MEF cells. Fluorescence-based experiments show that, upon photoinduced cleavage, the bound DNA is released from the nanoparticle surface to

the intracellular environment where it then localizes in the nucleus. A similar strategy has been developed to deliver anticancer drugs [36].

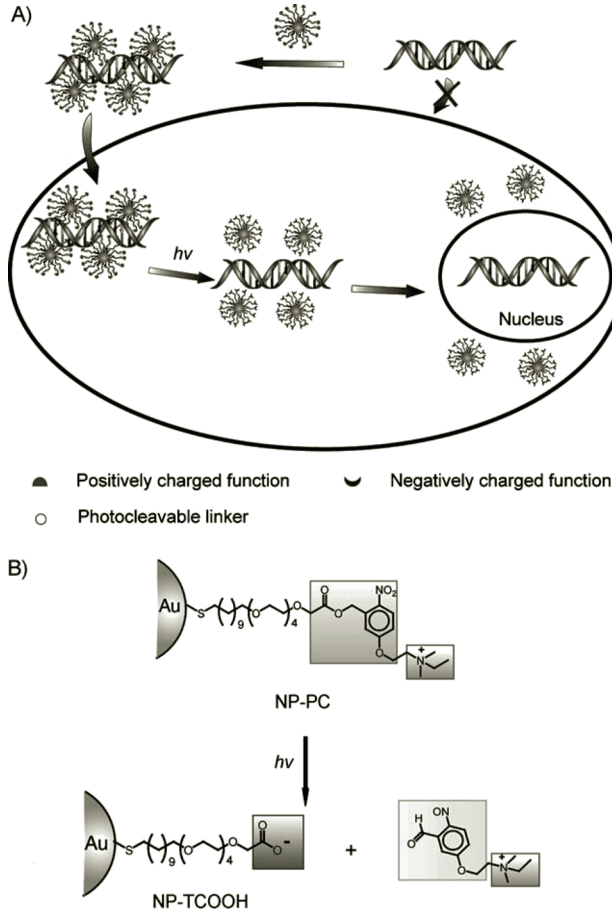

Figure 3.2 (A) Schematic illustration of the release of DNA from a photocleavable AuNP complex (NP-PC) upon UV irradiation within the cell. (B) Schematic presentation of light-induced surface transformation of NP-PC. Adapted with permission from Ref. [35]. Copyright © 2006, John Wiley and Sons.

Another study by Rotello and coworkers demonstrates an alternative method of releasing molecules from gold nanoparticle drug carriers. In this method, gold nanoparticles functionalized with

a mixed monolayer of amine-terminated and fluorophore-labeled alkyl thiol ligands were internalized by either HepG2 or MEF cells. Exposure to intracellular environments containing an elevated glutathione concentration (a thiol-possessing peptide) results in substitution and the passive release of the nanoconjugate ligands [37].

3.3.3 Stability

In addition to providing functional groups, surface-bound ligands also contribute to the stability of the AuNPs. The stability of the nanoconjugates is an important consideration for their potential use as therapeutic agents because they must maintain their stability under harsh conditions such as in the cell or in the bloodstream. In a study by Rotello and coworkers, the effect of surface charge on the stability of amine-functionalized gold nanoparticle was characterized [38]. In this study, 2 nm gold nanoparticles functionalized with combinations of positively charged amines, negatively charged carboxylates, and fluorescent ligands were used. Various thiol species were tested for their ability to displace ligands bound to the nanoparticle surface. It was found that increasing the net positive charge on the nanoparticle surface caused a more rapid displacement of ligands, whereas more negatively charged nanoconjugates did not display measurable displacement of surface-bound ligands [38]. This result is consistent with studies by our research group on the stability of 13 nm oligonucleotide/gold nanoparticle conjugates which found that the negatively charged thiolated oligonucleotide ligands are not easily displaced in intracellular environments or by small molecules such as glutathione [25].

3.4 Oligonucleotides

Over the past decade, our research group and others have synthesized, characterized, and applied polyvalent DNA-functionalized gold nanoconjugates (DNA-AuNPs) [4]. This unique class of nanomaterial consists of a gold nanoparticle core that is functionalized with a dense shell of synthetic oligonucleotides. DNA-AuNPs exhibit cooperative properties that result from their polyvalent surfaces [39–43], and

these properties have been applied to areas such as programmable crystallization [44–46] and enzyme-free biodiagnostic assays [47, 48]. Indeed, the optical, catalytic, and binding properties of DNA-AuNPs have been used for a variety of colorimetric [11, 49, 50], electronic [7], scanometric [51], and Raman-based [52] detection strategies, some of which have recently been commercialized and approved by the American Food and Drug Administration [51].

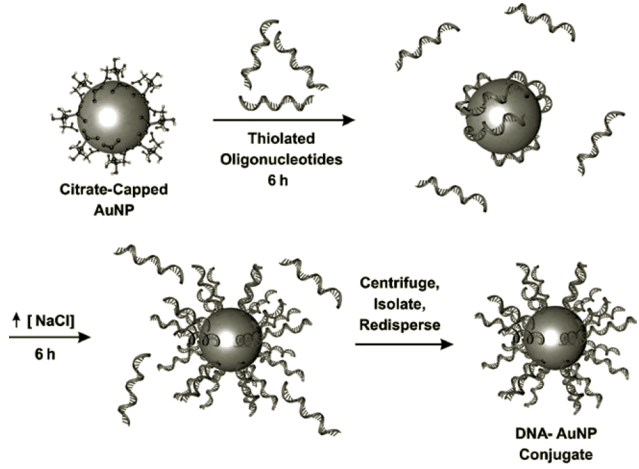

Figure 3.3 The synthesis of the oligonucleotide gold nanoconjugates: Alkanethiol-terminated oligonucleotides are added to citrate-stabilized AuNPs, thereby displacing the capping citrate ligands through formation of a gold–thiol bond. Subsequent addition of a salt shields repulsion between the strands, thus leading to a dense monolayer of oligonucleotides.

3.4.1 Synthesis

Nanoconjugates densely functionalized with synthetic oligonucleotides are prepared by mixing alkanethiol-terminated oligonucleotides and citrate-capped AuNPs. Oligonucleotide ligands displace the citrate from the AuNPs through formation of a gold–thiol bond. NaCl is added to the reaction mixture to shield charge repulsion, thus allowing a greater number of oligonucleotides to chemically adsorb to the nanoparticle surface, thereby resulting in a dense monolayer of oligonucleotides (Fig. 3.3). Approximately 250 oligonucleotides can be chemisorbed to the surface of 15 nm diameter AuNPs, thus creating polyvalent structures [53]. Methods

have been optimized for functionalizing particles with diameters ranging from 2 to 250 nm [54, 55]. This polyvalent material has a number of emergent properties that are unique from the properties of the oligonucleotides or the AuNPs alone.

3.4.2 Properties

One unusual but now fairly well understood property of DNA-AuNPs is their ability to bind complementary nucleic acids with a high affinity [56]. In fact, polyvalent particles exhibit binding constants as large as two orders of magnitude greater than the analogous molecular oligonucleotides of the same sequence [40]. Experimental data and later theoretical models show that this property likely arises from the dense packing and high local concentration of oligonucleotides on the gold surface [41, 57]. Additionally, the oligonucleotides on the AuNP surface are close enough such that the counterions associated with one oligonucleotide also act to screen negative charges on adjacent oligonucleotides. This additional charge screening causes increased stabilization of the oligonucleotide duplex, thereby increasing the effective binding constants associated with the DNA-AuNP compared with molecular oligonucleotides. Consistent with this observation, larger particles that have more DNA per particle, but less DNA per unit area exhibit affinities comparable to the molecular system and lower than the gold nanoconjugate structures [58]. In the context of cellular applications, it was hypothesized and subsequently demonstrated that the higher binding constant of the DNA-AuNP would lead to better intracellular binding of the target molecule, thereby increasing the effectiveness of antisense gene regulation (see Section 3.4.4.1) [25].

Nucleic acids are often hampered in biological investigations by enzymatic hydrolysis, which leads to degradation and renders them inactive [59, 60]. Another emergent property of DNA-AuNPs is resistance to degradation by enzymes such as DNase I [25]. Two explanations have been proposed as the origin of this enhanced stability: First, the dense packing of DNA on the surface of the particle could result in steric inhibition of enzyme binding, so that the inaccessible, particle-bound DNA would not be engaged or cleaved by the enzyme. An alternate hypothesis is that the high local ion concentration associated with the densely packed DNA inhibits

enzyme activity, since it is known that high concentrations of Na^+ ions result in a reduction of enzymatic activity [61, 62]. Experiments elucidating these two possibilities have recently been carried out [63]. Molecular DNA and DNA-AuNPs have similar enzymatic degradation rates under conditions where salt concentrations do not affect the enzymatic activity. However, the DNA-AuNP reaction rate is greatly slowed relative to that of molecular DNA under conditions where the salt concentrations affect enzymatic activity. The study concluded that the local Na^+ concentration is the dominant factor that contributes to the enhanced stability of DNA. The resistance of DNA-AuNPs to enzymatic degradation is an important property that renders these structures extremely promising candidates for introducing nucleic acids into cells, where oligonucleotide degradation has historically been a major challenge.

3.4.3 Cellular Uptake

Perhaps the most surprising property of DNA-AuNPs is their ability to enter a wide variety of cell types. The facile uptake of these structures into cells was not predicted, given that these structures contain a densely functionalized shell of polyanionic DNA (ca. 100 DNAs on the surface of each 13 nm gold particle), and that strategies for the introduction of oligonucleotides typically require that DNAs are complexed with positively charged agents to effect cellular internalization. Indeed, because of their high negative charge, most researchers at the time would have predicted that the nanoparticles would not enter cells [64]. Remarkably, it has been shown in all the cell types examined to date (which include over 30 cell lines, primary cells, and neurons, Table 3.2) that DNA-AuNPs can be added directly to cell culture media and are subsequently taken up by cells in high numbers (Fig. 3.4). Quantification of uptake using ICP-MS shows that while the number of internalized particles varies as a function of cell type, concentration, and incubation time, the cellular internalization of DNA-AuNPs is a general property of these materials. Importantly, the density of DNA on the particle surface was found to be the deciding factor of DNA-AuNP uptake. At DNA surface loadings of greater than about 18 $pmolcm^{-2}$, cellular uptake can exceed one million DNA-AuNPs per cell [65]. The importance of the polyvalent arrangement of oligonucleotides to cellular uptake can be further

emphasized when comparing DNA-AuNPs to other types of AuNPs. For example, HeLa cells internalize only a few thousand citrate-coated gold particles [19], compared to over one million DNA-AuNPs under nearly identical conditions [65]. Importantly, fluorescence spectroscopy studies reveal that the thiolated oligonucleotides remain bound to the AuNPs after cellular internalization (Fig. 3.4).

Table 3.2 Cell types that internalize polyvalent DNA gold nanoconjugates. Cellular internalization was determined using mass spectrometry and cell-associated fluorescence measurements

Cell type	Designation or source
Breast	SKBR3, MDA-MB-321, AU-565
Brain	U87, LN229
Bladder	HT-1376, 5637, T24
Colon	LS513
Cervix	HeLa, SiHa
Skin	C166, KB, MCF, 10 A
Kidney	MDCK
Blood	Sup T1, Jurkat
Leukemia	K562
Liver	HepG2
Kidney	293T
Ovary	CHO
Macrophage	RAW 264.7
Hippocampus neurons	primary, rat
Astrocytes	primary, rat
Glial cells	primary, rat
Bladder	primary, human
Erythrocytes	primary, mouse
Peripheral blood mononuclear cell	primary, mouse
T cells	primary, human
Beta islets	primary, mouse
Skin	primary, mouse

Given the surprising ability of DNA-AuNPs to enter cells, the mechanism of uptake is of great interest. Interestingly, biophysical

characterization of DNA-AuNPs after exposure to serum-containing media reveals changes in the charge and size of the nanoconjugates. Exposure to cell culture conditions results in greater positive charge and larger nanoparticle diameter (as measured by zeta potential and light scattering), which was further shown to be caused by the adsorption of proteins [65]. The interaction of polyvalent nanoparticle conjugates with proteins provides a possible mechanism of recognition and subsequent internalization of these highly negatively charged particles, the details of which are still under intensive investigation.

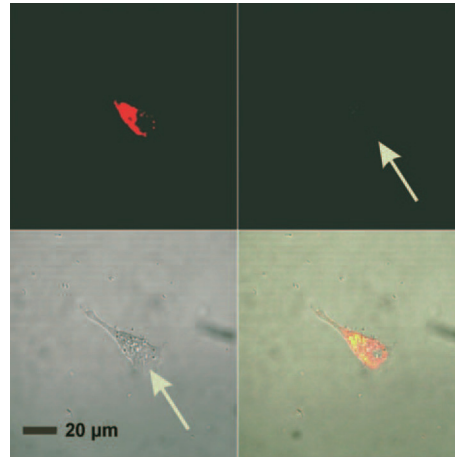

Figure 3.4 Fluorescent microscopy images of C166-EGFP cells incubated for 48 h with gold nanoconjugates functionalized with dual-fluorophore-labeled oligonucleotides (3′-Cy3 and 5′-Cy5.5) only reveal fluorescence from Cy5.5 (706–717 nm, upper left). Negligible fluorescence is observed in the emission range of Cy3 (565–615 nm, upper right). Transmission and composite overlay images are shown in the lower left and lower right quadrants, respectively. The arrows indicate the location of the cell. From Ref. [25]. Reprinted with permission from AAAS.

3.4.4 Applications in Cells

Methods based on nucleic acids for detecting and controlling gene expression have had a significant impact on fundamental studies of gene pathways and functions [29]. Methods for controlling gene

expression include the use of antisense oligonucleotides [66] and small interfering RNA (siRNA) [67], which can be directed against messenger RNA (mRNA) through Watson–Crick pairing. While the promise of "gene therapy" based on nucleic acids was recognized over 20 years ago, its development has faced challenges with regard to entry into cells, delivery of intact oligonucleotides, and efficacy [68]. Various transfection agents, such as cationic lipids and polymers [69], modified viruses [70], dendrimers [71], liposomes [72], and nanoparticles [26, 73], have thus been developed to shuttle nucleic acids into cells. Despite the use of these materials, the toxicity of these agents and their off-target effects limit the amount of oligonucleotides that can be delivered safely. An ideal gene regulation system—from a research standpoint—should feature high uptake efficiencies across all cell types, high intracellular stability, strong binding affinity for target nucleic acids, and very low toxicity. Recently DNA-AuNPs were used as agents to alleviate several of the challenges that are commonly associated with the application of nucleic acids in cells [25].

3.4.4.1 Antisense gene control

We hypothesized that, because of their enhanced binding properties, DNA-AuNPs could act as potent "sponges" for binding mRNA and preventing translation into proteins. As a demonstration of this concept, we developed DNA-AuNPs that target the mRNA sequences that code for enhanced green fluorescent protein (eGFP) expressed in mouse endothelial cells. An antisense sequence complementary to an internal coding region of the mRNA for eGFP was used in the design and synthesis of "antisense nanoparticles" [25]. Quantitative measurement of expression by using fluorescence assays demonstrates that these particles outperform lipid-complexed DNA used in a direct comparison. Initial experiments demonstrate a silencing of approximately 20%, but further optimization of the experimental parameters and conjugate structure has increased the gene silencing ability to greater than 75% (Fig. 3.5).

Although more than a decade of studies have been dedicated to the synthesis and characterization of DNA-AuNPs, functionalization is not limited to DNA-type oligomers. Indeed, AuNPs can be encoded

with a suite of designer oligonucleotides that confer enhanced properties, ranging from increased target specificity to catalytically enhanced biological processing [74, 75]. In a recent example, locked nucleic acid (LNA) nanoparticle conjugates have been synthesized and investigated [76, 77]. LNAs incorporate bridged sugars in their backbones, which have been shown to increase binding affinity and increase duplex stability [78]. AuNPs densely functionalized with LNA form remarkably stable duplexes with complementary nucleic acids, and can be easily handled and manipulated under biologically relevant conditions. For application in cells, the use of LNA-modified AuNPs increases the effectiveness of gene knockdown compared to analogous DNA-modified AuNPs [77].

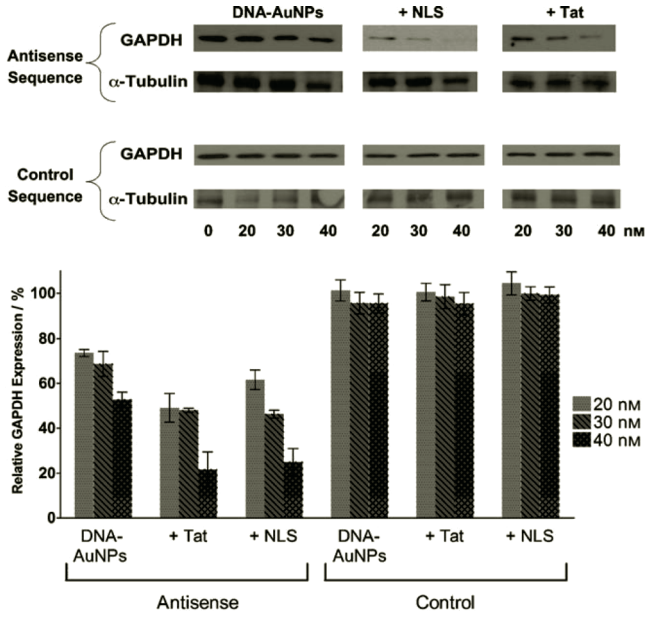

Figure 3.5 (A) Representative Western blots showing the expression of glyceradlehyde 3-phosphate dehydrogenase (GAPDH) in HeLa cells treated with various concentrations and compositions of the gold nanoconjugates. GAPDH expression is reduced in a dose- and sequence-dependent manner. α-Tubulin is shown as the loading control. (B) Relative decrease in GAPDH expression in HeLa cells. α-Tubulin was used as a loading control and for subsequent normalization of GAPDH knockdown. The error bars represent the standard deviation from at least three Western blots. From Ref. [102], Copyright (2008) National Academy of Sciences.

3.4.4.2 Intracellular detection and imaging

Oligonucleotide-based probes to visualize and detect intracellular RNA, including those used for in situ staining [79, 80], molecular beacons [81, 82], and fluorescence resonance energy transfer (FRET) probes [83, 84] are important biological tools to measure and quantify biological activity in living systems. However, cells do not readily internalize molecular probes, they require the use of transfection agents or microinjection for uptake. In addition, as a consequence of their oligonucleotide structure, such imaging agents can have limited stability to nuclease degradation, which can lead to a high background signal and decreased ability to specifically detect target structures.

Much work has thus gone into the development of structures that overcome these limitations, including chemically modified molecular beacons [85] or their corresponding peptide conjugates [86]. Recently, our research group has developed novel intracellular detection probes termed "nanoflares" that take advantage of the properties of DNA-AuNPs [87–89]. Nanoflares are oligonucleotide-functionalized gold nanoparticles that are hybridized to short, fluorophore-labeled complements designed to provide an intracellular fluorescence signal that correlates with the concentration of a specific nucleic acid or molecular target. In the absence of a target, the fluorophore is close to the nanoparticle surface, which quenches its fluorescence. Target binding releases the fluorophore, thereby generating a signal that can be detected inside a live cell. Nanoflares can distinguish between different cell types on the basis of the expression profile, and give a semiquantitative real-time readout of gene expression in a living sample (Fig. 3.6).

Several problems commonly associated with intracellular RNA detection, including the difficulty associated with cell entry, toxicity, and intracellular instability, are obviated as these nanoparticles are densely functionalized with oligonucleotides. These probes do not require microinjection or auxiliary reagents to enter cells and are more resistant than molecular nucleic acids towards enzymatic degradation, thus lowering background signal and improving detection ability.

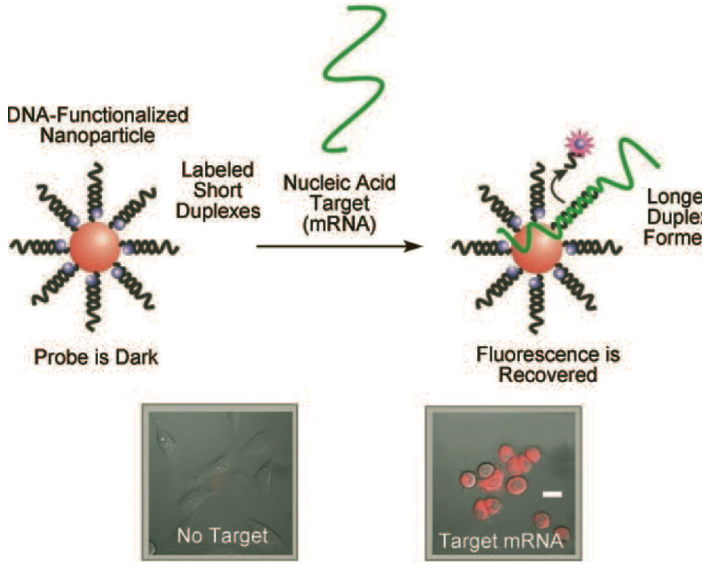

Figure 3.6 "Nanoflares" are gold nanoconjugates functionalized with oligonucleotide sequences complementary to a specific nucleic acid target (messenger RNA) hybridized to short fluorescent sequences. In the absence of a target the nanoflares are dark, because of quenching by the gold nanoparticle. In the presence of a target binding displaces the short flare through the formation of a longer (more energetically favorable) duplex. The result is a fluorescence signal inside the cell, which indicates the target has been detected. Scale bar: 20 µm. Adapted with permission from Ref. [87]. Copyright (2007) American Chemical Society.

3.4.4.3 RNA interference

Additional work is now underway on conjugates functionalized with RNA-capping ligands that are capable of acting in the highly potent RNA interference (RNAi) pathway. Recently, we determined that RNA-AuNPs can be synthesized and subsequently introduced into cells without the use of transfection agents [90]. Traditional RNAi uses molecular RNAs, which have extremely short half-lives as a result of the instability of ribonucleotides to RNase-type enzymes, thus limiting their efficacy [91, 92]. In the case of RNA-gold nanoconjugates, a dense monolayer of surface-immobilized RNA increases the protection from nonspecific degradation both in cell culture media and in the intracellular environment. These

structures are over six times more stable than molecular RNA in serum-containing media, and this enhanced stability does not rely on chemical modifications to the RNA molecular structure. We have further shown that the RNA-gold nanoconjugates have a more persistent ability to silence genes. The enhanced stability and high cellular uptake should result in these structures playing an important role in future fundamental studies as well as in the therapeutic application of RNAi.

3.4.4.4 Cellular detection

In addition to intracellular applications, Tan and coworkers have developed a colorimetric assay that uses DNA-AuNPs for the detection of cancer cells. Specifically, AuNPs were functionalized with a monolayer of aptamers selected to have a high affinity for surface receptors expressed by a cancer cell line (CCRF-CEM) [93]. The aptamer-functionalized nanoconjugates assemble on the cell surfaces, which causes their surface plasmon resonances to interact. This results in a red shift in the extinction spectra, thus providing a direct readout of target binding. The strong extinction of AuNPs means that the presence of cancer cells can be detected by the naked eye or by using a spectrometer, which eliminates the need for expensive and complicated instrumentation and makes the assay potentially useful for cancer diagnosis or disease screening.

3.5 Peptides

The targeting portions of many proteins are short stretches of oligopeptides. Peptide-based nuclear localization signals have been used to alter the intracellular localization and increase efficacy of conjugated biomolecules [94]. Such peptide signaling sequences are often composed of a stretch of positively charged amino acids such as arginine and lysine, which interact with Importin A for transport across the nuclear envelope [95]. Sequences derived from the HIV Tat protein (CYGRKKRRQRRR) and integrin binding domain (CKKKKKKGGRGDMFG) have been studied extensively for delivery of exogenous proteins and synthetic materials to the nucleus [23, 96–99].

3.5.1 Peptide Nanoconjugates

Recently, examples of peptide–gold nanoparticle conjugates have been reported. Feldheim, Franzen, and coworkers conjugated peptides to gold nanoparticles through attachment to bovine serum albumin (BSA) and subsequent electrostatic association [23, 100]. The resulting nanoconjugates enter the nucleus of HepG2 cells in culture. Interestingly, only nanoconjugates functionalized with peptides containing both a receptor-mediated endocytosis (RME) and nuclear localization signal (NLS) are able to enter the nucleus of these cells (Fig. 3.7). The same researchers recently investigated the ability of AuNPs modified with both peptides and polyethylene glycol (PEG) to enter cells. Interestingly, the particles are actively internalized even if the PEG molecule within the monolayer is large (molecular weight: 5000) [101]. These studies point to exciting opportunities in the design of multifunctional conjugates.

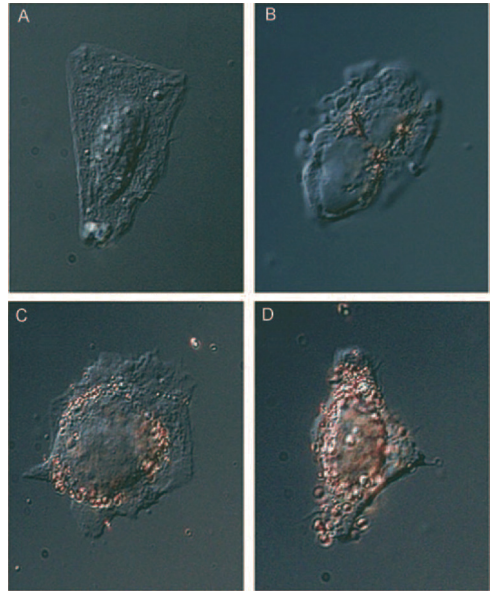

Figure 3.7 Images of nanoparticle–peptide complexes incubated with HepG2 cells for 2 h. Complexes were: (A) nuclear localization peptide, (B) receptor-mediated endocytosis peptide, (C) adenoviral fiber protein, and (D) both nuclear localization and receptor-mediated endocytosis peptides. Adapted with permission from Ref. [23]. Copyright (2003) American Chemical Society.

3.5.2 Peptide/DNA-Gold Nanoparticle Conjugates

We recently prepared gold nanoconjugates functionalized with both antisense oligonucleotides and NLS or HIV Tat peptides [102]. Our synthetic strategy uses thiolated oligonucleotides and cysteine-terminated peptides to functionalize the AuNP surfaces. As the oligopeptides and oligonucleotides are oppositely charged, the addition of salt is required to screen oppositely charged biomolecules during synthesis. When tested in cell culture, the resultant conjugates are internalized and localized in the perinuclear region. Consequently, these particles have a high gene silencing ability (>75% decrease in expression of the target protein).

3.5.3 Multifunctional and Multicomponent DNA Nanoconjugates

The versatility of nanoconjugates can be increased by incorporating multiple functional groups into each construct, or by rationally designing it to have multiple functions. Recently, our research group has demonstrated that nanoflares (see Section 3.4.4.2) can be adapted for both intracellular mRNA detection and gene knockdown [88]. These nanoflares enter cells and bind mRNA in a location suitable for gene knockdown, thereby decreasing the relative abundance of mRNA, while simultaneously releasing a fluorescent flare. Here, the nanoflare provides a read-out of gene regulation inside the cell. Such capabilities will provide valuable feedback, as the results of manipulating a cellular system can be observed in real time. In addition, one can, in principle, create all sorts of cell-sorting genetic screening asays by using the nanoflare approach.

Other therapeutic nanoconstructs have been designed to take advantage of the uptake of DNA-AuNPs by cells. For example, Pt^{IV} complexes are being explored for chemotherapy in an effort to reduce the side effects of cisplatin. Studies by the research groups of Lippard and Mirkin have shown that AuNPs can be modified with both oligonucleotides and cisplatin prodrugs. These constructs, similar to their canonical DNA counterparts, deliver the drug payload effectively to cells [127]. The prodrug consists of a Pt^{IV} complex designed to be reduced and released as active cisplatin in the acidic endosomes of cells. In addition, synthetic handles (in this case, a

carboxylic acid) can be added to the cisplatin precursor to allow for straightforward conjugation to the oligonucleotides through amide linkages. Future work in this area will examine regulating gene expression to chemosensitize the cells while delivering drugs. Such multicomponent conjugates should decrease the amount of chemotherapeutic agent needed for therapeutic efficacy while simultaneously reducing systemic toxicity.

3.6 Antibodies

Antibody-labeled gold nanoconjugates have been used in immunohistochemistry for almost 40 years [15]. Recently, however, there has been a resurgence in their use as a consequence of the development of gold nanoconjugates for live cell studies. Synthetic methods to produce antibody-gold nanoconjugates include adsorption [15], *N*-hydroxysuccinimide (NHS) ester chemistry [103], and oligonucleotide-directed immobilization [104]. Antibodies can adsorb to AuNPs through hydrophobic and ionic interactions, or through chemisorption of native thiol groups present in their chemical structure [105]. However, conjugates synthesized with this method have limited stability because the proteins are easily desorbed [106]. AuNPs functionalized with monolayers containing NHS esters can be reacted with the primary amine groups of the antibody to form more stable structures. Alternatively, DNA-AuNPs can be hybridized with antibodies that have been conjugated to complementary oligonucleotides [106].

3.6.1 Imaging

AuNPs modified with antibodies specific to cancer-associated proteins have been used to image cancerous cells. In one example, conjugates with antibodies to epithelial growth factor receptor (EGFR) were incubated with oral epithelial cancerous and noncancerous epithelial cells. Light microscopy experiments show that conjugates bind to cancerous cells with a six times greater affinity than the noncancerous controls, thus making this technique potentially useful for the detection of cancer cells [107].

3.6.2 Photothermal Therapy

Gold nanorods [108] and nanoshells [109] conjugated with antibodies are being developed as photothermal therapy agents that use antibody-coated surfaces to hone in on cancerous cells. For example, nanoshells conjugated to antibodies against human epidermal growth factor receptor 2 (HER2) were incubated with cancerous cells over-expressing HER2 receptors. These cells were then irradiated with near- IR light at a frequency that is resonant with the surface plasmon resonance of the nanoshell. Light absorption leads to heating, which causes cell death [110]. Nanoshells conjugated to control antibodies did not display this affect, because of the lack of nanoshell binding on the cell surfaces. These conjugates are also being developed as materials that combine photothermal therapy with near-IR imaging capabilities [107, 110].

3.7 Lipids

Recently, lipids have joined oligonucleotides, peptides, and antibodies as biomolecules used to modify AuNPs. Our research group and others have synthesized biomimetic high-density lipoprotein (HDL) nanostructures by adsorbing lipids and proteins to the surface of AuNPs [111]. In this synthesis, thiolated lipids or alkanethiols along with apolipoprotein A1 (APOA1), a protein component of HDL, are adsorbed onto the surface of AuNPs. Next, a second lipid is adsorbed onto the AuNP surface through hydrophobic interactions between the lipid tails and thiolated species. Simple methods for synthesizing HDL with control over the size, shape, and composition had not been demonstrated prior to these studies. It is being increasingly appreciated that size, shape, and chemistry of HDL has an impact on its in vivo physiology, and these structures may prove useful as therapeutics and imaging agents [111, 112].

3.7.1 Therapeutics

Natural HDL is critical for transporting cholesterol from macrophages in atherosclerotic plaques and from the body, and increasing the HDL levels may provide an approach to preventing or reversing

atherosclerosis. To that end, our research group synthesized HDL mimics called HDL AuNPs whose size as well as protein and lipid contents are similar to those of natural HDL (Fig. 3.8). Importantly, these nanostructures can be used to determine the strength of interactions between HDL and cholesterol. In our first example using these conjugates we showed that HDL AuNPs are capable of binding a fluorescent cholesterol analogue with a high binding affinity (K_d = 4 nm) [111]. To the best of our knowledge, this is the first measured binding constant for any form of HDL and a cholesterol derivative. This is important as it provides a key data point from which to evaluate future constructs and their ability to bind cholesterol as well as their potential as new therapeutic candidates.

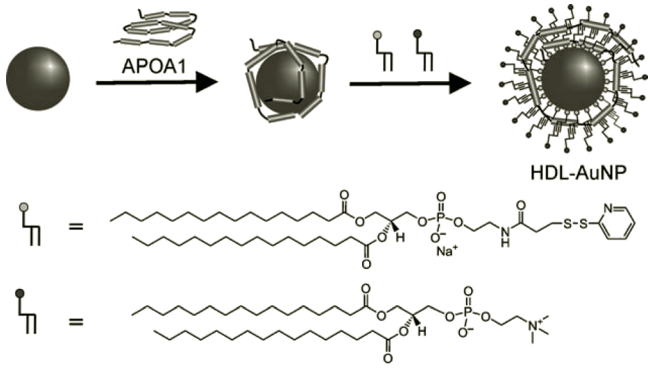

Figure 3.8 Templated synthesis of spherical HDL nanoparticles through use of thiol-terminated peptides and the protein (APOA1). Adapted with permission from Ref. [111]. Copyright (2009) American Chemical Society.

3.7.2 Imaging

In addition to cholesterol transport, HDL-AuNP mimics have been used to image macrophage cells in vivo [112]. Macrophage density is indicative of high-risk atherosclerotic plaque, thus making it an attractive imaging target. Mice fed high cholesterol diets, an established model for atherosclerosis, were injected with HDL-AuNPs. Tomography images of the mice aortas showed a build-up of HDL-AuNPs, thereby indicating that the nanoparticles could be applied to atherosclerotic imaging.

3.8 Summary and Outlook

Gold nanoconjugates are an important class of materials that have already proven useful in fundamental cell biology applications. As is the case with all nanomaterials, little is known about the interactions of gold nanoconjugates and cells at the molecular level, and the design criteria for research and therapeutic usage are still being formulated. In the next sections, we discuss emerging challenges in the field. In our opinion, these questions will be the key towards the further development of gold nanoconjugates into viable therapeutic agents.

3.8.1 Mechanism of Uptake in Cells

Several research groups have now confirmed the internalization of gold nanoconjugates in common cell-line models. The mechanism of cellular internalization is likely to differ for different classes of gold nanoconjugates because of differences in their surface chemistry, size, and charge. Indeed, substitution reactions can be used to modulate the ability of an AuNP to be internalized by a cell [24, 113]. In the case of AuNPs functionalized with positively charged amines or peptides, the mechanism likely involves the interaction of these positive moieties with the negatively charged cell surface [26]. In the case of antibody conjugates or those that possess peptidic internalization signals, interactions between specific cell-surface antigens are likely mechanistic steps [23]. Negatively charged gold nanoconjugates likely follow yet another uptake pathway. Studies by our research group and others suggest that internalization in the cell may involve the interaction of proteins with the nanoparticle surfaces [21, 65]. Identifying the proteins that allow the negatively charged gold nanoconjugates to penetrate cells stands as a formidable challenge.

3.8.2 Targeting

The use of gold nanoconjugates provides a highly effective method for introducing substances into cells. We have described how the unique ensemble properties of these materials allow for multivalent drug and antisense agents. These agents can be used to control

cellular function, regulate gene expression, and detect intracellular analytes with greater efficiency than molecular systems, which is in part due to composite properties and proven cellular uptake ability across diverse cell types. An important challenge for the continued development of these materials as therapeutics is to target specific cells and eventually tissues and organs. Strategies for targeted delivery may include the use of biomolecules such as antibodies [108], aptamers [114], peptides [23], or small molecule ligands [115].

Targeting strategies need to be integrated with functionality to create multifunctional particles for delivering oligonucleotides or other therapeutic cargos to target cells. For example, antibodies targeted against surface receptors for appropriate cellular targets should be able to effect cell-specific uptake and limit nonspecific uptake, but they must also maintain the other desired activity and properties of nanoconjugates. In the case of polyvalent DNA-AuNPs, moieties such as antibodies must be attached in a manner that does not limit the degree of DNA functionalization or the properties that result from the density of DNA. While this is not trivial, it is noteworthy that cofunctionalized AuNPs have already been synthesized and preliminarily studied, including structures which successfully incorporate peptides without compromising complementary binding to nucleic acids [102]. These results are promising steps towards the next generation of targeted polyvalent nanoconjugate therapeutics.

3.8.3 Toxicity

The toxicity of several types and sizes of gold nanoconjugates has been investigated by a number of independent research groups. Although results have varied to date, several important conclusions can be drawn from these studies. Perhaps the most salient is that the toxicity of gold nanoconjugates is dependent on the chemical composition of the surface ligands. In fact, it is often the surface group itself that leads to toxicity. For example, although gold nanoconjugates functionalized with cetyltrimethylammonium bromide (CTAB) were initially thought to be toxic, it was subsequently determined that the particles do not cause cytotoxicity if they are washed to remove excess ligand [18]. Additional work in this area,

has shown how the toxicity of a ligand such as CTAB is reduced when complexed with an AuNP [116], presumably because of an alteration of the cellular localization of the toxic agent. Rotello and coworkers have also shown how the chemical functionality and charge of nanoconjugate surface ligands influence toxicity. These researchers found that while amine-functionalized particles were only mildly toxic, particles functionalized with carboxylic acids were nontoxic under all the conditions examined [117].

Several recent studies have focused on the toxicity of citrate-capped nanoconjugates. One study investigating human dermal fibroblasts determined that the rate of cell proliferation, spreading, and adhesion is slowed by the presence of citrate-capped nanoconjugates [118]. The authors presented evidence that actin stress is the cause of these effects. A second, independent study also reports decreased cell growth in the presence of citrate-capped nanoconjugates, and in this case, the authors present evidence that this is the result of oxidative damage [119]. Similar results have also been reported when similar particles were used in myeloma cells [120]. Although acute and gross toxicity was not observed in these cases, the adverse effects of citrate-capped nanoconjugates merit further attention.

Intriguing recent investigations demonstrate that the size of the conjugate also determines its toxicity. In a recent study, Simon, Jahnen-Dechent, and coworkers examined a panel of phosphine-functionalized AuNPs with diameters ranging from 0.8 to 15 nm. These researchers found that 1.4 nm diameter particles were toxic, whereas 15 nm diameter particles were nontoxic, even at up to 100-fold higher concentrations [121]. In the case of these 1.4 nm diameter particles, evidence is presented that toxicity results from necrosis; however, neither 1.2 nor 1.8 nm diameter particles display this effect. Chan and coworkers have recently investigated the cell response to herceptin-coated gold nanoparticles within the 2–100 nm size range and found that 40 and 50 nm particles have the greatest effect on cell signaling functions [122]. Clearly, these are important findings that need to be explored further. The challenge will be preparing a range of particle sizes by using a common synthetic strategy and ensuring exact chemical surface functionality for accurate comparison.

Gold nanorods and nanoshells have recently been tested in mouse models. Halas, West, and coworkers have evaluated the

photothermal efficacy of PEG-coated nanoshells injected into tumors in a mouse model. These researchers found that tumors could be ablated by treatment with light, and the animals remained healthy after more than 90 days, thus pointing to a low toxicity of nanoconjugates in vivo [123]. A research group investigating the use of CTAB-functionalized gold nanorods as imaging agents found that the particles were rapidly cleared from the blood after injection into the tail vein [124]. Another study on very similar nanorod particles found that they are accumulated in the liver after 72 h [125]. Interestingly, however, when the surface groups were changed to PEG, very few particles remained in the liver after 72 h, and most were cleared. These initial animal studies are indeed promising, and should motivate future studies that investigate the biodistribution of gold nanoconjugates as a function of size, shape, and chemical properties of the ligands.

To date, no cytotoxicity of the DNA-AuNPs has been observed [25]. It is again important to note that these nanoconjugates have unique size, charge, and surface functionality, with properties derived from the combination of the DNA and the AuNP. Extensive toxicology screening of these unique materials will be a necessity, and determining what component or components of the structure contribute to a biological response will be an exciting endeavor. Preliminary work in our research group on the innate immune response, (as characterized by interferon production, one of the first pathways activated in an innate immune response) has shown little interferon-β production caused by the DNA-AuNPs compared to analogous molecular DNA [126]. Further work is required to examine any changes in the gene expression profile that may result from the introduction of these structures. In addition to in vitro assays, preliminary work to examine biodistribution and toxicity in vivo is now underway. While polyvalent DNA-AuNPs have already shown utility in cell culture assays, such animal studies will be required to assess the feasibility of these nanomaterials becoming possible therapeutic agents.

3.8.4 Conclusion

Although the properties of colloidal gold have been investigated for over a century, their application as intracellular agents in living cells

emerged only prominently a few years ago. These investigations have demonstrated that multivalent and/or composite nanomaterials can provide significant advantages over molecular systems in terms of uptake and efficacy in cellular models. More fundamentally, these studies have reinforced the underlying concept in nanotechnology that composition, surface derivatization, charge, size, and shape are all critical to materials properties, and that this translates into a unique ability to interact with a biological system such as a cell. The highlighted classes of gold nanoconjugates represent a small but important sample of possible conjugate materials. The study of these classes highlights one very important conclusion: Namely, unique nanomaterials must be investigated and evaluated individually. This is exemplified in the studies of nanoparticle toxicity, where surface functionalization has repeatedly been shown to be a key parameter that influences toxicity. If one were to conclude from earlier work using CTAB-functionalized nanoconjugates that all gold nanoconjugates were toxic, then important opportunities would have been missed, for example the use of DNA-AuNPs for genetic regulation [25] or amine-functionalized conjugates for drug delivery [36], where toxicity has been shown to be lower than polymer delivery systems [25]. As such, we encourage investigators to study and evaluate nanoconjugates on a case-by-case basis and avoid generalization wherever possible.

The preparation and use of functionalized gold nanoconjugates continues to be an extremely active and important area of research. This field continues to tantalize the chemical research community with major discoveries as well as new scientific challenges, while also involving cross-disciplinary investigators including materials scientists, biologists, engineers, and clinicians. The work carried out thus far provides only a glimpse of the wide range of potential applications for gold nanoparticles in biology and medicine.

Acknowledgments

C.A.M. acknowledges a Cancer Center for Nanotechnology Excellence (CCNE) award, the NSF-NSEC, and a U.S. Army Medical Research and Material Command Grant W81XWH-08-1-0766 for support of this work. C.A.M. is also grateful for a NIH Director's Pioneer Award. D.S.S. was supported by the LUNGevity Foundation—American Cancer

Society Postdoctoral Fellowship in Lung Cancer. P.C.P. was supported by a Ryan Fellowship.

References

1. Hayat, M. A. (1989). *Colloidal Gold: Principles, Methods, and Applications* (Academic Press, San Diego).
2. Edwards, P. P. and Thomas, J. M. (2007). *Angew. Chem*. **119**, 5576; *Angew. Chem*. *Int. Ed*. **46**, 5480.
3. Daniel, M.-C. and Astruc, D. (2004). *Chem. Rev*. **104**, 293.
4. Mirkin, C. A., Letsinger, R. L., Mucic, R. C. and Storhoff, J. J. (1996). *Nature* **382**, 607.
5. Park, S. Y., Lytton-Jean, A. K. R., Lee, B., Weigand, S., Schatz, G. C. and Mirkin, C. A. (1996). *Nature* **451**, 553.
6. Alivisatos, A. P., Johnsson, K. P., Peng, X. G., Wilson, T. E., Loweth, C. J., Bruchez, M. P. and Schultz, P. G. (1996). *Nature* **382**, 609.
7. Park, S. J., Taton, T. A. and Mirkin, C. A. (2002). *Science* **295**, 1503.
8. Wang, J., Liu, G. D. and Merkoci, A. (2003). *J. Am. Chem. Soc*. **125**, 3214.
9. Xiao, Y., Patolsky, F., Katz, E., Hainfeld, J. F. and Willner, I. (2003). *Science* **299**, 1877.
10. He, L., Musick, M. D., Nicewarner, S. R., Salinas, F. G., Benkovic, S. J., Natan, M. J. and Keating, C. D. (2000). *J. Am. Chem. Soc*. **122**, 9071.
11. Liu, J. and Lu, Y. (2003). *J. Am. Chem. Soc*. **125**, 6642.
12. Rosi, N. L. and Mirkin, C. A. (2005). *Chem. Rev*. **105**, 1547.
13. Katz, E. and Willner, I. (2004). *Angew. Chem*. **116**, 6166; *Angew. Chem*. *Int. Ed*. **43**, 6042.
14. Penn, S. G., He, L. and Natan, M. J. (2003). *Curr. Opin. Chem. Biol*. **7**, 609.
15. Faulk, W. P. and Taylor, G. M. (1971). *Immunochemistry* **8**, 1081.
16. Frens, G. (1973). *Nat. Phys. Sci*. **241**, 20.
17. Enustun, B. V. and Turkevich, J. (1963). *J. Am. Chem. Soc*. **85**, 3317.
18. Connor, E. E., Mwamuka, J., Gole, A., Murphy, C. J. and Wyatt, M. D. (2005). *Small* **1**, 325.
19. Chithrani, B. D., Ghazani, A. A. and Chan, W. C. W. (2006). *Nano Lett*. **6**, 662.
20. Yang, P. H., Sun, X. S., Chiu, J. F., Sun, H. Z. and He, Q. Y. (2005). *Bioconjugate Chem*. **16**, 494.

21. Chithrani, B. D. and Chan, W. C. W. (2007). *Nano Lett.* **7**, 1542.
22. Cho, E. C., Xie, J. W., Wurm, P. A. and Xia, Y. N. (2009). *Nano Lett.* **9**, 1080.
23. Tkachenko, A. G., Xie, H., Coleman, D., Glomm, W., Ryan, J., Anderson, M. F., Franzen, S. and Feldheim, D. L. (2003). *J. Am. Chem. Soc.* **125**, 4700.
24. Nativo, P., Prior, I. A. and Brust, M. (2008). *ACS Nano* **2**, 1639.
25. Rosi, N. L., Giljohann, D. A., Thaxton, C. S., Lytton-Jean, A. K. R., Han, M. S. and Mirkin, C. A. (2006). *Science* **312**, 1027.
26. Sandhu, K. K., McIntosh, C. M., Simard, J. M., Smith, S. W. and Rotello, V. M. (2002). *Bioconjugate Chem.* **13**, 3.
27. Brust, M., Walker, M., Bethell, D., Schiffrin, D. J. and Whyman, R. (1994). *J. Chem. Soc. Chem. Commun*. 801.
28. Hostetler, M. J., Templeton, A. C. and Murray, R. W. (1999). *Langmuir* **15**, 3782.
29. Patil, S. D., Rhodes, D. G. and Burgess, D. J. (2005). *AAPS J.* **7**, E61.
30. Thomas, M. and Klibanov, A. M. (2003). *Proc. Natl. Acad. Sci. U.S.A.* **100**, 9138.
31. Ghosh, P. S., Kim, C. K., Han, G., Forbes, N. S. and Rotello, V. M. (2008). *ACS Nano* **2**, 2213.
32. Torchilin, V. P. (2006). *Adv. Drug Delivery Rev*. **58**, 1532.
33. Gibson, J. D., Khanal, B. P. and Zubarev, E. R. (2007). *J. Am. Chem. Soc*. **129**, 11653.
34. Bowman, M. C., Ballard, T. E., Ackerson, C. J., Feldheim, D. L., Margolis, D. M. and Melander, C. (2008). *J. Am. Chem. Soc*. **130**, 6896.
35. Han, G., You, C. C., Kim, B. J., Turingan, R. S., Forbes, N. S., Martin, C. T. and Rotello, V. M. (2006). *Angew. Chem*. **118**, 3237; *Angew. Chem. Int. Ed*. **45**, 3165.
36. Kim, C. K., Ghosh, P., Pagliuca, C., Zhu, Z. J., Menichetti, S. and Rotello, V. M. (2009). *J. Am. Chem. Soc*. **131**, 1360.
37. Hong, R., Han, G., Fernandez, J. M., Kim, B. J., Forbes, N. S. and Rotello, V. M. (2006). *J. Am. Chem. Soc*. **128**, 1078.
38. Chompoosor, A., Han, G. and Rotello, V. M. (2008). *Bioconjugate Chem*. **19**, 1342.
39. Storhoff, J. J., Lazarides, A. A., Mucic, R. C., Mirkin, C. A., Letsinger, R. L. and Schatz, G. C. (2000). *J. Am. Chem. Soc*. **122**, 4640.
40. Lytton-Jean, A. K. and Mirkin, C. A. (2005). *J. Am. Chem. Soc*. **127**, 12754.
41. Jin, R. C., Wu, G. S., Li, Z., Mirkin, C. A. and Schatz, G. C. (2003). *J. Am. Chem. Soc*. **125**, 1643.

42. Hurst, S. J., Hill, H. D. and Mirkin, C. A. (2008). *J. Am. Chem. Soc*. **130**, 12192.
43. Demers, L. M., Mirkin, C. A., Mucic, R. C., Reynolds III, R. A., Letsinger, R. L., Elghanian, R. and Viswanadham, G. (2000). *Anal. Chem*. **72**, 5535.
44. Nykypanchuk, D., Maye, M. M., van der Lelie, D. and Gang, O. (2008). *Nature* **451**, 549.
45. Park, S. Y., Lytton-Jean, A. K., Lee, B., Weigand, S., Schatz, G. C. and Mirkin, C. A. (2008). *Nature* **451**, 553.
46. Hill, H. D., Macfarlane, R. J., Senesi, A. J., Lee, B., Park, S. Y. and Mirkin, C. A. (2008). *Nano Lett*. **8**, 2341.
47. Nam, J.-M., Thaxton, C. S. and Mirkin, C. A. (2003). *Science* **301**, 1884.
48. Stoeva, S. I., Lee, J. S., Smith, J. E., Rosen, S. T. and Mirkin, C. A. (2006). *J. Am. Chem. Soc*. **128**, 8378.
49. Elghanian, R., Storhoff, J. J., Mucic, R. C., Letsinger, R. L. and Mirkin, C. A. (1997). *Science* **277**, 1078.
50. Storhoff, J. J., Elghanian, R., Mucic, R. C., Mirkin, C. A. and Letsinger, R. L. (1998). *J. Am. Chem. Soc*. **120**, 1959.
51. Taton, T. A., Mirkin, C. A. and Letsinger, R. L. (2000). *Science* **289**, 1757.
52. Cao, Y. W. C., Jin, R. C. and Mirkin, C. A. (2002). *Science* **297**, 1536.
53. Hurst, S. J., Lytton-Jean, A. K. and Mirkin, C. A. (2006). *Anal. Chem*. **78**, 8313.
54. Lee, J.-S., Seferos, D. S., Giljohann, D. A. and Mirkin, C. A. (2008). *J. Am. Chem. Soc*. **130**, 5430.
55. Hurst, S. J., Lytton-Jean, A. K. R. and Mirkin, C. A. (2006). *Anal. Chem*. **78**, 8313.
56. Bao, Y. P., Huber, M., Wei, T. F., Marla, S. S., Storhoff, J. J. and Muller, U. R. (2005). *Nucleic Acids Res*. **33**, 7.
57. Long, H., Kudlay, A. and Schatz, G. C. (2006). *J. Phys. Chem. B* **110**, 2918.
58. Lytton-Jean, A. K. R. and Mirkin, C. A. (2005). *J. Am. Chem. Soc*. **127**, 12754.
59. Cazenave, C., Chevrier, M., Thuong, N. T. and Helene, C. (1987). *Nucleic Acids Res*. **15**, 10507.
60. Woolf, T. M., Jennings, C. G. B., Rebagliati, M. and Melton, D. A. (1990). *Nucleic Acids Res*. **18**, 1763.
61. Pan, C. Q. and Lazarus, R. A. (1997). *Biochemistry* **36**, 6624.
62. Shack, J. (1959). *J. Biol. Chem*. **234**, 3003.
63. Seferos, D. S., Prigodich, A. E., Giljohann, D. A., Patel, P. C. and Mirkin, C. A. (2009). *Nano Lett*. **9**, 308.

64. Niidome, T. and Huang, L. (2002). *Gene Ther*. **9**, 1647.
65. Giljohann, D. A., Seferos, D. S., Patel, P. C., Millstone, J. E., Rosi, N. L. and Mirkin, C. A. (2007). *Nano Lett*. **7**, 3818.
66. Uhlmann, E. and Peyman, A. (1990). *Chem. Rev*. **90**, 543.
67. Dorsett, Y. and Tuschl, T. (2004). *Nat. Rev. Drug Discovery* **3**, 318.
68. Lebedeva, I. and Stein, C. A. (2001). *Annu. Rev. Pharmacol. Toxicol*. **41**, 403.
69. Hwang, S. J. and Davis, M. E. (2001). *Curr. Opin. Mol. Ther*. **3**, 183.
70. Kamiya, H., Tsuchiya, H., Yamazaki, J. and Harashima, H. (2001). *Adv. Drug Delivery Rev*. **52**, 153.
71. Braun, C. S., Vetro, J. A., Tomalia, D. A., Koe, G. S., Koe, J. G. and Middaugh, C. R. (2005). *J. Pharm. Sci*. **94**, 423.
72. Hughes, M. D., Hussain, M., Nawaz, Q., Sayyed, P. and Akhtar, S. (2001). *Drug Discovery Today* **6**, 303.
73. Bharali, D. J., Klejbor, I., Stachowiak, E. K., Dutta, P., Roy, I., Kaur, N., Bergey, E. J., Prasad, P. N. and Stachowiak, M. K. (2005). *Proc. Natl. Acad. Sci. U.S.A.* **102**, 11539.
74. Kubo, T., Zhelev, Z., Ohba, H. and Bakalova, R. (2008). *Biochem. Biophys. Res. Commun*. **365**, 54.
75. Singh, S. K., Nielsen, P., Koshkin, A. A. and Wengel, J. (1998). *Chem. Commun*. 455.
76. McKenzie, F., Faulds, K. and Graham, D. (2007). *Small* **3**, 1866.
77. Seferos, D. S., Giljohann, D. A., Rosi, N. L. and Mirkin, C. A. (2007). *ChemBioChem* **8**, 1230.
78. Koshkin, A. A., Nielsen, P., Meldgaard, M., Rajwanshi, V. K., Singh, S. K. and Wengel, J. (1998). *J. Am. Chem. Soc*. **120**, 13252.
79. Femino, A. M., Fay, F. S., Fogarty, K. and Singer, R. H. (1998). *Science* **280**, 585.
80. Kloosterman, W. P., Wienholds, E., de Bruijn, E., Kauppinen, S. and Plasterk, R. H. (2006). *Nat. Methods* **3**, 27.
81. Tyagi, S. and Kramer, F. R. (1996). *Nat. Biotechnol*. **14**, 303.
82. Sokol, D. L., Zhang, X., Lu, P. and Gewirtz, A. M. (1998). *Proc. Natl. Acad. Sci. U.S.A.* **95**, 11538.
83. Sando, S. and Kool, E. T. (2002). *J. Am. Chem. Soc*. **124**, 9686.
84. Santangelo, P. J., Nix, B., Tsourkas, A. and Bao, G. (2004). *Nucleic Acids Res*. **32**, e57.
85. Wang, L., Yang, C. Y. J., Medley, C. D., Benner, S. A. and Tan, W. H. (2005). *J. Am. Chem. Soc*. **127**, 15664.

86. Nitin, N., Santangelo, P. J., Kim, G., Nie, S. and Bao, G. (2004). *Nucleic Acids Res*. **32**, e58.

87. Seferos, D. S., Giljohann, D. A., Hill, H. D., Prigodich, A. E. and Mirkin, C. A. (2007). *J. Am. Chem. Soc*. **129**, 15477.

88. Prigodich, A. E., Seferos, D. S., Massich, M. D., Giljohann, D. A., Lane, B. C. and Mirkin, C. A. (2009). *ACS Nano* **3**, 2147.

89. Zheng, D., Seferos, D. S., Giljohann, D. A., Patel, P. C. and Mirkin, C. A. (2009). *Nano Lett*. **9**, 3258.

90. Giljohann, D. A., Seferos, D. S., Prigodich, A. E., Patel, P. C. and Mirkin, C. A. (2009). *J. Am. Chem. Soc*. **131**, 2072.

91. Chiu, Y.-L. and Rana, T. M. (2003). *RNA* **9**, 1034.

92. Soutschek, J., Akinc, A., Bramlage, B., Charisse, K., Constien, R., Donoghue, M., Elbashir, S., Geick, A., Hadwiger, P., Harborth, J., John, M., Kesavan, V., Lavine, G., Pandey, R. K., Racie, T., Rajeev, K. G., Rohl, I., Toudjarska, I., Wang, G., Wuschko, S., Bumcrot, D., Koteliansky, V., Limmer, S., Manoharan, M. and Vornlocher, H.-P. (2004). *Nature* **432**, 173.

93. Medley, C. D., Smith, J. E., Tang, Z., Wu, Y., Bamrungsap, S. and Tan, W. H. (2008). *Anal. Chem*. **80**, 1067.

94. Vives, E., Schmidt, J. and Pelegrin, A. (2008). *Biochim. Biophys. Acta Rev. Cancer* **1786**, 126.

95. Goldfarb, D. S., Gariepy, J., Schoolnik, G. and Kornberg, R. D. (1986). *Nature* **322**, 641.

96. Biju, V., Muraleedharan, D., Nakayama, K., Shinohara, Y., Itoh, T., Baba, Y. and Ishikawa, M. (2007). *Langmuir* **23**, 10254.

97. Derfus, A. M., Chen, A. A., Min, D. H., Ruoslahti, E. and Bhatia, S. N. (2007). *Bioconjugate Chem*. **18**, 1391.

98. Lanford, R. E., Kanda, P. and Kennedy, R. C. (1986). *Cell* **46**, 575.

99. Oyelere, A. K., Chen, P. C., Huang, X., El-Sayed, I. H. and El-Sayed, M. A. (2007). *Bioconjugate Chem*. **18**, 1490.

100. Tkachenko, A. G., Xie, H., Liu, Y. L., Coleman, D., Ryan, J., Glomm, W. R., Shipton, M. K., Franzen, S. and Feldheim, D. L. (2004). *Bioconjugate Chem*. **15**, 482.

101. Liu, Y. L., Shipton, M. K., Ryan, J., Kaufman, E. D., Franzen, S. and Feldheim, D. L. (2007). *Anal. Chem*. **79**, 2221.

102. Patel, P. C., Giljohann, D. A., Seferos, D. S. and Mirkin, C. A. (2008). *Proc. Natl. Acad. Sci. U.S.A.* **105**, 17222.

103. Qian, X., Peng, X. H., Ansari, D. O., Yin-Goen, Q., Chen, G. Z., Shin, D. M., Yang, L., Young, A. N., Wang, M. D. and Nie, S. (2008). *Nat. Biotechnol*. **26**, 83.

104. Niemeyer, C. M. and Ceyhan, B. (2001). *Angew. Chem*. **113**, 3798; *Angew. Chem*. *Int. Ed*. **40**, 3685.

105. Hermanson, G. T. (1996). *Bioconjugate Techniques* (Academic Press, San Diego, CA).

106. Nitin, N., Javier, D. J. and Richards-Kortum, R. (2007). *Bioconjugate Chem*. **18**, 2090.

107. El-Sayed, I. H., Huang, X. H. and El-Sayed, M. A. (2005). *Nano Lett*. **5**, 829.

108. El-Sayed, I. H., Huang, X. H. and El-Sayed, M. A. (2006). *Cancer Lett*. **239**, 129.

109. Hirsch, L. R., Stafford, R. J., Bankson, J. A., Sershen, S. R., Rivera, B., Price, R. E., Hazle, J. D., Halas, N. J. and West, J. L. (2003). *Proc. Natl. Acad. Sci. U.S.A.* **100**, 13549.

110. Loo, C., Lowery, A., Halas, N., West, J. and Drezek, R. (2005). *Nano Lett*. **5**, 709.

111. Thaxton, C. S., Daniel, W. L., Giljohann, D. A., Thomas, A. D. and Mirkin, C. A. (2009). *J. Am. Chem. Soc*. **131**, 1384.

112. Cormode, D. P., Skajaa, T., van Schooneveld, M. M., Koole, R., Jarzyna, P., Lobatto, M. E., Calcagno, C., Barazza, A., Gordon, R. E., Zanzonico, P., Fisher, E. A., Fayad, Z. A. and Mulder, W. J. (2008). *Nano Lett*. **8**, 3715.

113. Huff, T. B., Hansen, M. N., Zhao, Y., Cheng, J. X. and Wei, A. (2007). *Langmuir* **23**, 1596.

114. Javier, D. J., Nitin, N., Levy, M., Ellington, A. and Richards-Kortum, R. (2008). *Bioconjugate Chem*. **19**, 1309.

115. Dixit, V., Van den Bossche, J., Sherman, D. M., Thompson, D. H. and Andres, R. P. (2006). *Bioconjugate Chem*. **17**, 603.

116. Hauck, T. S., Ghazani, A. A. and Chan, W. C. W. (2008). *Small* **4**, 153.

117. Goodman, C. M., McCusker, C. D., Yilmaz, T. and Rotello, V. M. (2004). *Bioconjugate Chem*. **15**, 897.

118. Pernodet, N., Fang, X. H., Sun, Y., Bakhtina, A., Ramakrishnan, A., Sokolov, J., Ulman, A. and Rafailovich, M. (2006). *Small* **2**, 766.

119. Li, J. J., Zou, L., Hartono, D., Ong, C. N., Bay, B. H. and Yung, L. Y. L. (2008). *Adv. Mater*. **20**, 138.

120. Bhattacharya, R., Patra, C. R., Verma, R., Kumar, S., Greipp, P. R. and Mukherjee, P. (2007). *Adv. Mater*. **19**, 711.

121. Pan, Y., Neuss, S., Leifert, A., Fischler, M., Wen, F., Simon, U., Schmid, G., Brandau, W. and Jahnen-Dechent, W. (2007). *Small* **3**, 1941.

122. Jiang, W., Kim, B. Y. S., Rutka, J. T. and Chan, W. C. W. (2008). *Nat. Nanotechnol*. **3**, 145.

123. Neal, D. P. O., Hirsch, L. R., Halas, N. J., Payne, J. D. and West, J. L. (2004). *Cancer Lett*. **209**, 171.

124. Wang, H. F., Huff, T. B., Zweifel, D. A., He, W., Low, P. S., Wei, A. and Cheng, J. X. (2005). *Proc. Natl. Acad. Sci. U.S.A.* **102**, 15752.

125. Niidome, T., Yamagata, M., Okamoto, Y., Akiyama, Y., Takahashi, H., Kawano, T., Katayama, Y. and Niidome, Y. (2006). *J. Controlled Release* **114**, 343.

126. Massich, M. D., Giljohann, D. A., Seferos, D. S., Ludlow, L. E., Horvath, C. M. and Mirkin, C. A. (2009). *Mol. Pharm*. **6**, 1934.

127. Dhar, S., Daniel, W. L., Giljohann, D. A., Mirkin, C. A. and Lippard, S. J. (2009). *J. Am. Chem. Soc*. **131**, 14652.

Chapter 4

Spherical Nucleic Acids*

Joshua I. Cutler, Evelyn Auyeung, and Chad A. Mirkin
Department of Chemistry, Northwestern University, 2145 Sheridan Road, Evanston, IL 60208, USA
International Institute for Nanotechnology, Northwestern University, 2145 Sheridan Road, Evanston, IL 60208, USA
chadnano@northwestern.edu

A historical perspective of the development of spherical nucleic acid (SNA) conjugates and other three-dimensional nucleic acid nanostructures is provided. This Perspective details the synthetic methods for preparing them, followed by a discussion of their unique properties and theoretical and experimental models for understanding them. Important examples of technological advances made possible by their fundamental properties spanning the fields of chemistry, molecular diagnostics, gene regulation, medicine, and materials science are also presented.

*Reprinted with permission from Cutler, J. I., Auyeung, E. and Mirkin, C. A. (2012). Spherical nucleic acids, *J. Am. Chem. Soc.* **134**(3), 1376–1391. Copyright (2012) American Chemical Society.

Spherical Nucleic Acids, Volume 1
Edited by Chad A. Mirkin

ISBN 978-981-4800-35-8 (Hardcover), 978-0-429-20015-1 (eBook)
www.jennystanford.com

4.1 Introduction

In 1996, we introduced a synthetic method for preparing polyvalent nucleic acid–nanoparticle conjugates, spherical nanostructures with densely functionalized and highly oriented nucleic acids covalently attached to their surfaces (Fig. 4.1) [1]. These structures represent the first well-characterized forms of spherical nucleic acid (SNA) conjugates and were originally made with gold cores and DNA shells [1]. Moreover, they exhibit properties that are distinct from those of both the nanoparticles (NPs) and DNA from which they derive. Since the initial work, these materials have been used in many important, and in certain cases, commercially viable applications; indeed, they have catalyzed worldwide interest in using well-characterized nanostructures as novel labels for in vitro biodetection schemes [2–7] and intracellular assays [8–11], and as potent cell transfection [12–15], therapeutic [16], and gene regulation materials [15, 17–19]. Subsequent studies have shown that the inorganic NPs serve two purposes: (1) they provide novel physical and chemical properties (e.g., plasmonic, catalytic, scattering, quenching) that are especially important in the contexts of materials design and nanoparticle probe design, and (2) they act as a scaffold for assembling and orienting the oligonucleotides into a dense arrangement that gives rise to many of their functional properties. Significantly, recent studies have shown that one can use the gold core as a scaffold, subsequently crosslink the DNA at the base of the particle, and dissolve the gold to create a new coreless form of SNAs, exhibiting many of the hallmark properties of the original gold nanoparticle (AuNP) conjugates, including the ability to cooperatively hybridize complementary nucleic acids and efficiently transfect cell membranes without the need for co-carriers [20]. This work underscored one of the fundamental features of SNAs, namely, that many of the properties of these nanostructures stem from a dense layer of oriented nucleic acids and are core-independent.

This perspective aims to provide a historical overview of the development of such SNA conjugates by first exploring synthetic methods for preparing them, followed by a discussion of their unique properties and a basis for understanding them. We will then highlight important examples of technological advances made possible by their fundamental properties spanning the fields of chemistry, biology, medicine, and materials science. As there is still

much to be learned from the use of these materials, an important goal of this Perspective is to inspire future investigations of spherical and other three-dimensional (3D) nucleic acid-based structures.

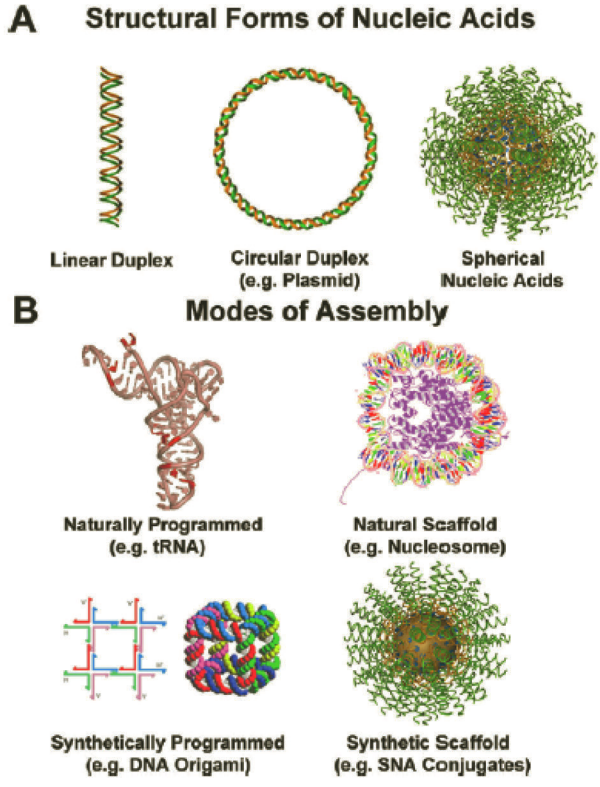

Figure 4.1 (A) Existing structural forms of nucleic acids include linear duplexes, circular plasmid DNA, and 3D SNA. (B) Nucleic acid structures with well-defined shapes are made naturally through sequence selection and base pairing interactions or through synthetic means (left). Alternatively, templates such as proteins or synthetic nanostructures can be used to make highly functional architectures based upon the size and shape of the template (right). Figures are not drawn to scale. Transfer RNA image adapted by permission from Springer Nature Customer Service Centre GmbH: Springer Nature, *Nature*, Ref. [33]. Copyright (2011). Nucleosome core adapted by permission from Springer Nature Customer Service Centre GmbH: Springer Nature, *Nature Structural & Molecular Biology*, Ref. [32]. Copyright (1997). DNA origami image adapted by permission from Springer Nature Customer Service Centre GmbH: Springer Nature, *Nature*, Ref. [36]. Copyright (2003).

4.2 The Emergence of DNA as a Surface Ligand for Nanoparticles

The ligands attached to a NP's surface (the ligand shell) are responsible for governing much of a NP's overall chemistry and its stability in complex media. These molecules are typically designed with a headgroup moiety suitable for attachment to the NP of interest and a tail group that extends into the solution, helps maintain colloidal stability, and controls particle reactivity. In the 1990s, the synthesis of chemically well-defined nanocrystals with well-characterized ligand shells [21, 22] became a major focus, with one of the intended uses of such structures being to prepare colloidal assemblies or superstructures [23]. Much of the work focused on using simple hydrocarbon surfactant ligands such as negatively charged carboxylates [24] or positively charged ammonium functional groups [25] that could influence the charge and solubility of the particles. However, if the intent is to use such particle building blocks to make superstructures and colloidal crystals, control over the architectural parameters of the resulting assemblies and materials is quite limited with conventional small-molecule adsorbates. Therefore, in 1996, we reported a novel strategy for preparing water-soluble conjugates from aqueous citrate-stabilized AuNPs and alkylthiol-functionalized DNA [1]. This approach, at the time, represented a departure from the concurrent and extensive efforts to characterize well-formed alkanethiol monolayers on gold surfaces [26, 27], but it was a natural extension of our work that focused on making redoxactive monolayers from ferrocenyl- and alkanethiol-capped oligonucleotides on bulk gold electrode surfaces [28].

The structures synthesized in the original work consisted of 13 nm gold cores densely functionalized with a surface shell of DNA coordinated via sulfur groups to the gold; they were the first well-characterized SNA–NP conjugates. Concurrently, Alivisatos and coworkers were developing techniques to prepare monovalent forms of smaller particles (2 nm) with the idea of using DNA templates to arrange individual particles in a controllable manner on such templates [29]. These structures have led to interesting advances in their own right, including the development of the concept of a

plasmon ruler [30, 31], but they do not possess the structure and properties of the SNA conjugate analogues, which are the focus of this perspective. Furthermore, it is important to differentiate the structure of SNA from other forms of nucleic acids (Fig. 4.1) [32–35]. The primary difference between SNAs and linear nucleic acids is that SNAs are dense, oriented spherical arrays of short oligonucleotides. While most forms of nucleic acids rely on the hybridized duplex as the fundamental structural unit that determines their overall shape, SNAs can be prepared from both single- and double-stranded nucleic acids, and their orientation is determined by the shape of the inorganic core. SNA nanostructures are also distinct from the synthetic structures made in the field, often referred to as "DNA nanotechnology and origami," wherein the recognition properties of DNA are used to assemble duplexes into rationally designed shapes [36–38]. The physical SNA structures described herein are synthesized independent of nucleic acid sequence and hybridization; they are formed via chemical bonds, not recognition processes.

4.3 Structural Considerations for SNA and SNA–NP Conjugates

SNA nanostructures are chemically quite sophisticated and can have markedly different properties depending upon the components and their placement within such structures (Fig. 4.2). For example, they have higher binding constants for their complements than free strands of the same sequence [39], exhibit cooperative binding and subsequent sharp melting transitions [1, 40], are resistant to nuclease degradation [41], and are capable of transfecting cell lines without the need for ancillary physical or chemical transfection methods [15]. Although these materials often contain an inorganic core, the emergent properties unique to SNAs stem in large part from the density and orientation of the oligonucleotides at the outer region of the nanostructure (Section 4.5). However, structures with cores (e.g., Au [1], Ag [42], Fe_3O_4 [43], CdSe [44], nanoshells [23], core–shell structures [45, 46], and polymers [47, 48]) can confer additional properties to the conjugate, which derive from the physical and chemical characteristics of the nanostructured core materials [49]. Finally, designer nucleic acids [50] can provide

additional functionality, all of which can be exploited in the design of molecular diagnostic systems [11] and gene regulating structures [51, 52], and in materials synthesis [20]. Below, we outline some of the general design considerations of SNA–NPs, their unusual properties, and what is understood about the structure–function relationships of these materials.

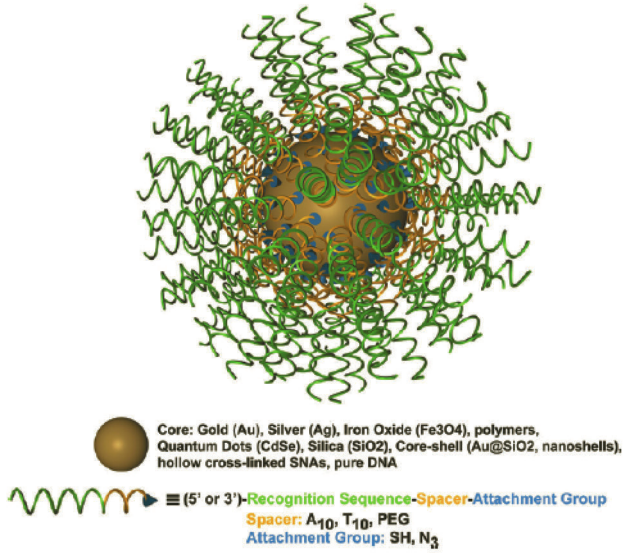

Figure 4.2 The anatomy of SNA nanostructures. An inorganic core is densely functionalized with oligonucleotides containing three segments: a recognition sequence, a spacer segment, and a chemical-attachment group. Additionally, other functional groups such as dye molecules, quenchers, modified bases, and drugs can be attached along any segment of the oligonucleotide.

An initial design consideration for SNA conjugates is the core material. The properties of the oligonucleotide shell are now well-studied and highly predictable based on its structure; an additional way to tailor the behavior of SNA conjugates is through the choice of the core material. Thus far, the most widely studied conjugates have consisted of AuNP cores functionalized with alkylthiolated oligonucleotides attached through an Au–S bond at the 3′ or 5′ end of the molecule [1, 53, 54]. AuNPs were chosen as initial candidates for the core material because they are easily synthesized over a range of particle diameters [55], have plasmon resonances with

high extinction coefficients, can be easily functionalized with a wide variety of chemical reagents, and exhibit well-defined catalytic properties. When modified with a dense monolayer of DNA, these particles, in addition to all SNAs, exhibit properties that are extremely useful in molecular diagnostic [5], therapeutic [15], and materials applications (Table 4.1) [56, 57]. In addition to gold, the physical properties of other inorganic NPs offer unique benefits within the SNA paradigm. To that end, there has been a significant effort to attach oligonucleotides to a wide range of particle types, including silver [42], semiconductor quantum dots (QDs) [44], silica [58], and metal oxides [43] to form SNA architectures. It is important to note that each of these methods requires specific chemistry tailored to the particles of interest, which is a nontrivial task due to the oligonucleotide densities necessary to achieve the properties unique to SNAs (Section 4.4). For example, the surfaces of aqueous silver nanoparticles (AgNPs) are easily oxidized [59, 60], which makes it difficult to prepare stable conjugates from monodentate alkylthiols. Therefore, SNAs from AgNPs are typically prepared from oligonucleotides with multiple cyclic disulfide anchoring groups [42]. Alternatively, silver nanoprisms have been functionalized with DNA by first coating them with a silica shell with subsequent bioconjugation [58]. Cadmium selenide (CdSe) QDs have been functionalized via a three-step processes that entails ligand exchange, solvent exchange, and incubation with alkylthiol-functionalized oligonucleotides [44]. Another method to prepare CdSe/ZnS QDs utilized a novel peptidic linker as an attachment group [61]. Superparamagnetic iron oxide nanoaparticles (SPIONs) have been modified with a SNA shell by using copper-catalyzed alkyne–azide "click" chemistry [43]. Importantly, the DNA binding behavior of these conjugates, which stems from their dense oligonucleotide monolayer, is nearly identical regardless of core material (*vide infra*, Table 4.1).

The oligonucleotides comprising SNAs consist of three main components: a particle attachment moiety (in the case of particle based structures), a spacer region, and a programmable recognition region. Each group serves an integral role for the function of the SNA, and each unit has been the subject of multiple studies. For AuNPs, a typical attachment group is a single propyl- or hexylthiol group, which can be incorporated through traditional

phosphoramidite chemistry (usually at the 5′ or 3′ ends, but in principle can be incorporated anywhere along the sequence). The lack of side reactions for the adsorption of thiols on gold allows for the functionalization reaction to proceed for as long as desired, and yields very high oligonucleotide densities on the surfaces of the AuNPs. Other attachment groups have been used to obtain conjugates with higher stabilities, such as those with chelating moieties, e.g., cyclic disulfides [62, 63] or branched thiol structures [53]. A typical test of conjugate stability involves an evaluation of the rate of oligonucleotide displacement with the disulfide reducing agent dithiothreitol [62]. The second segment of the oligonucleotide sequence, the spacer group, pushes the recognition region away from the AuNP surface, and can be composed of DNA bases (e.g., T_{10} or A_{10}) or other synthetic groups such as polyethylene glycol (PEG) units [64]. Finally, the recognition portion of the strand is tailored for each investigation or technological use and is generally the active segment that is available for further base pairing with other strands of interest (e.g., linker strands with sticky ends, target strands in detection assays, or complementary strands for the formation of siRNA). This portion can be composed of any such unit that can be incorporated via phosphoramidite chemistry, which in the simplest form is based on conventional nucleic acids (DNA or RNA).

In addition to DNA or RNA, the modularity afforded by phosphoramidite chemistry allows for incorporation of a wide variety of modifications to the nucleic acid strands within the SNA architecture. Locked nucleic acid (LNA) bases have been used to increase the binding strength of conjugates to their targets, which, in certain cases, can create a more potent construct [52]. In one example, by incorporating only four LNA bases into the particle sequence, the gene knockdown in A549 lung carcinoma cells by conjugates targeting the survivin gene was improved by 66.6% [52]. McKenzie et al. have shown that LNA–AuNP conjugates can be used to increase the melting temperature of such conjugates by ~3°C per LNA base (in a 14 bp sequence) [65]. This additional stability allows for higher selectivity in detection schemes. Peptide nucleic acids also have been used to prepare stable conjugates that have unusual properties because of the lack of negative charge on the peptide backbone [66].

Table 4.1

Property	Spherical nucleic acids	Linear nucleic acids
Melting transition	Cooperative and narrow (~2–8°C)	Broad (~20°C)
Cellular uptake	Transfection agents not required, (1–1.5) × 10^6 NPs per cell[a]	Transfection agents required (e.g., Dharma FECT, Lipofectamine, Ca^{2+})
Immune response	Minimal[141]	Elevated interferon-β levels (25-fold increase compared to DNA-AuNP conjugates)[141]
Stability	Nuclease resistance due to high local salt concentration[41]	Subject to degradation by nucleases (e.g., DNase degradation 4× higher rate than SNA)
Properties from inorganic core	Plasmonic, catalytic,[5,20] magnetic,[43] luminescent[44]	n/a
Binding strength[b]	K_{eq} = 1.8 × 10^{14}, activated binding motifs[150]	K_{eq} = 1.8 × 10^{12}

[a]Numbers vary depending on cell type and nucleic acid sequence.
[b]K_{eq} values for 15-mer AT-rich strand.[39]

Beyond substitutions of the oligonucleotide backbone, bases can be modified and sequences terminated with groups that provide additional functionality. For example, fluorescent tags, such as fluorescein or cyanine dyes, allow for quantification of the average number of strands per particle [64], and can be used as intracellular spectroscopic handles for the particles or as "flares" [11] in intracellular detection schemes (Section 4.10). Metal complexes, such as *cis*-diamminedichloroplatinum(II) analogues [67] or gadolinium chelates [68], have been coupled to conjugates to create potent drug delivery vehicles and magnetic resonance imaging contrast agents, respectively. Chemical tags such as alkynes and azides have been used to prepare probes that enable copper ion detection for environmental monitoring purposes [69]. Antibodies have been co-adsorbed with the oligonucleotides on the surface of the particle to create multifunctional probes that have been used in protein

detection assays [70, 71]. The high stability of the nucleic acid-modified nanostructures in aqueous media can be used to solubilize drugs that are inherently difficult to transfect, such as Paclitaxel [72], in aqueous media through attachment to the conjugate. Indeed, these are chemically versatile structures that allow one to prepare multifunctional materials using the SNA platform.

4.4 Controlling the Density of SNA Conjugates

Initial studies conducted with DNA-AuNPs have demonstrated the potential for utilizing SNA conjugates across a large number of disciplines. Indeed, the first reports of these structures touched off a decade and a half of research that continues today, which branched from materials synthesis to fundamental studies in DNA–NP-based assembly, diagnostics, and therapeutics (Sections 4.6, 4.8, and 4.9, respectively). The extension of these conjugates to such fields was predicated on their high stability and unique function, which is directly dependent on the structure and density of the monolayer of oligonucleotides on the surface of the NPs. Therefore, it was necessary to understand the important synthetic parameters for producing relatively well-defined conjugates exhibiting properties that have been optimized for an intended use. To that end, the variables that control the loading of oligonucleotides have been studied in detail. These include the salt concentration of the reaction solution, the size and shape of the NP, the bases closest to the particle surface, sonication or heating, and the identity of the chemical attachment moiety.

The first generation of SNA–NP conjugates consisted of citrate-stabilized 13 nm AuNPs that were functionalized with relatively short oligonucleotides through a terminal alkylthiol (e.g., 3′-propylthiol-TACCGTTG) [1]. However, because DNA is negatively charged and cannot pack densely without electrostatic screening, only a low-density monolayer was formed, and the resulting particles were only stable on the order of weeks. In a report published soon thereafter [73], we developed a method to prepare robust conjugates that introduced the concept of salt aging, which allows for high-density packing of oligonucleotides on the NP's surface, and is now the preferred method for synthesizing such conjugates (Fig. 4.3).

Increasing the sodium ion concentration of the reaction solution to >0.15 M (up to ~2.0 M with surfactants) screens the repulsive interactions between neighboring strands, thereby promoting higher densities as the oligonucleotides assemble on the surface of the AuNPs; higher salt concentrations generally result in higher oligonucleotide densities until steric constraints prohibit further adsorption. The monolayer of oligonucleotides formed by this method is especially stable because of the relatively strong Au–S interaction (compared to the Au–citrate interaction). Furthermore, the combined negative charge of the oligonucleotides on the surface of the NPs confers a high negative zeta potential (<−30 mV) that helps stabilize the colloid from flocculation [21, 74]. Indeed, particles functionalized in this way exhibit long-term (months) stability in solutions over a wide range of pH, solvent, and ionic strength conditions. Although DNA disassociation has been observed in certain cases [25], at room temperature or physiological conditions, we have not observed evidence of significant dissociation [15]. This stability is important for their use in intracellular gene regulation, in vitro molecular diagnostic, and materials assembly applications.

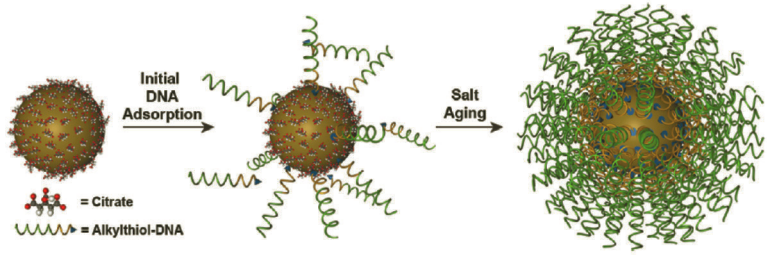

Figure 4.3 Synthesis of SNA–AuNP conjugates. Citrate-stabilized particles are incubated with alkylthiol-functionalized oligonucleotides in water to form a low-density monolayer. By incubating the nanoparticles in aqueous solutions with successively higher concentrations of salt (typically 0.15–1.0 M) and surfactants over ~12 h, a high-density SNA shell is formed.

The maximum possible surface density of DNA is dependent on the particle size and shape. In the case of spherical particles, smaller particles can support higher densities, substantially greater than values obtained on planar surfaces. For example, 10 nm particles can typically support ~2.0×10^{13} oligos/cm^2, while the surface

coverage for oligonucleotides of the same sequence assembled under identical conditions on a macroscopic planar gold surface is 5.8×10^{12} oligos/cm^2 [75]. In general, a smaller particle can support a higher oligonucleotide density than larger particles because the radius of curvature is higher, which confers a natural deflection angle between neighboring strands that creates additional space around individual strands (Fig. 4.4A). This effect diminishes as the particles increase in size; in fact, at diameters of 200 nm or larger, the surface coverage of DNA approaches that of planar gold [75]. The high-curvature particles result in surfaces with greater free volume and therefore minimized steric and electronic repulsion constraints, allowing for higher DNA surface densities. By increasing the salt concentration in the reaction solution, this screening is increased, allowing for a greater number of strands per particle (Fig. 4.4B). Finally, a geometric model developed by Hill et al. demonstrated that by combining the experimental density values for curved and flat surfaces, one could accurately predict the natural loading for anisotropic particles, such as gold nanorods and triangular prisms [75].

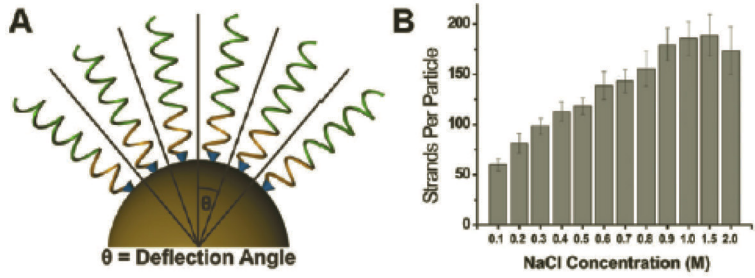

Figure 4.4 (A) The oligonucleotides that comprise SNAs are arranged in a dense, oriented fashion. On a nanoparticle surface, the geometric configuration confers a natural deflection angle between strands. On smaller particles, this angle is greater due to their higher relative curvatures. Ultimately, this results in reduced Coulombic repulsion at the termini of the strands, and hence higher densities in the overall structure. (B) The density of oligonucleotides of SNA–AuNP conjugates is controlled in part by the salt concentration of the NP/DNA incubation solution. A higher salt concentration results in a higher oligonucleotide density. For 15 nm particles, this range spans ~50–200 strands/particle. Reprinted with permission from Ref. [75]. Copyright (2009) American Chemical Society.

Another variable that controls the loading of oligonucleotides on AuNPs is the composition of the DNA bases closest to the particle surface [64]. In general, a spacer region of approximately 10 nucleotides (~3 nm) is often used to extend the active recognition portion of the oligonucleotide sequence away from the positively charged gold surface. This imparts flexibility that is important for binding and which also lowers steric barriers for accessing the full oligonucleotide sequence in the context of hybridization. DNA bases interact with gold surfaces to varying degrees [76], depending on the base (e.g., affinity of adenine > affinity of thymine), so the choice of bases used in the spacer region is important. Indeed, for 15 nm AuNPs, the density of oligonucleotides is highest when a T_{10} spacer is used (38 pmol/cm^2 for thymine compared to 19 pmol/cm^2 for adenine). Furthermore, higher densities can be obtained if PEG units, which minimally interact with the gold surface, are used as spacers (56 pmol/cm^2) [64]. Another method that has been used to increase the surface density of oligonucleotides is sonication [64], which allows one to facilitate the kinetics of immobilization, orientation, and packing of the oligonucleotides on the surface of the particle. Alternatively, one can get higher loadings and increased adsorption rates at elevated temperatures [64].

4.5 Cooperative Binding with High-Density SNA Conjugates

SNAs are entities with highly tailorable recognition properties by virtue of nucleic acid sequence. Direct particle–particle hybridization is possible [42, 43], in addition to assembly via linker strands [1], which occurs through the recognition region of the DNA sequences. One can think of the SNA–NP conjugates as individual building blocks, each with a unique identity dictated by their sequence. The NPs can be brought together through particle–DNA and linker design, which results in a polymeric macroscopic assembly. Because the particles are held together through DNA linkages and their cores do not interact or fuse, the DNA–NP conjugates can be released from the aggregate through dehybridization of the duplexes via heating or by lowering the solution salt concentration. DNA duplexes follow predictable “melting” dehybridization when the temperature is

raised above the melting point (T_m). The same holds true for SNA conjugates; however, their polyvalent binding behavior differs greatly from that of linear duplexes [40].

During the early studies of the chemical and physical properties of SNA–AuNP conjugates, a striking observation was made concerning the dehybridization of the aggregates (Fig. 4.5A,B). Typically, dehybridization or "melting" of oligonucleotides occurs over a broad temperature range (~20°C); however, when the duplex-assembled SNA–AuNPs are heated, this melting transition occurs over a very narrow temperature range (~2–8°C) and at a temperature higher than the Tm of the particle-free DNA duplex (at substantially lower concentrations, Fig. 4.5C). These sharp transitions were also observed for single layers of particles that were hybridized to a surface, for example in a chip-based assay [40, 77], although the transition is not as narrow as one observes in the aggregates. Experimentally, this phenomenon is observed for SNAs without particle cores as well [20]. The sharpness of the melting transition can be quantified mathematically by calculating the full width at half-maximum (fwhm) of the first derivative of the melting curve. Typical fwhm values for typical AT-rich duplexes, 10 bases in length, are ~10°C, while fwhm values for the transitions observed for hybridized aggregates of SNA conjugate structures formed from the same oligonucleotides are in the range of 1–3°C. As will be discussed in Section 4.8, the narrow melting transition observed for SNA nanostructures is important in their applications for diagnostics where a single oligonucleotide base-pair mismatch is enough to perturb the melting behavior of the aggregate, allowing it to be differentiated from the aggregates made from fully complementary duplex structures.

One explanation for the increase in melting temperature of the aggregate compared to the free strands is that the higher surface density of oligonucleotides on the particle surface gives rise to a greater number of interparticle connections that are collectively stronger and present at a higher effective concentration compared to DNA duplexes free in solution. Thus, decreasing the number of recognition strands on the particle surface (either through the addition of nonrecognition "diluent" strands or by decreasing the extent of chemisorption of the recognition strand during the functionalization/salting step) results in a broader melting transition that begins at a lower temperature. Additionally, the high local salt

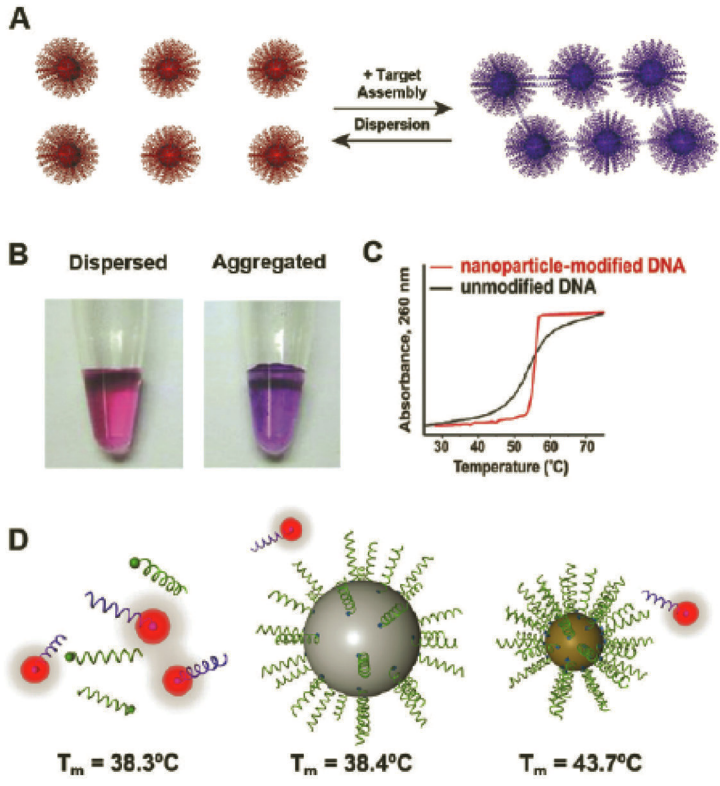

Figure 4.5 (A) Schematic illustration of the aggregation and dispersion of SNA–AuNP conjugates and the corresponding SPR shift of the Au cores. Dispersed particles are red, whereas aggregated particles are purple. Targets can be DNA, metal ions, or any molecule that the SNA shell has been programmed to recognize and bind. (B) Aggregation results in the red shift of the SPR (from 520 nm to ~600 nm) and a visible red-to-purple color transition of the particles in solution. Reproduced with permission from Ref. [78]. Copyright © 2011, John Wiley and Sons. (C) Compared to duplexes of free-strand DNA, which dissociates over a broad temperature range, the melting transitions of SNAs are sharp and occur over a very narrow temperature range due to the cooperative binding of the nucleic acids in the SNA shells. Reprinted with permission from Ref. [6]. Copyright (2005) American Chemical Society. (D) Melting temperatures of duplexes labeled with a quencher (green) and a fluorophore (purple), duplexes on silica particles (~100 nm in diameter), and SNA–AuNP conjugates (13 nm in diameter). The melting transition of free and silica particle-bound duplexes are similar because the density achieved on silica particles is typically low (1/30th that of the SNA–AuNP conjugates). The melting transition of SNA–AuNP conjugates occurs at higher temperatures due to the properties of the dense SNA shell.

environment in the area surrounding the NP, in certain cases, imparts greater stability to the duplexes and contributes to the increase in melting temperature (Fig. 4.5D) [79]. High local salt concentration is also believed to be responsible, in part, for the cooperative, narrow melting transition. At the start of the melting transition, when strands begin to dehybridize, there is a simultaneous decrease in the local salt concentration that decreases the melting temperature of the remaining strands. We and the Schatz group have provided both experimental and theoretical evidence to support a "shared ion cloud" theory in which cooperativity in oligonucleotide melting transitions arises from the dielectric environment of duplexed strands in close proximity to one another [80, 81]. Nguyen and coworkers have provided further experimental evidence for this theory using a molecular system in which sharp melting transitions were observed for systems containing only a few oligonucleotides, oriented in a manner such that shared ion interactions could take place [82, 83].

Importantly, the characteristic sharp melting of hybridized SNAs is a direct result of the collective behavior of the dense monolayer of oligonucleotides in the SNA shell. Indeed, subsequent studies have shown that the narrow melting transitions observed initially for the SNA–AuNPs are not core-dependent, but rather characteristic of all SNA–NP conjugates including QDs [44], SPIONs [43], AgNPs [42], and coreless SNAs [20], as well as anisotropic prisms, rods, and rhombic dodecahedra [84, 85]. The collective interactions of DNA can bring particles together even if the individual binding strength on a per strand basis is weak. This effect results in "three-dimensional hybridization," where the SNAs as single multistrand entities hybridize together [86]. For example, linear strands that are complementary by three base pairs will not hybridize in solution (e.g., 5′-GCG-3′ and 5′-CGC-3′). However, if particles are functionalized with strands terminated with the identical sequences, hybridization will occur and particles will aggregate. This effect is more prominent with larger NPs. For example, when 150 nm particles are aggregated, the total number of DNA linkages between particles is much greater than the number between aggregated 5 nm particles (hundreds compared to less than 10). Therefore, even a single base-pair interaction can cause aggregation of particles of larger sizes [86]. The fact that such weak interactions can aggregate particles is an

important consideration for sequence design of SNA conjugates. For instance, if a researcher intends to synthesize particles for an application in gene regulation or diagnostics, the sequence should be checked for self-complementarity; indeed, even a few bases can cause unanticipated and undesirable particle aggregation.

Interestingly, cooperative binding is not limited to canonical DNA binding. DNA binding modes that rely on G-quadruplex formation can also be accessed by the SNA structure [87]. One would normally expect the two sequences, 5′-CCCC-3′ and 5′- GGGG-3′, to have one melting transition. However, because the G-rich sequence can form quadruplexes, particles functionalized with these strands exhibit two melting transitions [88]. Furthermore, this has implications for sequence design; one should not synthesize SNAs with oligonucleotides terminated with G bases.

In some respects, DNA bases are to DNA strands as DNA strands are to SNA conjugates. This hierarchy makes interesting 3D modes of hybridization possible that are not expected if one only considers the dynamics of single linear strands in isolation. These considerations are exceedingly important, and only through understanding these fundamental polyvalent interactions of SNAs can researchers realize new ways of making macroscopic materials from these nanoscale building blocks.

4.6 Nanoparticle Assembly and Crystallization Programmed with Spherical and Other 3D Nucleic Acid Nanostructures

The SNA conjugate is a versatile and chemically programmable synthon that can be used to construct higher ordered materials, in particular colloidal crystals. Indeed, early work showed how linker strands could be used to assemble different particle building blocks into polymeric materials with unusual properties that derived from placement of the particles within such assemblies [1,89]. The property changes that accompanied such assembly events became the basis for many new nucleic acid-based diagnostic systems (Section 4.8). In addition to diagnostic applications, subsequent work began to show how one can force the assembly of such particles into colloidal crystals exhibiting short-range order, where interparticle distances

can be modulated by linker length [89]. Further work has shown the ability to create complex discrete structures, such as asymmetrically functionalized particles and programmably assembled clusters [90–92]. These works provided some of the fundamental knowledge necessary for the discovery in 2008 by our group and the Gang group (using related techniques) that SNA-modified AuNPs could be crystallized exclusively into either face-centered cubic (fcc) or body-centered cubic (bcc) lattices through judicious choice of linker strands and annealing (Fig. 4.6A) [93, 94]. A key insight was that the weak binding interactions of short DNA linker sequences combined with the polyvalent cooperative binding observed for SNA conjugates (Section 4.5) allows the system to self-correct defects and transform from an initial disordered aggregate into an energetically favored crystalline arrangement. Specifically, the large number of linkages can hold the aggregate together, yet because they are weak individually, they can hybridize and dehybridize dynamically. Thus, annealing an aggregate at a temperature slightly below its melting temperature provides the thermal energy required for the transition from a disordered to an ordered structure to take place. The NP superlattices synthesized using SNA conjugates exhibit a very high degree of crystalline order, as demonstrated by small-angle X-ray scattering (SAXS). SAXS is the primary characterization method for such structures because these superlattices typically exist only under conditions where DNA duplexes are stable, namely, aqueous saline solutions. As a secondary structural characterization technique to complement SAXS, we have recently developed a resin-embedding method for visualizing the NP superlattices by transmission electron microscopy (TEM) [85, 95]. These initial studies highlighted the use of DNA as a robust and programmable assembly tool for the formation of highly ordered NP superlattices and further demonstrated the potential materials applications made possible by the unique properties of SNA conjugates.

In addition to the reversible binding of short DNA sequences to the SNA shell, the ratio of DNA length to particle core size was found to be an important factor for determining whether a system reorganizes into a crystalline state. For fcc-type systems, a “zone of crystallization” was identified, as defined by this ratio, where ordered crystals are observed only when working within the constraints of the DNA length and particle core size parameters

[96]. These boundaries in the phase diagram exist because the ratio of DNA length to NP diameter affects both the number of stable DNA linkages that can be formed between particles and the rate at which those linkages are broken (k_{off}) and re-formed (k_{on}) during the reorganization process. At low ratios of DNA length to NP diameter, higher relative energetic penalties associated with DNA bending and stretching that are required to maximize the number of DNA connections between particles prevent crystal formation (it is harder to bend shorter duplexes than longer ones). For long, flexible DNA linkages between particles (>100 bp), i.e., high ratios of DNA length to NP diameter, a decrease in the local concentration of both salt and DNA "sticky ends" (short recognition elements at the terminus of the DNA sequence) results in a greater k_{off} for DNA binding between particles and disfavors the reorganization process toward crystal formation. In related work, Gang and coworkers adjusted two distinct variables, the DNA linker length and the number of DNA connections, to generate a phase diagram delineating the boundary between crystalline (bcc-type) and disordered aggregates [97]. It was observed that formation of ordered lattices required a greater number of linkages for longer linkers, most likely due to the destabilizing effects of lower effective linker concentrations on the reorganization process. Both phase diagrams are based upon the important concept that high-density DNA and the cooperative and reversible binding of the DNA linkages are required in the transformation from disordered aggregates to ordered superlattices.

One of the key advantages offered by DNA-mediated assembly is that parameters such as particle diameter, shape (Fig. 4.6B,C), DNA length, and sequence can be tuned independently. This provides a means to synthesize colloidal crystals with lattice parameters that can be controlled and predicted with nanometer precision (calculated rise per base pair = $0.255x + 11.1$ nm, with $R^2 = 0.987$, where x is the total number of bases between AuNPs; this rise per base differs from that of canonical B-form DNA) [98]. The packing density of the NP lattice is controlled by the sequence of the linker sticky ends: a self-complementary linker sequence (5′-GCGC-3′) allows every particle to bind to its nearest neighbor and favors the formation of a close-packed fcc lattice. In contrast, a pair of non-self-complementary linkers (e.g., 5′-TTCCTT-3′ and 5′- AAGGAA-3′) produces two particle types, "A" and "B," and favors the formation of

the non-close-packed bcc lattice if the particles are added in equal amounts [93]. In addition to a binary lattice consisting of particles that all have the same inorganic core, where the two particle types are differentiated by the identity of the DNA sequence, a bcc lattice composed of "A"-type AuNPs and "B"-type QDs has also been synthesized [99].

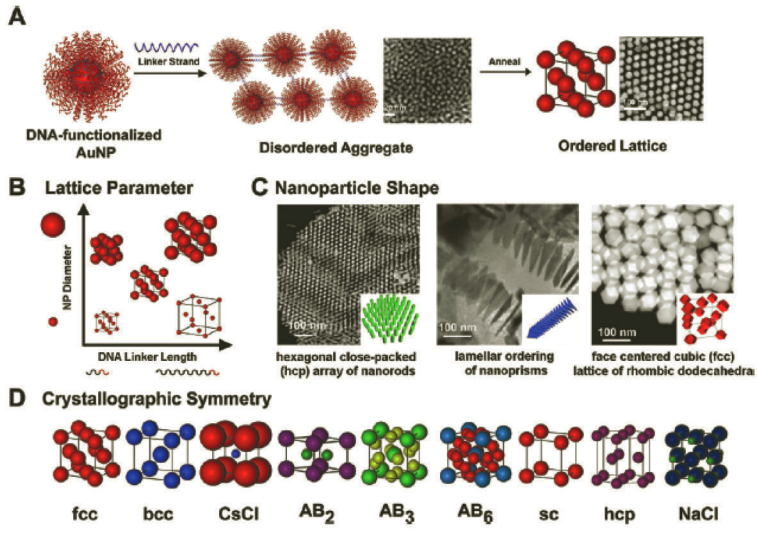

Figure 4.6 (A) Schematic illustration of DNA-programmable nanoparticle assembly into ordered superlattices (fcc lattice shown). TEM images show the transition from disordered aggregate (10 nm AuNPs shown) to ordered lattices (30 nm AuNPs shown) after annealing at a temperature slightly below the melting temperature of the aggregate. TEM image of the ordered NPs from Ref. [95]. Reprinted with permission from AAAS. The programmable parameters that can be controlled using this technique are (B) the lattice parameter, which can be tuned by using different linker lengths and NP diameters (figure not to scale), (C) NP shape, where directional bonding of different anisotropic NPs leads to a variety of one-, two-, and three-dimensional lattices, and (D) crystallographic symmetry, which can be controlled by linker lengths, linker sequences, and molar ratios of particles. Panel B is reprinted by permission from Springer Nature Customer Service Centre GmbH: Springer Nature, *Nature Materials*, Ref. [85]. Copyright (2011).

This system has evolved to one that offers a high level of predictability based upon a set of design rules that we recently

introduced [95]. The seven rules, which are summarized below but explained in detail elsewhere [95, 153], are as follows:

i. The most stable crystal structure maximizes all possible types of DNA hybridization interactions.
ii. For a system where all SNA–AuNPs possess the same hydrodynamic radii, each SNA–AuNP in the thermodynamic product will maximize the number of nearest neighbors with which it can form DNA connections.
iii. When two lattices are of similar energetic stability, the kinetic product can form if the rates of DNA linker de-and rehybridization are slowed.
iv. The hydrodynamic radii of the SNA–AuNP conjugates, rather than the size of the constituent AuNPs or the length of the oligonucleotides, dictate their assembly and packing behavior.
v. For binary systems, the size ratio and DNA linker ratio between particles dictate the thermodynamically favored crystal structure.
vi. Two systems with the same size ratio and DNA linker ratio produce the same thermodynamic product.
vii. Hollow SNAs can be used as spacer elements within nanoparticle superlattices to access symmetries not accessible with core-filled structures [153].

These six rules, which have been formulated on the basis of experiments and modeled phase diagrams, have been used to construct over 50 SNA–AuNP superlattices with nine distinct crystallographic symmetries (Fig. 4.6D). In addition to fcc and bcc lattices, superlattices with hexagonal close-packed (hcp), cesium chloride (CsCl), AB_2 (isostructural with aluminum diboride), AB_3 (isostructural with Cr_3Si), AB_6 (isostructural with the alkali-fullerene complex Cs_6C_{60}), sodium chloride (NaCl), and simple cubic (sc) symmetry have been synthesized. With the exception of hcp, all are assumed to be thermodynamic products, made by annealing the programmed structures at a temperature near the onset of the melting transition. The rules are analogous to Pauling's rules for determining the packing behavior of complex ionic solids [100], but in many ways afford greater predictability and tunability due to the ease with which DNA interactions can be programmed.

4.7 Moving beyond Spherical Conjugates to Other Forms of 3D Nucleic Acids

In addition to size-dependent properties, many physical and optical properties are dependent upon nanoparticle shape, and some are unique to NPs exhibiting anisotropy (e.g., rods, prisms, cubes). For example, the plasmon resonances of such structures are highly dependent on their shape and aspect ratio [101, 102]. The diverse properties of anisotropic NPs have been reviewed in detail elsewhere [103–106]; here, we will focus solely on the emergent properties of DNA-functionalized anisotropic particles in the formation of nonspherical 3D nucleic acids (Fig. 4.7A).

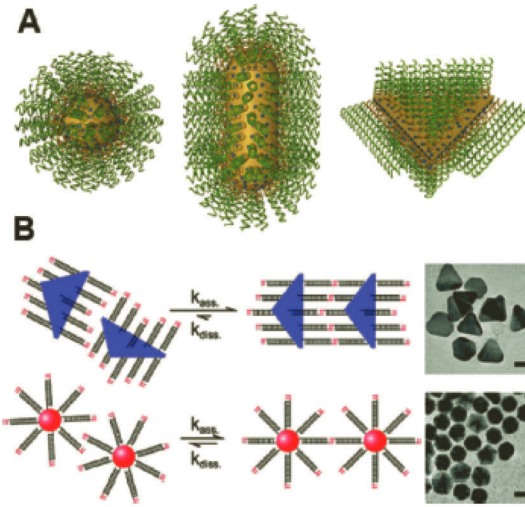

Figure 4.7 (A) Illustration of 3D SNA conjugates formed from different particle templates: spheres, rods, and triangular prisms. (B) Schematic demonstrating the difference between anisotropic 3D nucleic acid hybridization and SNA hybridization. Reprinted with permission from Ref. [115]. Copyright (2011) American Chemical Society.

Because the synthesis conditions for anisotropic particles are often distinct from those of spherical nanostructures, DNA surface-immobilization must be tailored for each of these particle types. For instance, many anisotropic Au nanostructures are synthesized in the presence of the capping agent cetyl trimethylammonium bromide

(CTAB) [107–109]. Because CTAB is a positively charged surfactant, it effectively complexes and sequesters the DNA, preventing it from adsorbing to the AuNP surface. Therefore, it must be removed by iterative centrifugation and washing steps before DNA functionalization can occur in an analogous way to how spherical AuNPs are functionalized [84, 85].

Like their spherical counterparts, these anisotropic particles have unusual and useful properties due to both their inorganic cores and dense surface coating of oligonucleotides. For example, the size- and shape-tunable near-infrared (NIR) absorption of many anisotropic particles has utility in the development of diagnostic and imaging tools. We and others have demonstrated light-mediated methods to release DNA from anisotropic NPs either through breakage of the Au–S bond [110] or through dehybridization of complementary DNA strands via local photothermal heating [110–114]. Because the size, and therefore the resonance wavelength, of these anisotropic particles can be finely controlled, one can selectively dehybridize strands from a given particle type within a mixture simply through appropriate choice of the laser irradiation wavelength [112]. This combination of the plasmonic properties of the NPs and the thermal properties of the anchored DNA strands allows one to wield spatiotemporal control over the local concentration and bioavailability of oligonucleotides in biological systems.

The degree of anisotropy associated with a particle scaffold can dramatically influence the collective behavior of the oligonucleotides comprising 3D nucleic acids. In recent work, we have shown that the binding affinity between complementary DNA-functionalized triangular nanoprisms is several million times higher than that of SNA–AuNP conjugates with similar oligonucleotide loadings [115]. As the sphericity of a structure decreases, more connections between 3D nucleic acids can be supported through greater interparticle surface contact, such as between two flat extended surfaces (Fig. 4.7B). This geometry increases the effective local concentration of oligonucleotides available for binding, which increases the "on" rate of hybridization. Additionally, the binding interactions between flat surfaces impart less conformational stress on the hybridized duplexes as compared to those that bridge SNAs. Taken together, these factors form the basis for beginning to understand the "valency" of nonspherical 3D nucleic acids. Furthermore, these

striking observations recapitulate the notion that the orientation and density of nucleic acids at the nanoscale are unique parameters that can be tailored to obtain nanostructures with a wide range of unusual and novel chemical and physical properties.

In the areas of materials synthesis and programmed colloidal crystallization, nonspherical 3D nucleic acid nanostructures provide access to NP superlattices with greater structural diversity than can be achieved with isotropic NPs. The introduction of the concept of NP shape into the DNA-based assembly methodology imparts a kind of "nanoparticle valency," where directional hybridization interactions between particles allow for the formation of one-, two-, and three-dimensional superlattices that would be difficult, if not impossible, to synthesize with other assembly or lithography methods [85]. These directional interactions occur because DNA base pairing between anisotropic particles is favored along directions that maximize parallel face-to-face interactions between particles. Thus, following DNA functionalization, nanoprisms assemble into 1D arrays along the prism faces, nanorods assemble into 2D sheets with hexagonal close-packed (hcp) ordering, and rhombic dodecahedra assemble into 3D fcc lattices (Fig. 4.6C). Analogous to the unique physical properties possessed by anisotropic NPs over their spherical counterparts, other forms of 3D DNA allow access to an entirely new design space for NP superlattices that is distinct from what is achievable with SNAs alone. Finally, efforts to face-selectively functionalize particles with different oligonucleotides [84, 90, 91] will dramatically increase valency control, the synthetic tunability of this system, and the sophistication of the types of materials and crystals that can be constructed.

4.8 Diagnostics

During the initial studies of the SNA–AuNP conjugates, we recognized immediately that their reversible melting behavior over a narrow temperature range and their corresponding hybridization-dependent optical changes could be useful for high-selectivity detection platforms (*vide infra*). Since that time, SNA nanostructures have been used to develop a wide variety of in vitro and intracellular molecular diagnostic systems for a range of analytes. These include

solution-based colorimetric [4] and chip-based scanometric systems for nucleic acid [5], protein [71], small-molecule [116], and metal-ion-based targets [117] (*vide infra*). The utility of SNA structures in diagnostic applications arises in part from both the properties of the SNA's polyvalent oligonucleotide shell and the physical and chemical properties of the inorganic core. Taken together, these two components yield probes that offer significant advantages over molecular counterparts.

In a typical colorimetric assay using SNA–AuNP probes, a target entity is captured by two distinct sets of AuNPs, each functionalized with a strand programmed or chemically modified to impart specificity to its target, such that the presence and subsequent capture of target triggers the reversible aggregation of the AuNP probes (Fig. 4.5A,B). This process results in a visible red-to-purple color transition due to a red shift in the SPR of the AuNPs, which can be monitored by eye or spectroscopically. Significantly, an aggregate formed from a perfectly complementary target nucleic acid sequence exhibits a very narrow melting transition (compared to duplex DNA) and can readily be differentiated from target strands containing a single base-pair mismatch, insertions, or deletions [40]. This observation is clinically relevant because single-nucleotide polymorphisms (SNPs) play a role in many diseases [118]. Furthermore, the high extinction coefficient of AuNPs allows one to detect targets at lower concentrations than conventional molecular dyes. To date, colorimetric detection systems designed with the appropriately functionalized SNA conjugates have been used to quantitatively measure the concentrations of nucleic acids [4, 73], enzymes [119], small-molecule targets (via aptamers) [120], enzymes [121], known DNA-binding molecules (e.g., 4′,6-diamidino-2-phenylindole (DAPI), ethidium bromide) [122], Hg^{2+} ions [123], copper ions (Cu^{+} and Cu^{2+}) [69], and other metal ions [124]. Particles do not need to be directly cross-linked by a target molecule to achieve target-specific aggregation. For example, Sato et al. have developed a system that takes advantage of conformational changes of the SNA shells when they bind to their targets. At high salt concentrations, particles will rapidly aggregate when they bind their complements due to reduced repulsive interactions between particles [54]. In principle, solution-based colorimetric detection

strategies can be used to detect any target that has the ability to bring plasmonic NPs together through interactions with suitably designed oligonucleotides. Reverse colorimetric detection platforms, whereby the presence of target triggers the dispersion of aggregated particles and a concomitant purple-to-red transition, have also been developed by Lu and coworkers [125]. In these systems, SNA–AuNPs are aggregated in the presence of a DNAzyme that can be cleaved upon binding of the appropriate target, which results in particle dispersion [126]. Finally, other systems that cause a change in the physical properties of the inorganic core of SNAs, based upon magnetic [127], Raman [128], or fluorescent signals [67], also have been developed.

The ability to differentiate SNPs by NP-based colorimetric detection was a significant advance in molecular diagnostics. In 2000, to increase the sensitivity offered by this system, we developed a chip-based method called the scanometric assay where the capturing of a desired target results in the immobilization of the AuNP probes onto a functionalized glass slide in a three-component, sandwich-type assay (Fig. 4.8A) [5]. Additionally, this assay utilized the catalytic properties of the AuNPs, namely its ability to promote the reduction of silver(I) in the presence of hydroquinone, as a method for signal amplification. Silver-coated AuNPs could then be readily detected by traditional flat-bed scanners, whereby the presence of more immobilized NPs, and hence more captured targets, resulted in a greater light scattering. A second gold [71] or silver deposition [5] step was shown to increase the limit of detection (LOD) offered by this assay, though subsequent depositions did not improve the LOD due to increased background signals for all target concentrations (Fig. 4.8B,C). Since its discovery in 2000, the scanometric assay has been extended to proteins [129], commercialized, FDA-cleared, and used in a variety of highly sensitive molecular diagnostic technologies [6, 30, 100]. In 2009, we developed an analogous scanometric immunoassay using antibody-modified SNA–NP conjugates where the target in this case was prostate-specific antigen (PSA) rather than DNA [71]. This study also showed that using gold deposition steps increased the LOD by 2 orders of magnitude from 30 fM to 300 aM, compared to the same assay using an equal number of silver deposition steps.

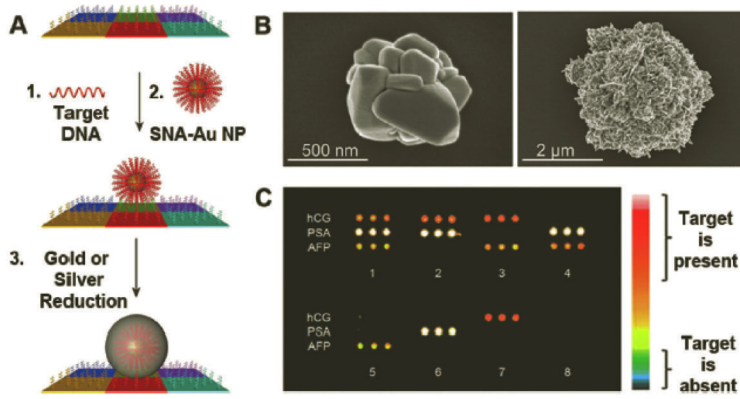

Figure 4.8 (A) Schematic illustration of a scanometric detection assay. A chip is synthesized with capture strands for a number of different targets. The targets will hybridize to the appropriate spots if they are present. The chip is then exposed to a solution of SNA–AuNP probes, which will hybridize to the appropriate targets if they are on the chip. The binding of the SNA–AuNP probes can be visualized by reducing metal ions (Ag or Au) on the NP cores, which creates a macroscopic structure. The SNA probes can be modified with many recognition elements, such as antibodies, which allows for the detection analytes beyond nucleic acid targets. (B) Large macroscopic structures created by reduction of Ag (left) and Au (right). The Au is a better signal enhancer due to its mechanism of reduction, which results in larger macroscopic particles. (C) Read-out of a scanometric detection assay. If the target is present, the macroscopic structure can be detected via light scattering and a conventional optical flat-bed scanner. A bright spot indicates that target is present, and the signal intensity permits quantification of target concentration. Panels B and C reprinted with permission from Ref. [71]. Copyright (2009) American Chemical Society.

Strategies that rely on more sophisticated versions of SNA conjugates, such as the bio-barcode assay [130], have been introduced. With such assays, a NP probe is designed with "barcode" DNA strands that are hybridized to an SNA conjugate functionalized with strands complementary to the barcode sequence as well an antibody for an antigen of interest (e.g., PSA). In the barcode assay, rather than directly detecting the antigen molecules, signal amplification is effected by releasing the barcode DNA strands, post antigen sequestration and isolation, followed by their detection with the scanometric assay. Further signal amplification is possible by using polymerase chain reaction (PCR) to increase the copies of the

barcode DNA, though the PCR-less technique using larger AuNPs (30 nm) was shown to effectively detect PSA at attomolar concentrations. Variants of this assay have been used to study clinical disease states including Alzheimer's disease [154] and prostate cancer [155].

4.9 Spherical Nucleic Acids as Single-Entity Gene Regulation Constructs

Regulation of gene expression with synthetic oligonucleotides has led to fundamental breakthroughs in the understanding of intracellular function [131] and may lead to viable treatment options for genetic-based diseases, such as many forms of cancer and neurological disorders [132, 133]. However, the delivery of synthetic nucleic acids to disease sites and across cell membranes is still a major challenge for gene regulation therapies (antisense DNA and siRNA). Indeed, Nature has created a defense network for foreign nucleic acids. For example, since nucleic acids are negatively charged, they cannot easily cross the negatively charged cell membrane. Furthermore, they are rapidly degraded by nucleases and activate the innate immune response in cells. Historically, researchers have required the use of transfection agents, such as cationic polymers [122, 134, 135], liposomes [136], and modified viruses [137], to shuttle the nucleic acids through the negatively charged cellular membrane and shield them from enzymatic degradation. Unfortunately, these methods are not ideal for systemic delivery because of their inability to be degraded naturally, severe immunogenicity, and toxicity at high concentrations (Table 4.1) [138, 139]. The most widely used agents, cationic polymers, complex the nucleic acid material and neutralize its charge, allowing the hybrid material to breach cellular membranes by fusing with them [140]. SNA constructs provide an alternative in this regard since, despite their large negative charge (zeta potential < -30 mV), they have been found to enter cells in very high numbers, without the need for ancillary transfection agents [15]. Additionally, SNA–NP conjugates have a unique set of properties specific for intracellular applications, such as high binding coefficients for complementary DNA and RNA (vide supra) [39], nuclease resistance [41], minimal immune response [141], no observed toxicity [74], and highly effective gene regulating capabilities [17, 20, 142]. Again,

all of these properties derive from the 3D structure of the densely packed, highly oriented oligonucleotide shell on the surface of the particles.

It has been shown that the dense DNA monolayer is primarily responsible for cellular uptake, as bare citrate-stabilized particles (the only other component in the system) or particles without DNA but passivated with BSA show orders of magnitude lower cellular uptake [74, 143]. Furthermore, this uptake is universal for any NP functionalized with a dense shell of DNA (~20 pmol/cm^2). Indeed, conjugates made from other cores, such as iron oxide NPs, also show high cellular uptake without transfection agents [43]. One of the most convincing pieces of evidence for the importance of this surface structure/ uptake relationship comes from studies of coreless SNAs (Fig. 4.9) [20]. These particles, which are as close as one can get to pure SNA, are composed only of cross-linked nucleic acids, which are oriented in the same fashion as SNA–AuNP conjugates. They can be synthesized from modified forms of DNA or RNA and exhibit many of the same properties of inorganic NP-based SNAs. Furthermore, they anticipate concerns about the potential toxicity of the inorganic gold core.

Importantly, SNAs (with or without an inorganic core) are capable of rapidly entering every cell type tested thus far (over 50), including primary cells, with the exception of mature red blood cells [15]. Inductively coupled plasma or radiolabeling allows for quantification of the number of particles that enter each cell, which often exceeds millions. This seemingly universal uptake phenomenon is facilitated in part by membrane-bound scavenger receptors [144], which are known to mediate endocytosis of specific polyanionic ligands, such as oligonucleotides [145], including phosphorothioate variants [146]. In a proposed mechanism, serum proteins (such as BSA) first adsorb to the SNA's oligonucleotide shell, slightly inhibiting uptake of particles [74]. Next, the serum proteins are displaced by scavenger receptors at the cell surface, a process that initiates endocytosis of the particles. By inhibiting these receptors with their natural agonists, such as poly-inosine (I) and fucoidan, the uptake of SNAs is significantly reduced [31]. The interaction between the dense nucleic acid shell of SNAs and cell membranes governs this uptake phenomenon; higher densities result in higher uptake of SNAs (Fig. 4.10A).

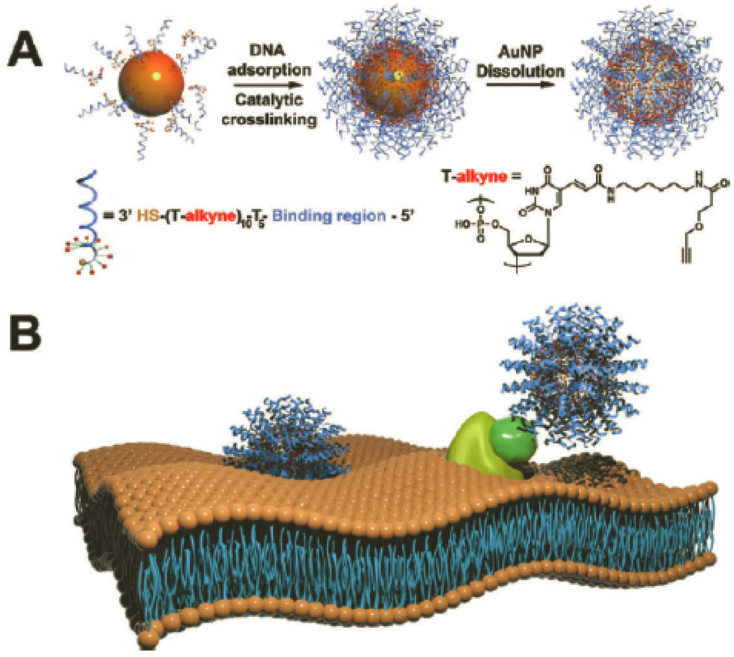

Figure 4.9 (A) Synthesis of hollow SNAs. Alkyne-modified oligonucleotides are adsorbed onto AuNPs, which then catalyze the cross-linking of the alkyne groups. After purification from excess oligonuceotides, the cores are dissolved with potassium cyanide, which yields hollow SNAs. (B) Schematic of hollow SNAs interacting with scavenger receptors in the cell membrane, which induces endocytosis of the particles. Reprinted with permission from Ref. [20]. Copyright (2011) American Chemical Society.

Beyond being able to enter cells easily without transfection agents, SNAs also possess important properties for function within a cell. The SNA's dense oligonucleotide shell is capable of deactivating enzymes in close proximity to the conjugate due to the high local sodium ion concentration [79, 147]. SNA conjugates exhibit remarkable serum and intracellular stability because of their ability to deactivate many nucleases in this way [41]. This property is exceedingly important in the context of nucleic acid delivery and gene regulation because oligonucleotides are otherwise rapidly degraded by such nucleases. In buffer, the rate of degradation of SNA (duplexes) by many nucleases is ~4 times slower than that of free duplexes, primarily due to a decreased rate of hydrolysis. In

serum, however, this rate difference is drastically increased because nonspecific serum proteins can adsorb to the particles' surface, which is hypothesized to block and further inhibit nucleases from accessing the surface strands (Fig. 4.10B) [148]. Furthermore, SNA conjugates can evade proteins that recognize foreign nucleic acid material, thereby avoiding the innate immune response that would otherwise be activated by foreign nucleic acids [141]. Thus, despite the very high number of NPs that can enter the cells, the immune response (as measured by the interferon-β level) is significantly lower (~25 times lower) as compared to that of DNA transfected by conventional polymeric agents (Fig. 4.10C).

Once inside the cell, SNA conjugates can carry out tasks related to their chemically programmed oligonucleotide shell. For example, if the shell is composed of DNA targeted for mRNA, the structures can regulate gene expression via the antisense pathway [15]. RNA conjugates also have been synthesized, which can regulate gene expression through the RNAi pathway [17]. These conjugates have been shown to be extremely potent, with only picomolar concentrations needed to see knockdown in some cases. Interestingly, the knockdown of mRNA and protein levels by SNAs is more persistent than knockdown via nucleic acids delivered with cationic agents (Fig. 4.10D) [15, 17]. This is likely due to the intracellular stability of SNAs discussed above. Additionally, the stability of the nucleic acid shells allows for attachment and delivery of other chemical agents, such as metal complexes. For example, platinum(IV) prodrugs have been covalently attached to SNA–AuNPs to create a potent delivery vehicle for cisplatin [67]. Once internalized in the cells with the SNA–AuNPs, the platinum(IV) complexes are reduced to a cytotoxic Pt(II) species and released into the cytosol through reductive elimination of their axial ligands. On a per platinum basis, the Pt–SNA–AuNP conjugates were significantly more effective than cisplatin or the prodrug alone. Additionally, drugs that are not soluble and thus difficult to administer, such as Paclitaxel, can be conjugated to the SNA shell [72]. This strategy takes advantage of the high stability and high cellular uptake of SNAs. The solubility of Paclitaxel can be increased by over 50 times, and when attached to SNA–AuNP conjugates, the drug exhibits lower IC_{50} values (4–10 times) compared to free drugs. The attachment of drugs to SNAs may become a general method to deliver drugs and other chemical agents for disease applications.

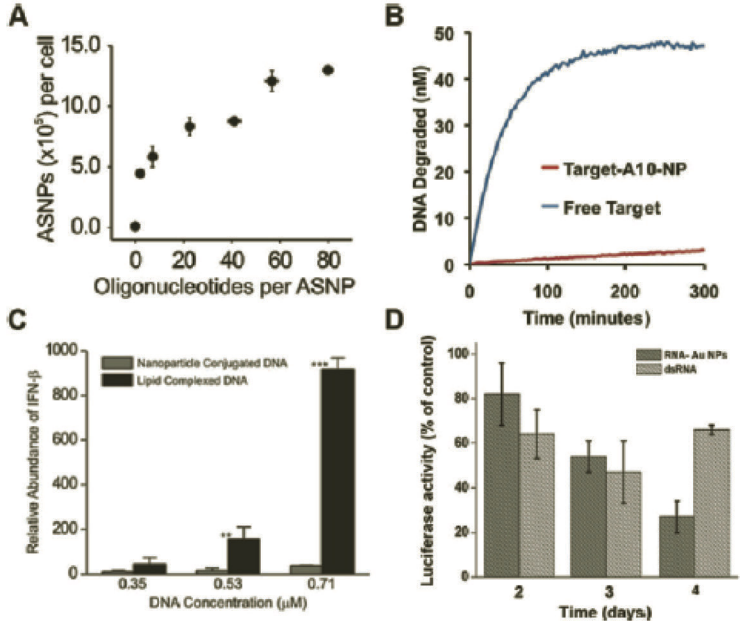

Figure 4.10 (A) Oligonucleotide density determines the cellular uptake numbers of SNA–NP conjugates; higher densities result in more particles per cell. Reprinted with permission from Ref. [74]. Copyright (2007) American Chemical Society. (B) SNAs are degraded much more slowly by nonspecific serum nucleases compared to duplexes of the same sequence. In an in vitro experiment where the concentration of nuclease was at elevated levels to shorten experimental time windows, less than 10% of the SNA duplexes were degraded after 300 min. In contrast, all of the free duplexes are completely degraded in 200 min. Reprinted with permission from Ref. [148]. Copyright (2011) American Chemical Society. (C) Relative amounts of interferon-*β* produced after transfection with SNA–AuNP conjugates and lipoplexed DNA. Reprinted with permission from Ref. [141]. Copyright (2009) American Chemical Society. (D) Gene knockdown of siRNA-based SNA conjugates is more persistent than with lipoplexed siRNA. Studies show that this effect is likely due to the higher stability of SNAs in biological media as compared to free duplexes. Reprinted with permission from Ref. [17]. Copyright (2009) American Chemical Society.

The high cellular internalization of SNAs is indeed promising for the field of gene regulation; however, their indiscriminant uptake may pose challenges for targeting in vivo. Indeed, in their present state of development they are ideal for local delivery applications where

targeting can be done at the genetic level. Unlike chemotherapy, where all cells are potentially subject to the cytotoxic effects of drugs, SNAs target the genetic expression profiles of cancerous cells only. Nevertheless, the chemical tailorability of the nucleic acid shell provides an ideal scaffold for chemical modification. For example, one can envision the covalent attachment of targeting moieties on the periphery of the shell through modified bases and bioconjugation. Alternatively, one could hybridize oligonucleotides with targeting "cargo" in a relatively straightforward fashion. SNAs can be synthesized over a range of particle sizes, which suggests that they may be tailored for specific disease types [149]. Collectively these strategies provide a blueprint for developing a wide variety of new therapeutic candidates based on SNAs. Taken together, these observations challenge the notion that one needs an auxiliary agent to deliver oligonucleotides to cells. Previous work has focused on how to tailor the carrier to be compatible with biological systems to minimize its toxicity and immunogenicity, while maximizing efficiency. Now, one can consider SNA and other 3D forms of nucleic acids as single-entity gene regulation agents, capable of freely entering a wide variety of cell lines and effecting gene regulation in a very potent manner (Fig. 4.11).

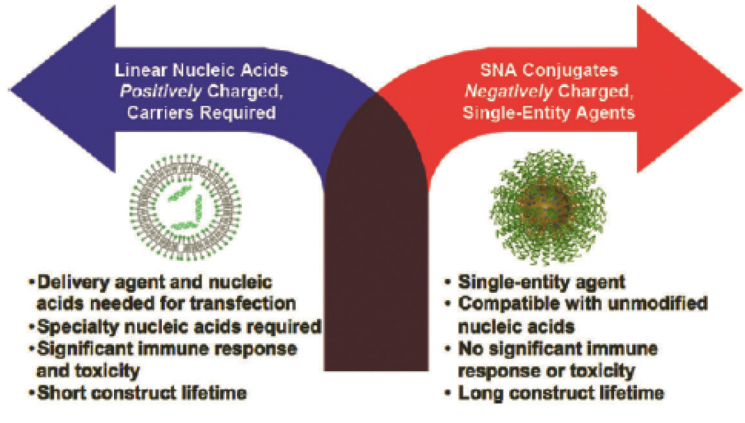

Figure 4.11 SNAs offer a different paradigm for gene regulation. Negatively charged nucleic acids do not need to be precomplexed with synthetic positively charged carriers to enter cells and effect gene regulation. If the nucleic acids are densely oriented at the nanoscale, they enter cells in high numbers, resist degradation, exhibit nuclease resistance, show no apparent toxicity, and do not activate the innate immune response.

4.10 Combined Intracellular Diagnostics and Imaging

SNAs are also leading to intracellular diagnostic and imaging tools and platforms. Fluorophore tags can be attached to them, making it straightforward to locate and image particles in cells [15]. Furthermore, by attaching gadolinium chelates to such particles, one can synthesize multimodal particles useful for magnetic resonance imaging techniques [50]. As discussed in Section 4.8, SNAs are highly specific for target sequences and can thus be used to detect and measure the concentration of over- or under-expressed mRNA in cells that may indicate disease or be representative of a particular cell state (e.g., cancerous vs. noncancerous). Static measurements of such disease markers are important; however, the ability to measure and quantify activity dynamically (e.g., in response to stimuli) on a per cell basis can give valuable information that a measurement on a bulk cell sample cannot capture. SNA conjugates provide a solution in this regard, as they can enter cells autonomously with no significant disruption to normal cellular function and they resist enzymatic degradation. Moreover, they can be designed to target only specific genes of interest (Section 4.9). In the case of AuNPs, one can take advantage of the highly efficient fluorescence quenching ability of the gold core to create a dynamic fluorophore-based "off–on" system that responds to varying levels of mRNA expression in the cell [11]. These probes, termed "nanoflares," are designed with strands complementary to disease-related mRNA (~18 bases long), such as survivin, and a fluorophore-labeled "flare" sequence (~10 bases long) that is hybridized to the particle. In this state, the fluorophore label is close to the particle surface, and its fluorescence is predominantly quenched. In the cell, the nanoflare particle encounters and binds to its complementary mRNA target, which is longer than the short flare sequence. This action displaces the flare from the particle surface and causes an increase in signal (Fig. 4.12A). One interesting aspect of the nanoflare architecture is that the short flare sequence makes the strands at the surface more rigid and pushes the mRNA complement away from the NP surface, which results in an activated binding site for the mRNA target [150]. Indeed, the kinetics of target binding to sequences with nanoflares is 5 times faster than to single-stranded SNA–AuNP conjugates of the same sequence but without flares [150]. Cells treated with flares

of the sequence complementary to the target exhibit much higher fluorescence than cells incubated with noncomplementary flares (Fig. 4.12B). Moreover, the background fluorescence of nanoflares is substantially lower than that of molecular beacons, which is due to increased nuclease resistance of the SNA-based nanoflare structure; indeed, intracellular degradation of the probe beacon leads to significant background fluorescence. Finally, nanoflares allow for simultaneous gene knockdown and mRNA detection from a single conjugate [51].

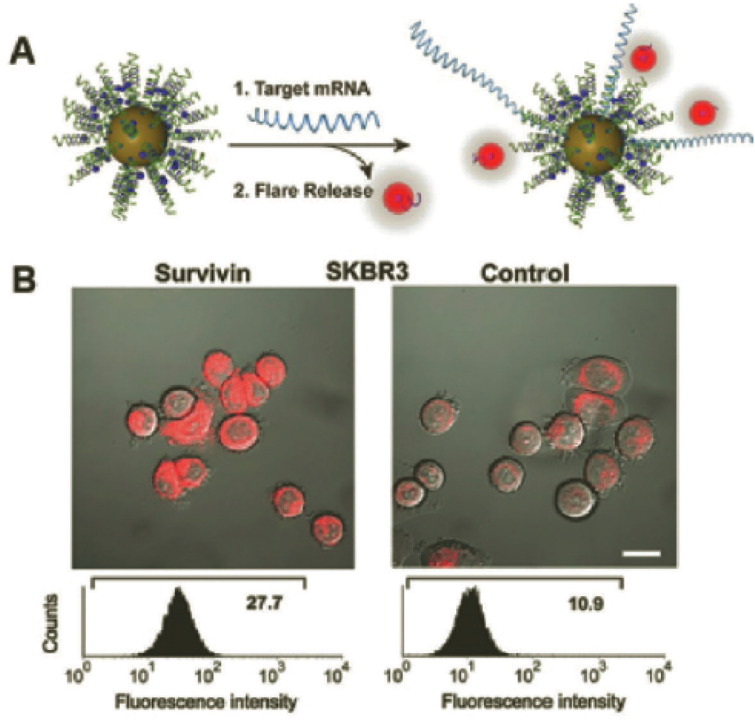

Figure 4.12 (A) Schematic of nanoflares. Short fluorophore-labeled "flare" sequences are hybridized to SNAs targeted for a disease gene of interest. Upon flare particle binding to its mRNA complement, the short flare sequence is displaced and released from the gold core. The flare is no longer quenched when it is released, and therefore a large signal increase is observed. (B) SKBR3 cells, which overexpress survivin, are treated with nanoflare probes targeted for survivin (left) and a nonsense control (right). Samples treated with the survivin flare show 3 times the fluorescence of cells treated with the control flare particles. Reprinted with permission from Ref. [11]. Copyright (2007) American Chemical Society.

One can build upon the nanoflare concept by introducing moieties that rely on other mechanisms of signal transduction or by targeting small molecules instead of mRNA. Nuclear magnetic resonance (NMR) probes have been synthesized by replacing the fluorophore moiety on the flare strand with a sequence of five NMR-active fluorine-19 (^{19}F)-modified 5-fluorouracil nucleobases. ^{19}F is a good choice for this system because fluorine is not very abundant in biological systems. In addition, ^{19}F is nearly NMR invisible when on the particle but shows a strong signal when released [151]. These probes have a high signal-to-noise ratio (~27) and show a marked increase in signal when they bind their targets. Probes can also be synthesized that target small molecules instead of DNA or RNA sequences. For example, aptamers [152] are oligonucleotides selected for binding affinity and specificity toward a target molecule, and they can be used as the recognition element on the particles to create "aptamer nanoflares" (ANFs) [125]. In a proof-of-concept system, ANFs were targeted to adenosine triphosphate (ATP) because of its importance in cellular metabolism regulation and biochemical pathways. Duplexes formed from the known ATP aptamer sequence and short complementary flare sequences were conjugated to AuNPs to form ATP-ANFs. In the presence of ATP, the ATP aptamer changes its conformation to bind ATP, which displaces the flare sequence and results in a large fluorescence increase. Significantly, ATP-ANFs can be used to quantify intracellular amounts of ATP in live cells. In principle, the nanoflare design can be tailored for many intracellular molecular targets and with many possible labeling and readout strategies. In principle, these include techniques like computed tomography and positron emission tomography. These strategies may lead to a broader impact on medicine and cancer treatments in general, including treatments specific for gene expression profiles or live small-molecule tracking within organs.

4.11 Conclusions and Outlook

SNAs have emerged as a fundamental new class of nucleic acid constructs with a set of properties distinct from linear forms of nucleic acids of the same sequence. These properties have led to powerful new concepts in materials synthesis and colloidal

crystallization and laid the foundation for important new technologies in the life sciences and medicine. They were initially made to introduce a simple concept for nanoparticle assembly whereby programmable base pairing interactions could be used to reversibly form macroscopic materials from nanoscale components. However, the discovery that the arrangement of oligonucleotides into highly oriented, densely packed spherical structures results in entities capable of interacting with biological materials in unique ways provided venues to use them in molecular diagnostics, gene regulation, and medicine. These constructs do not simply provide different ways of accomplishing what can be done with molecular systems but rather superior approaches. This is apparent in in vitro molecular diagnostics where SNA cooperative binding and subsequent melting lead to higher selectivity in assays based upon SNA probes, in gene regulation, where the densely packed and oriented nucleic acids in SNAs can support the binding of scavenger proteins, which trigger endocytosis, and in the case of nanoflares, where the ability of SNAs to freely enter cells combined with their ability to resist nuclease degradation gives rise to a powerful new class of live single-cell assays.

Significantly, the understandings garnered from the studies of SNAs as diagnostic and gene-regulating constructs brought the initial study of DNA-mediated assembly full circle through the realization of some of the key insights required for nanoparticle crystallization, which has emerged as a rich field of study in the past few years. Many researchers around the globe have made significant contributions to the field of SNAs as it continues to expand across diverse scientific and technological disciplines. However, there is still much to be learned about the fundamental properties of SNAs, their scope of utility, and the diversity of possible conjugate materials. We still do not understand their modes of intracellular trafficking at the molecular level, why they can penetrate tissues and organs much more effectively than analogous molecular systems, and how they move from cell to cell within living systems. The bulk of the technologies based upon them have focused on the life sciences, but there are significant opportunities in the areas of electronics, catalysis, and energy harvesting, storage, and conversion. The realization of such opportunities will rely on our ability to synthesize broader classes of conjugate materials. Indeed, although the majority of the work

carried out thus far has focused on SNA–AuNP conjugates, we and others have shown that SNAs can be prepared from magnetic [43], insulator [58], semiconductor [44], and metallic materials [1], and even pure DNA cores prepared by DNA origami techniques [156].

Anisotropic SNA nanostructures are just beginning to be explored, and their use as near-infrared plasmonic heating materials and surface-enhanced Raman spectroscopy labels may prove useful not only in the development of new biodiagnostic and imaging tools but also in the realization of plasmonic energy conversion materials. Because of their tailorable binding strengths, anisotropic 3D nucleic acids may find use in novel detection assays with higher sensitivities than analogous assays with SNAs. Collectively, these SNA conjugate structures, combined with a fundamental understanding of their properties, will establish a new paradigm in bioprogrammable particle design. Indeed, they should inspire new syntheses of bioconjugated nanomaterials based on the functions one can realize from the cooperative behavior of ligand shells combined with the exquisitely tailorable properties of nanomaterial cores.

Acknowledgments

C.A.M. acknowledges the DOE Office (Award No. DESC0000989) for support through the Northwestern Nonequilibrium Energy Research Center (NERC). He also acknowledges the NSF-NSEC and the AFOSR for grant support, and is grateful for an NSSEF Fellowship from the DoD. E.A. acknowledges the NDSEG for a Graduate Research Fellowship and Northwestern University for a Ryan Fellowship.

References

1. Mirkin, C. A., Letsinger, R. L., Mucic, R. C. and Storhoff, J. J. (1996). *Nature* **382**, 607–609.
2. Jain, K. K. (2003). *Exp. Rev. Mol. Diagn*. **3**, 153–161.
3. Farokhzad, O. C. and Langer, R. (2006). *Adv. Drug Delivery Rev*. **58**, 1456–1459.
4. Storhoff, J. J., Elghanian, R., Mucic, R. C., Mirkin, C. A. and Letsinger, R. L. (1998). *J. Am. Chem. Soc*. **120**, 1959–1964.
5. Taton, T. A., Mirkin, C. A. and Letsinger, R. L. (2000). *Science* **289**, 1757–1760.

6. Rosi, N. L. and Mirkin, C. A. (2005). *Chem. Rev*. **105**, 1547–1562.
7. Weiss, S., Bruchez, M., Moronne, M., Gin, P. and Alivisatos, A. P. (1998). *Science* **281**, 2013–2016.
8. Morrow, D. A., Wilson, S. R., Sabatine, M. S., Braunwald, E., Sloan, S. and Murphy, S. A. (2009). *Am. Heart J*. **158**, 386–391.
9. Verma, A., Simard, J. M., Worrall, J. W. and Rotello, V. M. (2004). *J. Am. Chem. Soc*. **126**, 13987–13991.
10. Xu, X. H. N., Kyriacou, S. V. and Brownlow, W. J. (2004). *Biochemistry* **43**, 140–147.
11. Seferos, D. S., Giljohann, D. A., Hill, H. D., Prigodich, A. E. and Mirkin, C. A. (2007). *J. Am. Chem. Soc*. **129**, 15477–15479.
12. Giljohann, D. A., Seferos, D. S., Daniel, W. L., Massich, M. D., Patel, P. C. and Mirkin, C. A. (2010). *Angew. Chem. Int. Ed*. **49**, 3280–3294.
13. Sandhu, K. K., McIntosh, C. M., Simard, J. M., Smith, S. W. and Rotello, V. M. (2002). *Bioconjugate Chem*. **13**, 3–6.
14. Lehr, C. M., Kumar, M. N. V. R., Sameti, M., Mohapatra, S. S., Kong, X., Lockey, R. F., Bakowsky, U., Lindenblatt, G. and Schmidt, H. (2004). *J. Nanosci. Nanotechnol*. **4**, 876–881.
15. Rosi, N. L., Giljohann, D. A., Thaxton, C. S., Lytton-Jean, A. K. R., Han, M. S. and Mirkin, C. A. (2006). *Science* **312**, 1027–1030.
16. von Maltzahn, G., Park, J. H., Lin, K. Y., Singh, N., Schwoppe, C., Mesters, R., Berdel, W. E., Ruoslahti, E., Sailor, M. J. and Bhatia, S. N. (2011). *Nat. Mater*. **10**, 545–552.
17. Giljohann, D. A., Seferos, D. S., Prigodich, A. E., Patel, P. C. and Mirkin, C. A. (2009). *J. Am. Chem. Soc*. **131**, 2072–2073.
18. Davis, M. E., Chen, Z. and Shin, D. M. (2008). *Nat. Rev. Drug Discov*. **7**, 771–782.
19. Dobson, J. (2006). *Gene Ther*. **13**, 283–287.
20. Cutler, J. I., Zhang, K., Zheng, D., Auyeung, E., Prigodich, A. E. and Mirkin, C. A. (2011). *J. Am. Chem. Soc*. **133**, 9254–9257.
21. Leff, D. V., Brandt, L. and Heath, J. R. (1996). *Langmuir* **12**, 4723–4730.
22. Kataby, G., Cojocaru, M., Prozorov, R. and Gedanken, A. (1999). *Langmuir* **15**, 1703–1708.
23. Johnson, S. R., Evans, S. D. and Brydson, R. (1998). *Langmuir* **14**, 6639–6647.
24. Zheng, W., Maye, M. M., Leibowitz, F. L. and Zhong, C.-J. (1999). *Analyst* **125**, 17–20.

25. Galow, T., Boal, A. and Rotello, V. (2000). *Adv. Mater*. **12**, 576–579.
26. Dubois, L. H. and Nuzzo, R. G. (1992). *Annu. Rev. Phys. Chem*. **43**, 437–463.
27. Bain, C. D. and Whitesides, G. M. (1989). *Angew. Chem., Int. Ed*. **28**, 506–512.
28. Mucic, R. C., Herrlein, M. K., Mirkin, C. A. and Letsinger, R. L. (1996). *Chem. Commun*. 555–557.
29. Alivisatos, A. P., Johnsson, K. P., Peng, X. G., Wilson, T. E., Loweth, C. J., Bruchez, M. P. and Schultz, P. G. (1996). *Nature* **382**, 609–611.
30. Sonnichsen, C., Reinhard, B. M., Liphardt, J. and Alivisatos, A. P. (2005). *Nat. Biotechnol*. **23**, 741–745.
31. Liu, N., Hentschel, M., Weiss, T., Alivisatos, A. P. and Giessen, H. (2011). *Science* **332**, 1407–1410.
32. Luger, K., Mader, A. W., Richmond, R. K., Sargent, D. F. and Richmond, T. J. (1997). *Nature* **389**, 251–260.
33. Fei, J., Richard, A. C., Bronson, J. E. and Gonzalez, R. L. (2011). *Nat. Struct. Mol. Biol*. **18**, 1043–1051.
34. Bansal, M. and Ghosh, A. (2003). *Acta. Crystallogr. D* **59**, 620–626.
35. Dean, D. A., Vaughan, E. E. and DeGiulio, J. V. (2006). *Curr*. *Gene Ther*. **6**, 671–681.
36. Seeman, N. C. (2003). *Nature* **421**, 427–431.
37. Seeman, N. (1999). *Trends Biotechnol*. **17**, 437–443.
38. Han, D., Pal, S., Nangreave, J., Deng, Z., Liu, Y. and Yan, H. (2011). *Science* **332**, 342–346.
39. Lytton-Jean, A. K. R. and Mirkin, C. A. (2005). *J. Am. Chem. Soc*. **127**, 12754–12755.
40. Jin, R. C., Wu, G. S., Li, Z., Mirkin, C. A. and Schatz, G. C. (2003). *J. Am. Chem. Soc*. **125**, 1643–1654.
41. Seferos, D. S., Prigodich, A. E., Giljohann, D. A., Patel, P. C. and Mirkin, C. A. (2009). *Nano Lett*. **9**, 308–311.
42. Lee, J. S., Lytton-Jean, A. K. R., Hurst, S. J. and Mirkin, C. A. (2007). *Nano Lett*. **7**, 2112–2115.
43. Cutler, J. I., Zheng, D., Xu, X. Y., Giljohann, D. A. and Mirkin, C. A. (2010). *Nano Lett*. **10**, 1477–1480.
44. Mitchell, G. P., Mirkin, C. A. and Letsinger, R. L. (1999). *J. Am. Chem. Soc*. **121**, 8122–8123.

45. Han, M. Y. and Liu, S. H. (2005). *Adv. Funct. Mater*. **15**, 961–967.

46. Stoeva, S. I., Huo, F. W., Lee, J. S. and Mirkin, C. A. (2005). *J. Am. Chem. Soc*. **127**, 15362–15363.

47. Li, Z., Zhang, Y., Fullhart, P. and Mirkin, C. A. (2004). *Nano Lett*. **4**, 1055–1058.

48. Liu, H. P., Zhu, Z., Kang, H. Z., Wu, Y. R., Sefan, K. and Tan, W. H. (2010). *Chem.–Eur. J*. **16**, 3791–3797.

49. Redl, F. X., Black, C. T., Papaefthymiou, G. C., Sandstrom, R. L., Yin, M., Zeng, H., Murray, C. B. and O'Brien, S. P. (2004). *J. Am. Chem. Soc*. **126**, 14583–14599.

50. Keefe, A. D. and Wilson, C. (2006). *Curr. Opin. Chem. Biol*. **10**, 607–614.

51. Prigodich, A. E., Seferos, D. S., Massich, M. D., Giljohann, D. A., Lane, B. C. and Mirkin, C. A. (2009). *ACS Nano* **3**, 2147–2152.

52. Seferos, D. S., Giljohann, D. A., Rosi, N. L. and Mirkin, C. A. (2007). *ChemBioChem* **8**, 1230–1232.

53. Li, Z., Jin, R. C., Mirkin, C. A. and Letsinger, R. L. (2002). *Nucleic Acids Res*. **30**, 1558–1562.

54. Sato, K., Hosokawa, K. and Maeda, M. (2003). *J. Am. Chem. Soc*. **125**, 8102–8103.

55. Frens, G. (1973). *Nature Phys. Sci*. **241**, 20–22.

56. Park, S. Y., Lytton-Jean, A. K. R., Lee, B., Weigand, S., Schatz, G. C. and Mirkin, C. A. (2008). *Nature* **451**, 553–556.

57. Nykypanchuk, D., Maye, M. M., van der Lelie, D. and Gang, O. (2008). *Nature* **451**, 549–552.

58. Xue, C., Chen, X., Hurst, S. J. and Mirkin, C. A. (2007). *Adv. Mater*. **19**, 4071–4072.

59. Cao, Y. W., Jin, R. and Mirkin, C. A. (2001). *J. Phys. Chem. B* **123**, 7961–7962.

60. Yin, Y. D., Li, Z. Y., Zhong, Z. Y., Gates, B., Xia, Y. N. and Venkateswaran, S. (2002). *J. Mater. Chem*. **12**, 522–527.

61. Medintz, I. L., Berti, L., Pons, T., Grimes, A. F., English, D. S., Alessandrini, A., Facci, P. and Mattoussi, H. (2007). *Nano Lett*. **7**, 1741–1748.

62. Dougan, J. A., Karlsson, C., Smith, W. E. and Graham, D. (2007). *Nucleic Acids Res*. **35**, 3668–3675.

63. Letsinger, R. L., Elghanian, R., Viswanadham, G. and Mirkin, C. A. (2000). *Bioconjugate Chem*. **11**, 289–291.

64. Hurst, S. J., Lytton-Jean, A. K. R. and Mirkin, C. A. (2006). *Anal. Chem*. **78**, 8313–8318.

65. McKenzie, F., Faulds, K. and Graham, D. (2007). *Small* **3**, 1866–1868.

66. Lytton-Jean, A. K. R., Gibbs-Davis, J. M., Long, H., Schatz, G. C., Mirkin, C. A. and Nguyen, S. T. (2009). *Adv. Mater*. **21**, 706–707.

67. Dhar, S., Daniel, W. L., Giljohann, D. A., Mirkin, C. A. and Lippard, S. J. (2010). *J. Am. Chem. Soc*. **132**, 17335–17335.

68. Song, Y., Xu, X. Y., MacRenaris, K. W., Zhang, X. Q., Mirkin, C. A. and Meade, T. J. (2009). *Angew. Chem. Int. Ed*. **48**, 9143–9147.

69. Xu, X. Y., Daniel, W. L., Wei, W. and Mirkin, C. A. (2010). *Small* **6**, 623–626.

70. Nam, J. M., Thaxton, C. S. and Mirkin, C. A. (2003). *Science* **301**, 1884–1886.

71. Kim, D., Daniel, W. L. and Mirkin, C. A. (2009). *Anal. Chem*. **81**, 9183–9187.

72. Zhang, X.-Q., Xu, X., Lam, R., Giljohann, D., Ho, D. and Mirkin, C. A. (2011). *ACS Nano* **5**, 6962–6970.

73. Elghanian, R., Storhoff, J. J., Mucic, R. C., Letsinger, R. L. and Mirkin, C. A. (1997). *Science* **277**, 1078–1081.

74. Giljohann, D. A., Seferos, D. S., Patel, P. C., Millstone, J. E., Rosi, N. L. and Mirkin, C. A. (2007). *Nano Lett*. **7**, 3818–3821.

75. Hill, H. D., Millstone, J. E., Banholzer, M. J. and Mirkin, C. A. (2009). *ACS Nano* **3**, 418–424.

76. Storhoff, J. J., Elghanian, R., Mirkin, C. A. and Letsinger, R. L. (2002). *Langmuir* **18**, 6666–6670.

77. Taton, T. A., Mucic, R. C., Mirkin, C. A. and Letsinger, R. L. (2000). *J. Am. Chem. Soc*. **122**, 6305–6306.

78. Wang, H., Xu, W., Zhang, H., Li, D., Yang, Z., Xie, X., Li, T. and Liu, X. (2011). *Small* **7**, 1987–1992.

79. Zwanikken, J. W., Guo, P. J., Mirkin, C. A. and de la Cruz, M. O. (2011). *J. Phys. Chem. C* **115**, 16368–16373.

80. Gibbs-Davis, J. M., Nguyen, S. T. and Schatz, G. C. (2007). *J. Am. Chem. Soc*. **129**, 15535–15540.

81. Park, S. Y., Gibbs-Davis, J. M., Nguyen, S. B. T. and Schatz, G. C. (2007). *J. Phys. Chem. B* **111**, 8785–8791.

82. Eryazici, I., Prytkova, T. R., Schatz, G. C. and Nguyen, S. T. (2010). *J. Am. Chem. Soc*. **132**, 17068–17070.

83. Stepp, B. R., Gibbs-Davis, J. M., Koh, D. L. F. and Nguyen, S. T. (2008). *J. Am. Chem. Soc*. **130**, 9628–9629.
84. Millstone, J. E., Georganopoulou, D. G., Xu, X. Y., Wei, W., Li, S. Y. and Mirkin, C. A. (2008). *Small* **4**, 2176–2180.
85. Jones, M. R., Macfarlane, R. J., Lee, B., Zhang, J., Young, K. L., Senesi, A. J. and Mirkin, C. A. (2010). *Nat. Mater*. **9**, 913–917.
86. Hurst, S. J., Hill, H. D. and Mirkin, C. A. (2008). *J. Am. Chem. Soc*. **130**, 12192–12200.
87. Wu, Z. S., Guo, M. M., Shen, G. L. and Yu, R. Q. (2007). *Anal. Bioanal. Chem*. **387**, 2623–2626.
88. Hurst, S. J., Hill, H. D., Macfarlane, R. J., Wu, J., Dravid, V. P. and Mirkin, C. A. (2009). *Small* **5**, 2156–2161.
89. Park, S. J., Lazarides, A. A., Storhoff, J. J., Pesce, L. and Mirkin, C. A. (2004). *J. Phys. Chem. B* **108**, 12375–12380.
90. Huo, F. W., Lytton-Jean, A. K. R. and Mirkin, C. A. (2006). *Adv. Mater*. **18**, 2304–2305.
91. Xu, X. Y., Rosi, N. L., Wang, Y. H., Huo, F. W. and Mirkin, C. A. (2006). *J. Am. Chem. Soc*. **128**, 9286–9287.
92. Maye, M. M., Nykypanchuk, D., Cuisinier, M., van der Lelie, D. and Gang, O. (2009). *Nat. Mater*. **8**, 388–391.
93. Park, S. Y., Lytton-Jean, A. K. R., Lee, B., Weigand, S., Schatz, G. C. and Mirkin, C. A. (2008). *Nature* **451**, 553–556.
94. Nykypanchuk, D., Maye, M. M., Lelie, D. v. d. and Gang, O. (2008). *Nature* **451**, 549–552.
95. Macfarlane, R. J., Lee, B., Jones, M. R., Harris, N., Schatz, G. C. and Mirkin, C. A. (2011). *Science* **334**, 204–208.
96. Macfarlane, R. J., Jones, M. R., Senesi, A. J., Young, K. L., Lee, B., Wu, J. and Mirkin, C. A. (2010). *Angew. Chem. Int. Ed*. **49**, 4589–4592.
97. Xiong, H., Lelie, D. v. d. and Gang, O. (2009). *Phys. Rev. Lett*. **102**, 1–4.
98. Hill, H. D., Macfarlane, R. J., Senesi, A. J., Lee, B., Park, S. Y. and Mirkin, C. A. (2008). *Nano Lett*. **8**, 2341–2344.
99. Sun, D. and Gang, O. (2011). *J. Am. Chem. Soc*. **133**, 5252–5254.
100. Pauling, L. (1929). *J. Am. Chem. Soc*. **51**, 1010–1026.
101. Xia, Y. N., Xiong, Y. J., Lim, B. and Skrabalak, S. E. (2009). *Angew. Chem. Int. Ed*. **48**, 60–103.
102. Jones, M. R., Osberg, K. D., Macfarlane, R. J., Langille, M. R. and Mirkin, C. A. (2011). *Chem. Rev*. **111**, 3736–3827.

103. Odom, T. W. and Nehl, C. L. (2008). *ACS Nano* **2**, 612–616.
104. Kelly, K. L., Coronado, E., Zhao, L. L. and Schatz, G. C. (2003). *J. Phys. Chem. B* **107**, 668–677.
105. Dick, K. A., Deppert, K., Larsson, M. W., Martensson, T., Seifert, W., Wallenberg, L. R. and Samuelson, L. (2004). *Nat. Mater*. **3**, 380–384.
106. Hyeon, T., Park, S. J., Kim, S., Lee, S., Khim, Z. G. and Char, K. (2000). *J. Am. Chem. Soc*. **122**, 8581–8582.
107. Nikoobakht, B. and El-Sayed, M. A. (2003). *Chem. Mater*. **15**, 1957–1962.
108. Millstone, J. E., Park, S., Shuford, K. L., Qin, L. D., Schatz, G. C. and Mirkin, C. A. (2005). *J. Am. Chem. Soc*. **127**, 5312–5313.
109. Smith, D. K. and Korgel, B. A. (2008). *Langmuir* **24**, 644–649.
110. Poon, L., Zandberg, W., Hsiao, D., Erno, Z., Sen, D., Gates, B. D. and Branda, N. R. (2010). *ACS Nano* **4**, 6395–6403.
111. Jones, M. R., Millstone, J. E., Giljohann, D. A., Seferos, D. S., Young, K. L. and Mirkin, C. A. (2009). *ChemPhysChem*. **10**, 1461–1465.
112. Wijaya, A., Schaffer, S. B., Pallares, I. G. and Hamad-Schifferli, K. (2009). *ACS Nano* **3**, 80–86.
113. Huschka, R., Zuloaga, J., Knight, M. W., Brown, L. V., Nordlander, P. and Halas, N. J. (2011). *J. Am. Chem. Soc*. **133**, 12247–12255.
114. Lee, S. E., Liu, G. L., Kim, F. and Lee, L. P. (2009). *Nano Lett*. **9**, 562–570.
115. Jones, M. R., Macfarlane, R. J., Prigodich, A. E., Patel, P. C. and Mirkin, C. A. (2011). *J. Am. Chem. Soc*. **133**, 18865–18869.
116. Han, M. S., Lytton-Jean, A. K. R., Oh, B. K., Heo, J. and Mirkin, C. A. (2006). *Angew. Chem. Int. Ed*. **45**, 1807–1810.
117. Liu, C. W., Hsieh, Y. T., Huang, C. C., Lin, Z. H. and Chang, H. T. (2008). *Chem. Commun*. 2242–2244.
118. Lander, E. S., Altshuler, D., Pollara, V. J., Cowles, C. R., Van Etten, W. J., Baldwin, J. and Linton, L. (2000). *Nature* **407**, 513–516.
119. Zheng, G. F., Daniel, W. L. and Mirkin, C. A. (2008). *J. Am. Chem. Soc*. **130**, 9644–9645.
120. Liu, J. W. and Lu, Y. (2006). *Angew. Chem. Int. Ed*. **45**, 90–94.
121. Xu, X., Han, M. S. and Mirkin, C. A. (2007). *Angew. Chem. Int. Ed*. **46**, 3468–3470.
122. Han, M. S., Lytton-Jean, A. K. R., Oh, B. K., Heo, J. and Mirkin, C. A. (2006). *Angew. Chem. Int. Ed*. **45**, 1807–1810.
123. Lee, J. S., Han, M. S. and Mirkin, C. A. (2007). *Angew. Chem. Int. Ed*. **46**, 4093–4096.

124. Liu, J. and Lu, Y. (2003). *J. Am. Chem. Soc*. **125**, 6642–6643.

125. Lu, Y. and Liu, J. W. (2004). *J. Am. Chem. Soc*. **126**, 12298–12305.

126. Wang, Z. D., Lee, J. H. and Lu, Y. (2008). *Adv. Mater*. **20**, 3263–3267.

127. Perez, J. M., O'Loughin, T., Simeone, F. J., Weissleder, R. and Josephson, L. (2002). *J. Am. Chem. Soc*. **124**, 2856–2857.

128. Graham, D., Thompson, D. G., Smith, W. E. and Faulds, K. (2008). *Nat. Nanotechnol*. **3**, 548–551.

129. Nam, J.-M., Thaxton, C. S. and Mirkin, C. A. (2003). *Science* **301**, 1884–1886.

130. Nam, J. M., Stoeva, S. I. and Mirkin, C. A. (2004). *J. Am. Chem. Soc*. **126**, 5932–5933.

131. Fire, A., Xu, S. Q., Montgomery, M. K., Kostas, S. A., Driver, S. E. and Mello, C. C. (1998). *Nature* **391**, 806–811.

132. Pardridge, W. M., Zhang, Y. and Schlachetzki, F. (2003). *Mol. Ther*. **7**, 11–18.

133. Pardridge, W. M., Zhang, Y. and Zhu, C. N. (2002). *Mol. Ther*. **6**, 67–72.

134. Herr, A. E., Tia, S. Q., He, M. and Kim, D. (2011). *Anal. Chem*. **83**, 3581–3588.

135. Mintzer, M. A. and Simanek, E. E. (2009). *Chem. Rev*. **109**, 259–302.

136. Kim, D., Halpern, A. R., Chen, Y. L. and Corn, R. M. (2011). *Anal. Chem*. **83**, 2801–2806.

137. Young, L. S., Searle, P. F., Onion, D. and Mautner, V. (2006). *J. Pathol*. **208**, 299–318.

138. Shenoy, D. B. and Amiji, M. M. (2007). *CSH Protoc*. No. pdb.top9.

139. Xia, F., Zuo, X. L., Yang, R. Q., Xiao, Y., Kang, D., Vallee-Belisle, A., Gong, X., Yuen, J. D., Hsu, B. B. Y., Heeger, A. J. and Plaxco, K. W. (2010). *Proc. Natl. Acad. Sci. U.S.A*. **107**, 10837–10841.

140. Liu, J. W. and Lu, Y. (2004). *Chem. Mater*. **16**, 3231–3238.

141. Massich, M. D., Giljohann, D. A., Seferos, D. S., Ludlow, L. E., Horvath, C. M. and Mirkin, C. A. (2009). *Mol. Pharmaceutics* **6**, 1934–1940.

142. Han, M. S., Ryou, S. M., Kim, S., Jang, H. H., Kim, J. H., Yeom, J. H., Eom, M. S., Bae, J. and Lee, K. (2010). *Biochem. Biophys. Res. Commun*. **398**, 542–546.

143. Chithrani, B. D., Ghazani, A. A. and Chan, W. C. W. (2006). *Nano Lett*. **6**, 662–668.

144. Matsumoto, A. (1990). *Proc. Natl. Acad. Sci. U.S.A*. **87**, 9133–9137.

145. Greaves, D. R. and Gordon, S. (2005). *J. Lipid Res*. **46**, 11–20.

146. Bijsterbosch, M. K., Manoharan, M., Rump, E. T., DeVrueh, R. L. A., vanVeghel, R., Tivel, K. L., Biessen, E. A. L., Bennett, C. F., Cook, P. D. and vanBerkel, T. J. C. (1997). *Nucleic Acids Res*. **25**, 3290–3296.

147. Schatz, G. C. and Lee, O. S. (2009). *J. Phys. Chem. C* **113**, 2316–2321.

148. Prigodich, A. E., Alhasan, A. H. and Mirkin, C. A. (2011). *J. Am. Chem. Soc*. **133**, 2120–2123.

149. De Jong, W. H., Hagens, W. I., Krystek, P., Burger, M. C., Sips, A. J. A. M. and Geertsma, R. E. (2008). *Biomaterials* **29**, 1912–1919.

150. Prigodich, A. E., Lee, O. S., Daniel, W. L., Seferos, D. S., Schatz, G. C. and Mirkin, C. A. (2010). *J. Am. Chem. Soc*. **132**, 10638–10641.

151. Kieger, A., Wiester, M. J., Procissi, D., Parrish, T. B., Mirkin, C. A. and Thaxton, C. S. (2011). *Small* **7**, 1977–1981.

152. Ellington, A. D. and Szostak, J. W. (1990). *Nature* **346**, 818–822.

153. Auyeung, E., Cutler, J. I., Macfarlane, R. J., Jones, M. R., Wu, J., Liu, G., Zhang, K., Osberg, K. D. and Mirkin, C. A. (2012). *Nature Nanotech*. **7**, 24–28.

154. Georganopoulou, D. G., Chang, L., Nam, J.-M., Thaxton, C. S., Mufson, E. J., Klein, W. L. and Mirkin, C. A. (2005). *Proc. Natl. Acad. Sci. U.S.A*. **102**, 2273–2276.

155. Thaxton, C. S., Elghanian, R., Thomas, A. D., Stoeva, S. I., Lee, J.-S., Smith, N. D., Schaeffer, A. J., Klocker, H., Horninger, W., Bartsch, G. and Mirkin, C. A. (2009). *Proc. Natl. Acad. Sci. U.S.A*. **106**, 18437–18442.

156. Walsh, S. A., Yin, H., Erben, C. M., Wood, M. J. A. and Tuberfield, A. J. (2011). *ACS Nano* **5**, 5427–5432.

Chapter 5

Nucleic Acid-Modified Nanostructures as Programmable Atom Equivalents: Forging a New "Table of Elements"*

Robert J. Macfarlane, Matthew N. O'Brien, Sarah Hurst Petrosko, and Chad A. Mirkin
Department of Chemistry, Northwestern University, 2145 Sheridan Road, Evanston, IL 60208, USA
International Institute for Nanotechnology, Northwestern University, 2145 Sheridan Road, Evanston, IL 60208, USA
chadnano@northwestern.edu

5.1 Introduction

The establishment of the Periodic Table of the elements almost 150 years ago was the first step towards transforming how scientists organized and understood the elemental building blocks of matter. Before its introduction, elements were viewed as separate and

*Reproduced with permission from Macfarlane, R. J., O'Brien, M. N., Petrosko, S. H. and Mirkin, C. A. (2013). Nucleic acid-modified nanostructures as programmable atom equivalents: forging a new "table of elements," *Angew. Chem. Int. Ed.* **52**, 5688–5698. Copyright © 2013, John Wiley and Sons.

Spherical Nucleic Acids, Volume 1
Edited by Chad A. Mirkin

ISBN 978-981-4800-35-8 (Hardcover), 978-0-429-20015-1 (eBook)
www.jennystanford.com

independent entities, each with their own unique set of properties. By arranging elements based upon their characteristics, the Periodic Table enabled scientists to understand their behavior as members of collective sets. Their properties could be discussed in the context of logical trends, and these trends could be used to predict the properties of as-of-yet undiscovered elements and yet-to-be synthesized molecules, bulk materials, and extended lattice structures. Indeed, for decades the Periodic Table has served as a guide for the synthesis of new structures and given us a framework to understand important scientific advances.

Today, the field of nanoscience and nanotechnology offers scientists new ways to think about materials synthesis. Nanoscience is an interdisciplinary field focused on the synthesis, manipulation, characterization, and application of structures with at least one dimension on the 1 to 100 nm length scale. In this size regime, materials possess properties that are significantly different than their macroscopic analogues, and these properties are highly dependent on the nanostructure's composition, size, shape, and local environment [1–7]. In 2000, with the introduction of the National Nanotechnology Initiative (NNI) [8], nanoscience research and development were prioritized in the United States, and since then US scientists and other researchers around the globe have devised myriad methodologies to generate nanoparticles of many compositions (e.g., metallic [3, 9], semiconducting [10–12], insulating [13], carbon-based [14], polymeric [15–17]) in high yield in the solid, solution, and gas phases, as well as on surfaces. Several methods also have been introduced to tune the size and shape of nanoparticles with nanometer precision [18–22], and to couple materials of different compositions together to create hybrid structures (e.g., alloys [23], core–shell structures [24, 25]). These new nanoparticles have a variety of interesting chemical and physical properties, which have been applied in a range of fields from catalysis [26, 27] to biomedicine [28–30] to energy [31]. This explosion in research aimed at discovering, understanding, and refining nanoparticle syntheses to realize highly sophisticated nanoscale architectures can be likened to the early rush in chemistry to discover new elements.

A key area of nanotechnology research deals with the assembly of these building blocks into more complex structures [18, 32–41], just as the discovery of different elements led to the synthesis

of many new materials. Although analogues consisting of small clusters of nanoparticles have also been developed, we will focus herein primarily on extended networks [18, 42–46]. In many cases, these assemblies have been shown to exhibit novel and extremely useful emergent properties [18, 26, 40, 41] that are a direct result of the arrangement of the individual nanostructures within the assembly. As a result of these promising but nascent discoveries with nanoparticle-based constructs, there has been intense interest in devising strategies that can be used to organize nanoparticles of all types into well-defined hierarchical arrays, in which the spacing and symmetry between the particles are precisely controlled. Indeed, one of the main challenges currently facing nanoscience researchers is the development of a methodology whereby nanoparticles can be thought of as "atom equivalents," in which bonding interactions between particles are just as well understood and characterized as those between atoms in molecules and solid-state lattices. The development of such a methodology would open the door to more rigorous explanation and understanding of the emergent properties of assemblies based upon these atom-equivalent structures.

It is important to note that we use the term "atom equivalent" when referring to the use of nanoparticles as building blocks, rather than the often used term "artificial atom," which has different meanings across scientific disciplines. Historically, "artificial atom" has referred to a metal or semiconductor nanoparticle whose electrons are confined into discrete states by its physical size or an applied electric field, thereby mimicking the quantized energy states of electrons found in atoms [47–49]. Coupling between the discrete electronic states of "artificial atoms" leads to the formation of extended states, as with atoms, which are described as "artificial bonds." However, while this analogy provides significant insight into the electronic properties of discrete nanoparticles and their assemblies, it fails in the context of forming materials, as nanoparticles alone do not inherently have the necessary components to create physical bonds between themselves in a controllable manner.

In 1996, we introduced the concept of a nucleic acid-nanoparticle conjugate that could be used as a "programmable atom equivalent" (PAE) to build higher ordered materials through deliberately designed hybridization events [32]. Initial research focused both on developing these constructs and understanding their fundamental

behavior [33–36], as well as applications in small molecule and biomolecule sensing and diagnostics [50–56]. More recently, they have also proven useful in the context of therapeutics and intracellular diagnostics [57–59].

Table 5.1 The design rules for PAE assembly

Rule 1:	PAEs will arrange themselves in a lattice that maximizes the number of DNA duplex bonds formed.
Rule 2:	PAEs of equal hydrodynamic radii will form an FCC lattice when using self-complementary DNA sequences, and BCC or CsCl lattices when using two PAEs with complementary DNA sequences.
Rule 3:	The overall hydrodynamic radius of a PAE, rather than the sizes of its individual NP or oligonucleotide components, dictates its assembly and packing behavior.
Rule 4:	In a binary system based upon complementary PAEs, favored products will tend to have equivalent numbers of each complementary DNA sequence, evenly spaced throughout a unit cell.
Rule 5:	Two systems with the same size ratio and DNA linker ratio exhibit the same thermodynamic product.
Rule 6:	PAEs can be functionalized with more than one oligonucleotide bonding element, providing access to crystal structures not possible with single element PAEs.
Rule 7:	The crystal symmetry of a lattice is dictated by the position of the inorganic cores; a PAE with no inorganic core can be used to "delete" a particle at a specified position within a unit cell.
Rule 8:	PAEs based upon anisotropic particles with flat faces can be used to realize valency and will assemble into a lattice that maximizes the amount of parallel, face-to-face interactions between particles.

Since the initial development of the nucleic acid-nanoparticle conjugate, we and other research groups have made significant synthetic advances that have allowed us to create nanoparticle superlattices of multiple distinct crystalline symmetries with sub-nanometer control over their lattice parameters [60–63]. We have even developed a set of design rules [37] analogous to Pauling's Rules for ionic solids [64] that can be used as a guide for the rational construction of functional nanoparticle-based materials

with specific structures (Table 5.1). Unlike atoms, however, which have a fixed set of properties and bonding possibilities dictated by their inherent electronic structure, the properties and bonding behaviors of PAEs can be tuned by manipulating their structure over a wide range of possibilities. These design possibilities allow for the development of nanoparticle-based materials that have exotic and versatile structures, properties, and functions.

Although structures built via DNA origami [65–68] are sometimes compared to the PAE superlattices that will be discussed herein (both utilize DNA base pairing to build nanostructured materials), these two fields are actually quite distinct. DNA origami is defined as "*the process in which ... DNA molecules are folded into arbitrary nanostructures*" [69]; the DNA in these structures is both the assembly agent and the functional material being assembled. In the PAE lattices discussed herein, the DNA acts only as a synthetically programmable "glue," used to dictate how nanoparticles are positioned next to one another, and is not typically used outside of its regular linear duplex form. The final nanoparticle superlattice therefore is defined not by the positions or arrangement of DNA strands, but rather by the positions of the inorganic cores. DNA origami is more like line-drawing, where the DNA outlines the edges (or in some cases the faces) of the object being constructed. Therefore, although significant advances have been made in the field of DNA origami, this Essay will not further discuss this area of research.

To more rationally think about our rapidly growing knowledge of nanoparticle superlattice design and synthesis, we often liken the nanoparticle-based PAEs to elements that fill the Periodic Table. However, PAEs are defined according to their nanoscale architectural features (e.g., composition, size, shape, and surface functionality; Fig. 5.1) as opposed to their electronic properties. Although the Periodic Table of the elements is marked by incremental, stepwise changes in atomic properties, the table of PAEs is marked by a continuum of structures along multiple axes. Using this table as a guide, we discuss the design considerations associated with using nucleic acids to assemble PAEs into superlattices. Further, we compare these materials with their atomic analogues, as many aspects of the nanoparticle-based system parallel the atomic system and offer a new way of looking at fundamental concepts in chemistry (such as bonding, valency, lattice packing, phase, and

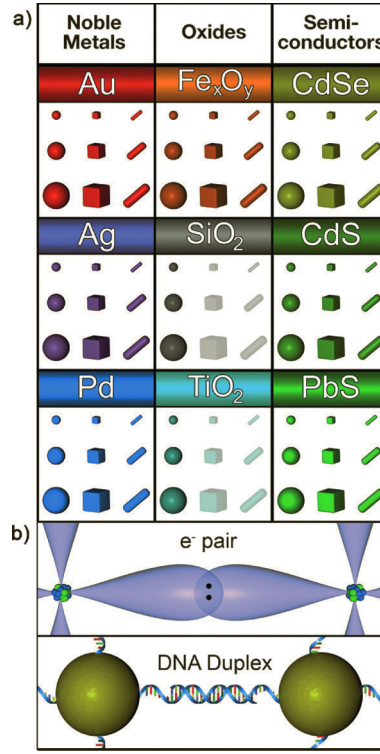

Figure 5.1 (a) The table of "programmable atom equivalents" arranges nucleic acid–nanoparticle conjugates across multiple dimensions: composition, shape, and size. In reality, this table extends nearly infinitely in the size dimension within the nanoscale regime, and for many material compositions, further into the shape dimension. Not all particles in this nanoscale 'periodic table' have been experimentally realized, and some (semi-transparent images in the table) represent potential building blocks that may be discovered in future synthetic efforts. This table merely presents a representative concept to demonstrate that the table of PAEs has an inherently larger number of variables than the corresponding Periodic Table of the elements, rather than imply that there is a specific relationship between different blocks in the table. Thus, it is best used as an empirical guide to aid in materials development, rather than an inherent representation of the intrinsic properties and characteristics of these materials. (b) The core composition and manner of bonding are compared between atoms and PAEs. Note that the comparison being drawn is only in the structural sense—DNA strands are the "glue" holding the nanoparticles in place and are not expected to directly mimic all of the inherent properties of electrons (such as band structure or orbital shape). In this sense, bonds between spherical PAEs could be considered more analogous to metallic-type bonds, while more covalent-like interactions can be observed by imparting anisotropy to nanoparticle interactions.

even impurities and doping). Our specific purpose herein is not to recreate the Periodic Table and replace its constituent parts with nanoparticles, but rather to use the analogy to help understand the similarities and differences between synthesizing extended matter with atomic and nanoparticle-based building blocks, respectively. The Periodic Table is a man-made arrangement designed to aid in understanding the behavior of naturally occurring structures that have inherent and unchangeable properties. In contrast, organizing nanoparticle-based PAEs according to structural feature enables one to realize both the continuum of nanostructures that can be created, as well as the necessity of developing a means to rationally assemble these structures in a predictable manner. Like its atomic analogue, the table of PAEs presents a map of current knowledge, but also highlights the necessity for continued discovery of new PAEs, and the continued development of means to control their behavior and explore the chemical and physical properties of these structures and their assemblies.

5.2 Discussion

A variety of different ligands have been utilized to control interactions between nanoparticles [38, 39, 42, 70–73]. In 1996, we proposed that DNA is the ideal ligand to direct nanoparticle bonding in a manner analogous to atomic bonding [32]. This is because the length, strength, and character of nucleic acid bonds between particles can be systematically varied by changing the length, nucleobase sequence, or number of DNA strands conjugated to a nanoparticle. Furthermore, DNA is a ligand that exists on the same nanometer length scale as the nanoparticle building blocks. However, unlike the atomic system, where the electronic properties of a given atom are immutable, the nucleic acid bonds linking nanoparticles to one another can be changed, independent of the properties of the nanoparticle core. Therefore, while a given atom cannot be assembled into any desired structure with a given coordination number and lattice parameter, any nanoparticle core that can be functionalized with nucleic acids can be assembled into a wide range of structures using the universal bonding capabilities of nucleic acids. The analogy we draw between bonds based upon atomic interactions and ones formed by DNA-based PAEs extends only to

structural considerations. Phenomena that emerge from orbital overlap behavior, such as the formation of valence and conduction bands are not directly represented in our analogy (although orbital directionality can be loosely mimicked in the context of nucleic acid modified nonspherical particles, as discussed later).

The first type of nucleic acid functionalized nanostructure that was developed by our group utilized a spherical gold nanoparticle core as a scaffold for the covalent attachment of single-stranded oligonucleotides in a densely functionalized and highly oriented manner. We described this PAE as a spherical nucleic acid (SNA)–nanoparticle conjugate because of the novel arrangement and dense packing of nucleic acids enabled by the shape of the nanoparticle core [32, 74]. To date, nucleic acid-based PAEs have been developed using nanoparticles of different sizes (2–250 nm in diameter) [75] and compositions (e.g., silver [76], Fe_2O_3 [77], silica [78, 79], CdSe [80]) for a variety of different classes of nucleic acids (e.g., ssDNA [57], dsDNA [32, 50, 58], RNA [81, 82], LNA [83]). Hollow, core-free versions of PAEs also have been developed by crosslinking the nucleic acids at the surface of the nanoparticle and subsequently dissolving the inorganic core [84, 85]. Other three-dimensional arrangements of nucleic acids have been created by employing different-shaped nanoparticle cores as scaffolds (e.g., triangular prisms, rods, octahedra, rhombic dodecahedra) [86]. In addition to being novel building block materials for the construction of lattices, these hybrid structures exhibit interesting properties that are a synergistic combination of those of the core and shell. For example, the nanoparticle core can impart upon the conjugate structure unique plasmon-based optical phenomena [4, 34, 87] or novel catalytic properties [84]. In addition, the tight packing and orientation of strands within the oligonucleotide shell leads to many interesting cooperative binding properties, and even leads to new properties that are not observed with free, linear DNA strands [74, 88–91].

Initial assemblies made from SNA–gold nanoparticle PAEs were synthesized by combining sets of complementary conjugates in solution below the melting temperature of the nucleic acid duplexes [32, 50]. In these systems, particle arrangements and bonding patterns were not well defined, but this early work introduced the concept of building programmable matter from nucleic acid–

nanoparticle conjugates and held promise for generating the desired atomic lattice analogues. Indeed, subsequent steps were taken in 2004 to demonstrate that annealing the conjugates allowed one to generate systems that exhibited short-range order, and also allowed for control over the distances between particles [92].

In 2008, the first crystalline superlattices were generated using DNA as a programmable linker by our group and independently by the Gang group [60, 61, 93]. A key development in our strategy that enabled the formation of crystalline lattices of nanoparticles was to utilize only "weak" DNA interactions between particles [60]. Unlike the previous systems in which tracts of complementary bases between 10 and 30 bases long were used to effect assembly, short "sticky ends" containing as few as four complementary bases were employed. These weak interactions enable the reorganization of the PAEs within a lattice even after they have bonded to one another, such that any DNA bonds that trap particles in thermodynamically unfavorable states are easily broken to allow for particle reorganization [62, 94, 95]. By hypothesizing that the most stable lattice will always be the one that maximizes the number of DNA bonds formed, we have developed a set of design rules that can be used to precisely position a variety of nanoparticle types into multiple distinct crystalline lattices with sub-nanometer precision, including structures that have no mineral equivalent, with tunable control over lattice parameters (Table 5.1) [37, 96].

These design rules are analogous to Pauling's Rules for ionic solids [64], but in many respects more powerful, because they provide both greater predictive power and enhanced programmability. While Pauling's Rules present a masterful understanding of the complexity of atomic arrangements, these rules are merely guidelines, and the structure of many atomic systems cannot be perfectly predicted by these rules. The lack of control over factors such as ionic radius or electronegativity makes true predictability in assembled atomic lattices challenging, and the programmability of these lattices impossible. In other words, once a set of atomic or molecular building blocks is chosen, the resulting set of lattices that can be constructed is also predetermined. By using nucleic acid functionalized nanostructures however, one can recreate the diversity observed in atomic lattices, but also surpass the limitations in programmability and predictability inherent in atomic systems. Therefore, these PAEs

can be used as a guide for the rational construction of functional nanoparticle-based materials for plasmonic, photonic, and catalytic applications [18, 26, 31].

The first in this set of rules, from which the rest of the rules are derived, is: PAEs will arrange themselves in a lattice that maximizes the number of DNA duplex bonds formed. Because it is the DNA strands that are stabilizing the lattice, the more DNA bonds formed between particles, the more stable the lattice will be. Thus, the thermodynamic product will always maximize the number of DNA connections being formed, and the set of rules we present herein makes the synthesis of a stable crystal structure a simple matter of determining which DNA strands must be used to place a nanoparticle-based PAE at a desired lattice position.

The second of the design rules states: PAEs of equal hydrodynamic radii will form an FCC lattice when using self-complementary DNA sequences, and BCC or CsCl lattices when using two PAEs with complementary DNA sequences [37]. When the DNA "sticky ends" presented on the nanoparticle surface are self-complementary, every particle in solution can bind to all other nanoparticles in solution. In these systems, the number of DNA connections within the lattice is therefore maximized when each particle's total number of nearest neighbors is maximized. Thus, a face-centered cubic (FCC) lattice (the densest packing of spheres of a single size) is predicted to be most favorable, and this is the type of structure observed for this system (Fig. 5.2). However, in a binary system, where two different sets of PAEs present, "sticky ends" that are complementary to each other and particles in solution that can only bind to their complement, the number of DNA connections is maximized when the particles are in a body-centered cubic (BCC) arrangement (Fig. 5.2). While each individual nanoparticle in a BCC system does not have as many nearest neighbors as in an FCC lattice, it does have the maximum number of complementary nearest neighbors to which it can "bond." Importantly, this rule holds for nanoparticles of a large size range (5–80 nm) and for DNA lengths of up to 100 nm [62, 96]. Further, the rise per base pair value (the additional distance between nanoparticles gained by making the linking DNA strands one nucleobase longer) was found to be approximately 0.26 nm for all combinations of nanoparticle size and DNA length [62, 96, 97]. This indicates that by using DNA to link nanoparticles together,

sub-nm level precision in interparticle distances (i.e., "bond lengths"), can be attained, simply by synthesizing a DNA strand of a specified number of nucleobases.

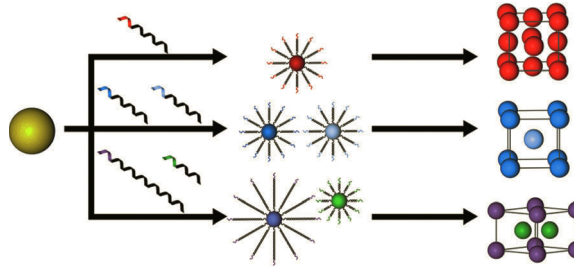

Figure 5.2 Different crystal structures can be constructed from nanoparticle building blocks of the same size and composition by changing the nature of the nucleic acid bonds (e.g. nucleobase sequence, length). Top: a single, self-complementary nucleic acid sequence enables all PAEs to bond to one another. This situation results in a crystal structure that maximizes the total number of nearest neighbors for each particle within a lattice: face-centered cubic (FCC). Middle: the terminus on the nucleic acid bonds has been changed from a single self-complementary sequence to two different, non-self-complementary sequences. Each sequence can bind to the other, but not to itself, which results in a body-centered cubic crystal structure (BCC). Bottom: nanoparticle size is kept constant, but two different DNA lengths are used. This results in nanoparticles with different hydrodynamic radii, and makes an AlB_2-type lattice most favorable.

In addition to altering superlattice symmetry by controlling the number, length, and nature of the self- or non-self-complementary sticky ends on the particle surface, the programmability of the DNA can also be used to control the strength of an individual DNA "bond," allowing kinetic products to be accessed. Therefore, a corollary to this second rule is: for two lattices of similar stability, kinetic products can be produced by slowing the rate at which individual DNA linkers de- and subsequently re-hybridize [37]. For example, each particle in a hexagonal close-packed (HCP) lattice has the same number of nearest neighbors as a particle in an FCC lattice. HCP lattices are only observed as kinetic products, owing to a slight favorability in the energetics of FCC lattices, as has been predicted by theory [98]. However, HCP lattices that are observed as kinetic products can be stabilized by slowing the rate of reorganization within a lattice (i.e., slowing the rate at which DNA bonds are formed

and/or broken during the crystallization process). This promotes the growth of HCP seeds (present at early stages of crystal growth) over their reorganization to the more favored FCC lattice. Importantly, the ability to stabilize these structures by controlling the crystal formation rate highlights the exquisite level of control possible in these systems as a result of the programmable nature of the DNA interactions.

Because the DNA sticky ends that link nanoparticles together are found at the periphery of the hydrodynamic radius of a nucleic acid functionalized nanostructure, the third rule is: The overall hydrodynamic radius of a PAE, rather than the sizes of its individual NP or oligonucleotide components, dictates its assembly and packing behavior [37]. In other words, two PAEs behave equivalently, so long as they have the same overall hydrodynamic radius, even if they have different DNA lengths or inorganic nanoparticle core sizes. This rule was demonstrated by synthesizing binary CsCl-type lattices (which exhibit the same connectivity as the BCC lattices generated using Rule 2, see Table 5.1), in which each of the two nanoparticle types has the same overall hydrodynamic radius, but different inorganic core sizes. This rule provides an interesting comparison to the first of Pauling's Rules for atoms, which states that interatomic distances are also dictated by the sum of the radii of the atomic building blocks. However, because the PAE system allows us to independently control the nanoparticle radii and DNA lengths, we can control the lattice parameters of a crystal separately from the sizes of the nanoparticles used.

The fourth and fifth rules in DNA-programmed nanoparticle assembly are: in a binary system based upon complementary PAEs, favored products will tend to have equivalent numbers of each complementary DNA sequence, evenly spaced throughout a unit cell, and two systems with the same size ratio and DNA linker ratio exhibit the same thermodynamic product [37]. These rules truly highlight the simplicity of the DNA programmed assembly process as compared to the complex nature of atomic assembly, as they enable the formation of a large number of crystal symmetries in a predictable manner (Fig. 5.3). In all cases, the most stable lattice is the one that maximizes the number of DNA connections formed. This means that determining which crystal structure is most stable for a given set of parameters is a simple means of counting the number of DNA strands present

in a unit cell of a given crystal symmetry, and determining which of these DNA strands are able to physically contact one another to form a DNA duplex. The hydrodynamic size ratio is therefore important because it determines both the distances between particles and how many nearest neighbors each particle can have. The DNA linker ratio (defined as the number ratio of DNA strands on the two particle types) dictates the relative amount of each type of DNA strand that is present in a given lattice unit cell. The general trends therefore are that: particles in the most stable arrangement are positioned such that the majority of the DNA strands can bind to DNA strands on adjacent particles, and the nanoparticle stoichiometry in the lattice is such that the overall number of each DNA type in a unit cell is nearly equal. This draws an interesting parallel to Pauling's second rule, which dictates that opposite charges in an ionic lattice must be balanced; the most stable PAE lattices typically balance the number of complementary DNA linker types within a unit cell.

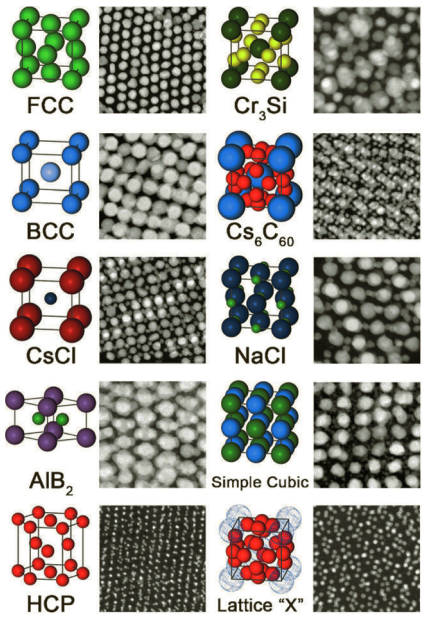

Figure 5.3 By varying the length and sequence of the nucleic acid "bonds," as well as the size and number of nanoparticle cores, a variety of crystal structures are accessible. Only a small number of those that have been made are shown, each with their corresponding TEM image. Over 100 different crystal structures, spanning 17 different crystal symmetries, have been made.

In comparison to the complexity of atomic interactions, these two rules provide a very simple means of understanding the stability of a given crystal symmetry as a function of the nanoparticle size and DNA linker ratios. They also allow us to create a phase diagram that enables the synthesis of lattices whose symmetry and lattice parameters can be determined prior to synthesis [37, 95]. In fact, to date, we have synthesized well over 100 unique lattices; the phase diagram and rules we have developed correctly predict the crystal structure obtained for over 95% of the crystals formed.

The sixth rule is: PAEs can be functionalized with more than one oligonucleotide bonding element, providing access to crystal structures not possible with single element PAEs [37]. In the ionic lattices examined in Pauling's Rules, each ion is attracted to ions of opposite charge and repelled by ions of the same charge, and there are only two fundamental types of building blocks: cations and anions. However, nanoparticles can be functionalized with many different DNA sequences, where interactions between particles occur when their respective DNA sequences are complementary. This effect allows the complexity of these lattices to be increased by adding multiple types of DNA linkers to a given nanoparticle. For example, a bi-functionalized nanoparticle can be synthesized that expresses both self-complementary and non-self-complementary sticky ends. On their own, the self-complementary sticky ends would favor the formation of an FCC lattice (as per the second design rule); the non-self-complementary sticky ends would favor the formation of a binary lattice when an appropriately functionalized second particle type is added. Together, however, the most stable crystal structure would allow for both of these types of interactions to be present. This principle was demonstrated in the synthesis of NaCl-type lattices: the self-complementary sticky ends on a bi-functionalized particle allow it to form an FCC lattice, while additional, non-self-complementary sticky ends also allow it to bind to a second particle type. When the hydrodynamic radii of the two particle types are appropriate, this secondary binding interaction allows the second particle type to fill the octahedral holes within the FCC lattice of the first particle type as that lattice forms; the end result is a NaCl arrangement of particles (Fig. 5.3).

Another fundamental concept in chemistry and materials science that can be translated to PAE-based lattices is that of vacancies.

In atomic lattices, vacancies represent point defects in crystalline lattices. In lattices of PAEs, the placement of vacancies within a unit cell can be precisely controlled using hollow, core-free nucleic acid functionalized structures, which exhibit the same binding and assembly behavior as the original gold nanoparticle conjugates [85, 99]. We refer to this strategy as "design by deletion," which leads to the seventh design rule: The crystal symmetry of a lattice is dictated by the position of the inorganic cores; a PAE with no inorganic core can be used to "delete" a particle at a specified position within a unit cell. In any of the lattices discussed that contain more than one type of PAE, any set can be replaced with three-dimensional spacers that are composed solely of DNA attached to an organic shell that contains no inorganic core, and are therefore silent from the perspective of X-ray scattering and electron microscopy (EM) analyses. In this way, new types of lattices with structures never before seen in nature have been readily synthesized (e.g., "Lattice X," Fig. 5.3). Unlike atomic vacancies, which are positioned randomly throughout a crystal, the "vacancies" introduced by using these core-free PAEs are placed at specified positions in every unit cell within a lattice and can therefore be used to control the overall symmetry of the lattice of inorganic nanoparticle core positions. However, because these "hollow" PAEs are indistinguishable from the PAEs with inorganic cores in terms of how they assemble, one can envision doping in a specified amount of the core-free NPs to introduce vacancies at random positions within a superlattice.

In the synthesis and assembly of PAEs described thus far, spherical nanoparticle cores were utilized to template an isotropic arrangement and spherical orientation of nucleic acid "bonds." Such an architecture is amenable to changes in the number, strength, and specificity of the DNA bonds, but ultimately confined to isotropic interactions. Directional bonding interactions, achieved via anisotropic surface functionalization of both isotropic and anisotropic particles (e.g., Janus particles [100], asymmetric or face-selective functionalization [45, 46, 101–104], patchy particles [105]) or anisotropic nanoparticle scaffolds [86, 106] extend the range of possible binding motifs and thus crystalline geometries achievable. The use of anisotropic functionalizion of particles relies upon spatial localization of certain molecules capable of forming bonds with incoming species. The use of anisotropic nanoparticle

scaffolds, more relevant to this discussion, utilizes the shape of the nanoparticle scaffold as a template to control the orientation of the resulting DNA bonds, similar to a covalent bond. Thus, PAEs formed from anisotropic building blocks—nanoparticles with at least one unique dimension (e.g., triangular prisms [107–111], rods [112–114], rhombic dodecahedra [115, 116], concave cubes [117], octahedra [118, 119])—provide synthetic control over another design dimension and allow novel superlattice structures to be accessed that cannot be realized with spherical particles (Fig. 5.4).

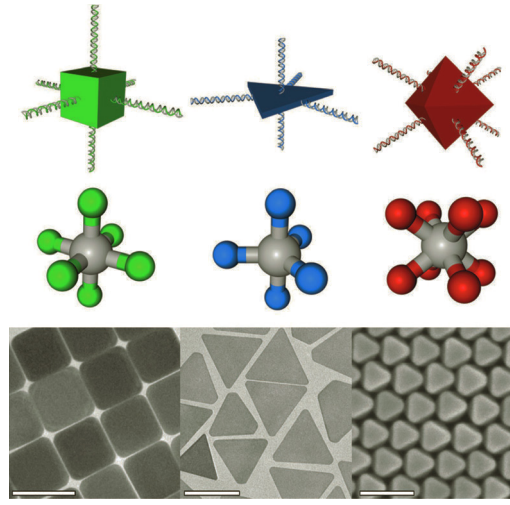

Figure 5.4 The distinct crystallographic facets of anisotropic nanoparticles enable directional hybridization (covalent-like) interactions between nanoparticles. Six-sided cubes, five-sided triangular prisms, and eight-sided octahedra are shown with DNA strands that demonstrate the directional bonding interactions for each particle shape. Note, however, that in this assembly strategy, each surface is densely functionalized with oligonucleotides. Below each nanoparticle is the corresponding ball-and-stick model of its bonding pattern and an electron microscopy image of synthesized particles. Scale bars in electron microscopy images are 100 nm.

Atoms rely on valency—the oriented overlap of atomic orbitals—to control molecular and crystallographic shape and symmetry. Among the tenets of valency is the relationship between electron density and bond strength: the greater the amount of shared electron density between two atoms, the stronger the bond. If this concept is extended to PAEs with anisotropic nanoparticle cores, one

would expect particle orientations that align the largest faces of the particles in a parallel placement to be favored, as this would result in a greater number of DNA connections and create stronger bonds between particles. For example, two-dimensional triangular prism structures will form stronger "bonds" with their large triangular faces aligned parallel to one another, as compared to orientations that align their (relatively smaller) rectangular sides (Fig. 5.4). This effect results in triangular prisms assembled into 1D lamellar stacks. This relationship has been further demonstrated with octahedra, rod, and rhombic dodecahedra nanoparticle templates, where each structure assembles along the crystal facet that forms the greatest number of nucleic acid bonds [86]. The eighth design rule is therefore: PAEs based upon anisotropic particles with flat faces can be used to realize valency and will assemble into a lattice that maximizes the amount of parallel, face-to-face interactions between particles. These assemblies are also accessible by alternative bonding methods, such as with the pH-mediated association of carboxylic acid-terminated ligands attached to gold triangular prisms, demonstrating that anisotropic nanoparticle assembly is ligand general, where the ultimate structure is heavily influenced by the shape of the nanoparticle [120].

Alignment of DNA bonds along the lengths of flat crystal facets also negates the radius of curvature effects associated with spherical particles, which enables greater overlap of DNA bonds and results in stronger connections between particles [120–122]. In fact, thermodynamic and kinetic enhancement of the bonding (hybridization) events between functionalized anisotropic nanoparticles leads to binding constants (analogous to bond strengths) several orders of magnitude higher than their spherical counterparts. For example, the directionality imparted by the large, flat triangular faces of triangular prisms results in a sizeable increase in nanoparticle binding constant over spheres (5.3×10^{17} M^{-1} vs. 1.5×10^{11} M^{-1}; over six orders of magnitude) [120].

Differences in the binding constants of PAEs of different shapes and/or sizes enable the separation of nanoparticle mixtures in a manner similar to the separation of elemental or molecular impurities. For example, molecular impurities are often isolated from organic syntheses by crystallization, a technique in which a desired product is isolated from a mixture by the thermodynamic

favorability of creating an ordered crystal consisting of only a single substance. When nanoparticles of disparate shape are functionalized with DNA, differences in binding constants (and therefore melting temperatures) can be used to separate them in an analogous manner. For example, for a solution of DNA-functionalized triangular prisms and spheres held between the melting temperatures of aggregates of the two shapes, the prisms are selectively associated with one another and precipitated out of solution, while the spheres remain free in solution, disassociated from one another. The precipitated phase (containing prisms) can then be easily separated from the solution phase (containing spheres) to obtain a pure solution of the desired product [123]. This concept of purification by crystallization has also been demonstrated with spherical nanoparticles of different sizes (where larger particles precipitate at higher temperatures because of the larger number of DNA connections that can be formed between particles with greater surface area) [124, 125], but with less-pronounced separation, owing to the lack of directional bonding interactions.

5.3 Outlook

Despite the rapid progress in the area of nucleic acid functionalized nanoparticle assembly, especially since 2008, several challenges remain as the focus of ongoing efforts. A primary challenge is to expand the nanoscale table of PAEs, filling in the empty spots with additional PAEs of varying size, shape, and composition. Much like the early versions of the Periodic Table, one can project the existence of many different nanoparticles that cannot yet be synthesized, but whose properties can be predicted based upon theoretical calculations and general trends established for existing nanoparticles [1, 4]. Certain existing building blocks also cannot currently be utilized because they only exist in impure mixtures containing multiple nanoparticle types (much like elements that were initially unknown as isolated species) [87, 126, 127]. Therefore, in order to expand the table of PAEs, one must first develop methods to synthesize a wider range of nanostructures in a controlled and predictable fashion, where the factors that influence size and shape are well understood. Furthermore, purification techniques (such as

the one described above) must also be explored to separate desired products from undesirable ones. Together, the development of these methodologies should allow for the synthesis of new nanoparticle building blocks with highly tunable structural characteristics and physical properties.

An additional challenge beyond simply synthesizing the nanoparticle building blocks is to functionalize them with nucleic acids without altering their structure or desired physical properties. However, other nanoparticle shapes, compositions, and sizes are not necessarily as amenable to surface modification with a high density of nucleic acids as the spherical gold nanoparticle systems that employ robust thiol gold chemistry [77–80, 86, 128]. Two potential approaches are: (1) to develop appropriate nucleic acid linking chemistries for each particle type or (2) to devise a general methodology for the surface modification of any nanoparticle core. Toward this end, methods have been developed in which particles have been coated in a shell of another material, such as silica [78, 79], polymer [18], or metal [25, 129], such that DNA can be attached to this layer using a more well-established methodology. However, at the present time, no truly universal strategy exists.

Another challenge focuses on increasing the stability of the nanoparticle superlattice structures after they have been synthesized. Since such lattices are held together by DNA bonding interactions, they are only stable in aqueous saline solutions at temperatures below the melting temperature of the DNA duplex linkages. To be useful in a wide range of applications, methods must be found to increase their stability toward changes in temperature, pH value, and solvent, and the presence of denaturing molecules or harsh environmental factors (such as the X-ray beams currently used to analyze the superlattices). We have recently made steps in this direction by developing a method that can be used to encase the nanoparticle lattices in porous silica [130]. Small-angle X-ray scattering (SAXS) and electron microscopy data confirm that the encapsulated lattices maintain their original symmetry and lattice parameters when dispersed in organic solvents (e.g., ethanol, acetone), at elevated temperatures above the melting temperature of the DNA duplex linkages, and in air and vacuum with no solvent present. Further, the encapsulated lattices were shown to be relatively unaffected by the X-ray beams utilized for structural

characterization. These data indicate that the nanoparticles have been locked in place by the silica network, which is chemically and physically more robust than the DNA duplexes. Ongoing work in this area involves understanding the full extent of stability conferred and examining the collective plasmonic, catalytic, and magnetic behaviors of the encased structures and comparing them to the unencapsulated structures where possible. Although this strategy represents a step in the right direction, other strategies may still be needed depending on the intended use of the lattices.

It would also be beneficial to either transfer superlattice materials from the solution phase to surfaces, or to grow the superlattices directly at a specific surface location. Ideally, a method to control layer-by-layer deposition of PAEs in a manner analogous to atomic layer deposition needs to be developed, such that each layer could be uniquely tailored [131–133]. This would both allow for integration of these materials into prototype devices, where chemical and physical properties can be measured, and allow for greater control of superlattice size.

One can also envision that it would also be advantageous to design and synthesize dynamic nanoparticle structures in which the lattice parameters or the crystal symmetry of a given nanoparticle superlattice can be varied at will, effectively turning these static lattices into "smart" functional structures. Steps in this direction have already been made utilizing the temperature or ionic strength of the solution to vary the lattice parameter of these crystals, albeit over a limited range [62, 134]. It is also possible to imagine using DNA hairpins to bring about such structural changes in a reversible manner, as initial work by Gang and coworkers suggests this is a viable strategy [135].

Finally, now that substantial progress has been made towards reliably synthesizing nanoparticle superlattices, more research effort must be put into developing new ways to analyze and ultimately utilize their properties (e.g., optical, plasmonic, magnetic, catalytic). It has long been known that individual nanoparticles possess a wide variety of tunable phenomena that are significantly affected by the local environment and position of nearby nanoscale objects [3, 4, 18, 26, 32, 40, 41]. The DNA-based assembly strategy discussed herein allows such parameters to be tailored (these parameters include interparticle distance, number of nearest neighbors, number of

unique nanoparticle types) and thus dictate the resulting physical and chemical characteristics. Recent developments in understanding how to individually control this parameter space coupled with the silica embedding methodology that makes the superlattices stable to a wider range of environmental conditions (including those necessary to perform certain types of characterization) allow us to begin to explore this area. Once desirable properties are elucidated and potential functions are defined, research will likely shift toward applications for these novel structures in many areas of chemistry, materials science, physics, and biology.

Ultimately, determination of the chemical and physical properties of these crystal structures will involve both experimental measurements as well as theoretical calculations. Theory has been used in this system as a guide for determining the relative stability of different lattice structures and for explaining their behavior [4, 36, 37, 95, 136]. It will also be helpful for determining which structures should be targeted for a given purpose and how the assembly process can be expanded to create additional crystal symmetries and lattices with larger (or smaller) lattice parameters than those currently accessible. Fundamental investigations of the kinetics of crystallization, probed by both experiment and theory, may also allow the size and morphology of the crystal domains to be controlled and the role of defects—such as grain boundaries, vacancies, and interstitial sites—to be understood. Each of these factors can be used in atomic systems to control materials properties, and we expect similar effects to be seen with the nanoparticle superlattice systems.

While the goals outlined in this Essay are most certainly ambitious, they are well worth the efforts it would take to achieve them. The potential benefit to understanding scientific phenomena at the nanoscale, developing novel materials by design, and predictably creating and controlling the physical and chemical characteristics of nanoparticle-based structures holds promise to usher in a new era of materials science. Despite the magnitude of this scientific challenge, the progress both our group and others have made in recent years in synthesizing nanoparticle building blocks and developing a means to assemble them in a programmable manner

indicates that these goals are achievable with the appropriate level of effort and innovation. The coming years undoubtedly hold promise for discoveries that fill out the table of PAEs, allow for new lattices to be realized, and demonstrate uses for the novel plasmonic, photonic, magnetic, and catalytic properties of these structures. We therefore invite the scientific community to adopt the concept of the nucleic acid–nanoparticle conjugate as a "programmable atom equivalent" and to use the table and design rules presented herein as a guiding principle in materials development. Approaching the field of nanoscience and technology with the same level of scientific rigor and intensity as chemists approached elemental discovery and usage in the previous two centuries will enable this burgeoning field to take on an important and highly influential role in the development of the chemistry, materials science, physics, biology, and engineering communities.

Since the document's initial submission, additional work not covered in this manuscript has been done in this field to further the concept of PAEs as nanoscale building blocks that warrants mention here [137, 138].

Acknowledgments

This material is based upon work supported by AFOSR Awards FA9550-11-1-0275, FA9550-12-1-0280, and FA9550-09-1-0294, DoD/NSSEFF/NPS Awards N00244-09-1-0012 and N00244-09-1-0071, the Defense Advanced Research Projects Agency (DARPA) Microsystems Technology Office (MTO) under award number HR0011-13-0002, the National Science Foundation's MRSEC program (DMR-1121262) at the Materials Research Center at Northwestern University, and the Non-equilibrium Energy Research Center (NERC), an Energy Frontier Research Center funded by the DoE, Office of Science, Office of Basic Energy Sciences under Award DESC0000989. Any opinions, findings, and conclusions or recommendations expressed in this publication are those of the author(s) and do not necessarily reflect the views of the sponsors. R.J.M. is grateful to Northwestern University for a Ryan Fellowship. M.N.O. is grateful to the NSF for a Graduate Research Fellowship.

References

1. Rossetti, R., Nakahara, S. and Brus, L. E. (1983). *J. Chem. Phys.* **79**, 1086–1088.
2. Brus, L. E. (1983). *J. Chem. Phys.* **79**, 5566–5571.
3. Daniel, M. C. and Astruc, D. (2004). *Chem. Rev.* **104**, 293–346.
4. Kelly, K. L., Coronado, E., Zhao, L. L. and Schatz, G. C. (2003). *J. Phys. Chem. B* **107**, 668–677.
5. Link, S. and El-Sayed, M. A. (1999). *J. Phys. Chem. B* **103**, 8410 –8426.
6. Xia, Y. N., Yang, P. D., Sun, Y. G., Wu, Y. Y., Mayers, B., Gates, B., Yin, Y. D., Kim, F. and Yan, Y. Q. (2003). *Adv. Mater.* **15**, 353–389.
7. Burda, C., Chen, X. B., Narayanan, R. and El-Sayed, M. A. (2005). *Chem. Rev.* **105**, 1025–1102.
8. Roco, M. C., Williams, R. S. and Alivisatos, A. P. (1999). *Nanotechnology Research Directions: IWGN Workshop Report* (National Science and Technology Council, Washington).
9. Xia, Y. N., Xiong, Y. J., Lim, B. and Skrabalak, S. E. (2009). *Angew. Chem.* **121**, 62–108; *Angew. Chem. Int. Ed.* **48**, 60–103.
10. Alivisatos, A. P. (1996). *Science* **271**, 933–937.
11. Trindade, T., O'Brien, P. and Pickett, N. L. (2001). *Chem. Mater.* **13**, 3843–3858.
12. Law, M., Goldberger, J. and Yang, P. D. (2004). *Annu. Rev. Mater. Res.* **34**, 83–122.
13. Fernández-García, M., Martínez-Arias, A., Hanson, J. C. and Rodriguez, J. A. (2004). *Chem. Rev.* **104**, 4063–4104.
14. Ajayan, P. M. (1999). *Chem. Rev.* **99**, 1787–1799.
15. Oh, M. and Mirkin, C. A. (2005). *Nature* **438**, 651–654.
16. Spokoyny, A. M., Kim, D., Sumrein, A. and Mirkin, C. A. (2009). *Chem. Soc. Rev.* **38**, 1218–1227.
17. Rolland, J. P., Maynor, B. W., Euliss, L. E., Exner, A. E., Denison, G. M. and DeSimone, J. M. (2005). *J. Am. Chem. Soc.* **127**, 10096 –10100.
18. Jones, M. R., Osberg, K. D., Macfarlane, R. J., Langille, M. R. and Mirkin, C. A. (2011). *Chem. Rev.* **111**, 3736–3827.
19. Langille, M. R., Personick, M. L., Zhang, J. and Mirkin, C. A. (2012). *J. Am. Chem. Soc.* **134**, 14542.
20. Sun, Y. G. and Xia, Y. N. (2002). *Science* **298**, 2176–2179.

21. Peng, X. G., Manna, L., Yang, W. D., Wickham, J., Scher, E., Kadavanich, A. and Alivisatos, A. P. (2000). *Nature* **404**, 59–61.
22. Arnold, M. S., Green, A. A., Hulvat, J. F., Stupp, S. I. and Hersam, M. C. (2006). *Nat. Nanotechnol.* **1**, 60–65.
23. Cortie, M. B. and McDonagh, A. M. (2011). *Chem. Rev.* **111**, 3713 –3735.
24. Caruso, F. (2001). *Adv. Mater.* **13**, 11–22.
25. Cao, Y. W., Jin, R. and Mirkin, C. A. (2001). *J. Am. Chem. Soc.* **123**, 7961–7962.
26. Bell, A. T. (2003). *Science* **299**, 1688–1691.
27. Christopher, P., Xin, H. L. and Linic, S. (2011). *Nat. Chem.* **3**, 467–472.
28. Rosi, N. L. and Mirkin, C. A. (2005). *Chem. Rev.* **105**, 1547–1562.
29. Giljohann, D. A., Seferos, D. S., Daniel, W. L., Massich, M. D., Patel, P. C. and Mirkin, C. A. (2010). *Angew. Chem.* **122**, 3352–3366; *Angew. Chem. Int. Ed.* **49**, 3280–3294.
30. Gratton, S. E. A., Ropp, P. A., Pohlhaus, P. D., Luft, J. C., Madden, V. J., Napier, M. E. DeSimone, J. M. (2008). *Proc. Natl. Acad. Sci. U.S.A.* **105**, 11613–11618.
31. Hochbaum, A. I. and Yang, P. D. (2010). *Chem. Rev.* **110**, 527–546.
32. Mirkin, C. A., Letsinger, R. L., Mucic, R. C. and Storhoff, J. J. (1996). *Nature* **382**, 607–609.
33. Mucic, R. C., Storhoff, J. J., Mirkin, C. A. and Letsinger, R. L. (1998). *J. Am. Chem. Soc.* **120**, 12674–12675.
34. Storhoff, J. J., Lazarides, A. A., Mucic, R. C., Mirkin, C. A., Letsinger, R. L. and Schatz, G. C. (2000). *J. Am. Chem. Soc.* **122**, 4640 –4650.
35. Park, S. J., Lazarides, A. A., Mirkin, C. A., Brazis, P. W., Kannewurf, C. R. and Letsinger, R. L. (2000). *Angew. Chem.* **122**, 4003 –4006; *Angew. Chem. Int. Ed.* **39**, 3845–3848.
36. Jin, R. C., Wu, G. S., Li, Z., Mirkin, C. A. and Schatz, G. C. (2003). *J. Am. Chem. Soc.* **125**, 1643–1654.
37. Macfarlane, R. J., Lee, B., Jones, M. R., Harris, N., Schatz, G. C. and Mirkin, C. A. (2011). *Science* **334**, 204–208.
38. Kalsin, A. M., Fialkowski, M., Paszewski, M., Smoukov, S. K., Bishop, K. J. M. and Grzybowski, B. A. (2006). *Science* **312**, 420–424.
39. Shevchenko, E. V., Talapin, D. V., Kotov, N. A., O'Brien, S. and Murray, C. B. (2006). *Nature* **439**, 55–59.
40. Talapin, D. V., Lee, J. S., Kovalenko, M. V. and Shevchenko, E. V. (2010). *Chem. Rev.* **110**, 389–458.

41. Halas, N. J., Lal, S., Chang, W. S., Link, S. and Nordlander, P. (2011). *Chem. Rev.* **111**, 3913–3961.

42. Alivisatos, A. P., Johnsson, K. P., Peng, X. G., Wilson, T. E., Loweth, C. J., Bruchez, M. P. and Schultz, P. G. (1996). *Nature* **382**, 609 –611.

43. Wang, Y., Wang, Y., Breed, D. R., Manoharan, V. N., Feng, L., Hollingsworth, A. D., Weck, M. and Pine, D. J. (2012). *Nature* **491**, 51–55.

44. Wang, Y., Chen, G., Yang, M. X., Silber, G., Xing, S. X., Tan, L. H., Wang, F., Feng, Y. H., Liu, X. G., Li, S. Z. and Chen, H. Y. (2010). *Nat. Commun.* **1**, 87.

45. Huo, F. W., Lytton-Jean, A. K. R. and Mirkin, C. A. (2006). *Adv. Mater.* **18**, 2304.

46. Xu, X. Y., Rosi, N. L., Wang, Y. H., Huo, F. W. and Mirkin, C. A. (2006). *J. Am. Chem. Soc.* **128**, 9286–9287.

47. Kastner, M. A. (1993). *Phys. Today* **46**, 24–31.

48. Ashoori, R. C. (1996). *Nature* **379**, 413–419.

49. Hanrath, T. (2012). *J. Vac. Sci. Technol. A* **30**, 030802.

50. Elghanian, R., Storhoff, J. J., Mucic, R. C., Letsinger, R. L. and Mirkin, C. A. (1997). *Science* **277**, 1078–1081.

51. Storhoff, J. J., Elghanian, R., Mucic, R. C., Mirkin, C. A. and Letsinger, R. L. (1998). *J. Am. Chem. Soc.* **120**, 1959–1964.

52. Taton, T. A., Mirkin, C. A. and Letsinger, R. L. (2000). *Science* **289**, 1757–1760.

53. Park, S. J., Taton, T. A. and Mirkin, C. A. (2002). *Science* **295**, 1503–1506.

54. Nam, J. M., Thaxton, C. S. and Mirkin, C. A. (2003). *Science* **301**, 1884–1886.

55. Georganopoulou, D. G., Chang, L., Nam, J. M., Thaxton, C. S., Mufson, E. J., Klein, W. L. and Mirkin, C. A. (2005). *Proc. Natl. Acad. Sci. U.S.A.* **102**, 2273–2276.

56. Thaxton, C. S., Elghanian, R., Thomas, A. D., Stoeva, S. I., Lee, J. S., Smith, N. D., Schaeffer, A. J., Klocker, H., Horninger, W., Bartsch, G. and Mirkin, C. A. (2009). *Proc. Natl. Acad. Sci. U.S.A.* **106**, 18437–18442.

57. Rosi, N. L., Giljohann, D. A., Thaxton, C. S., Lytton-Jean, A. K. R., Han, M. S. and Mirkin, C. A. (2006). *Science* **312**, 1027–1030.

58. Seferos, D. S., Giljohann, D. A., Hill, H. D., Prigodich, A. E. and Mirkin, C. A. (2007). *J. Am. Chem. Soc.* **129**, 15477–15479.

59. Zheng, D., Giljohann, D. A., Chen, D. L., Massich, M. D., Wang, X. Q., Iordanov, H., Mirkin, C. A. and Paller, A. S. (2012). *Proc. Natl. Acad. Sci. U.S.A.* **109**, 11975–11980.

60. Park, S. Y., Lytton-Jean, A. K. R., Lee, B., Weigand, S., Schatz, G. C. and Mirkin, C. A. (2008). *Nature* **451**, 553–556.

61. Nykypanchuk, D., Maye, M. M., van der Lelie, D. and Gang, O. (2008). *Nature* **451**, 549–552.

62. Macfarlane, R. J., Jones, M. R., Senesi, A. J., Young, K. L., Lee, B., Wu, J. S. and Mirkin, C. A. (2010). *Angew*. *Chem*. **122**, 4693–4696; *Angew*. *Chem*. *Int*. *Ed*. **49**, 4589–4592.

63. Xiong, H. M., van der Lelie, D. and Gang, O. (2009). *Phys*. *Rev*. *Lett*. **102**, 015504.

64. Pauling, L. (1960). *The Nature of the Chemical Bond and the Structure of Molecules and Crystals; An Introduction to Modern Structural Chemistry*, 3rd ed. (Cornell University Press, Ithaca).

65. Seeman, N. C. (2003). *Nature* **421**, 427–431.

66. Rothemund, P.W. K. (2006). *Nature* **440**, 297–302.

67. Le, J. D., Pinto, Y., Seeman, N. C., Musier-Forsyth, K., Taton, T. A. and Kiehl, R. A. (2004). *Nano Lett*. **4**, 2343–2347.

68. Yan, H., Park, S. H., Finkelstein, G., Reif, J. H. and LaBean, T. H. (2003). *Science* **301**, 1882–1884.

69. Kuzuya, A. and Komiyama, M. (2010). *Nanoscale* **2**, 309–321.

70. Connolly, S. and Fitzmaurice, D. (1999). *Adv*. *Mater*. **11**, 1202–1205.

71. Caswell, K. K., Wilson, J. N., Bunz, U. H. F. and Murphy, C. J. (2003). *J*. *Am*. *Chem*. *Soc*. **125**, 13914–13915.

72. Chen, C. L., Zhang, P. J. and Rosi, N. L. (2008). *J*. *Am*. *Chem*. *Soc*. **130**, 13555–13577.

73. Young, K. L., Jones, M. R., Zhang, J., Macfarlane, R. J., Esquivel-Sirvent, R., Nap, R. J., Wu, J. S., Schatz, G. C., Lee, B. and Mirkin, C. A. (2012). *Proc*. *Natl*. *Acad*. *Sci*. *U.S.A*. **109**, 2240–2245.

74. Cutler, J. I., Auyeung, E. and Mirkin, C. A. (2012). *J*. *Am*. *Chem*. *Soc*. **134**, 1376–1391.

75. Hurst, S. J., Lytton-Jean, A. K. R. and Mirkin, C. A. (2006). *Anal*. *Chem*. **78**, 8313–8318.

76. Lee, J. S., Lytton-Jean, A. K. R., Hurst, S. J. and Mirkin, C. A. (2007). *Nano Lett*. **7**, 2112–2115.

77. Cutler, J. I., Zheng, D., Xu, X. Y., Giljohann, D. A. and Mirkin, C. A. (2010). *Nano Lett*. **10**, 1477–1480.

78. Xue, C., Chen, X., Hurst, S. J. and Mirkin, C. A. (2007). *Adv*. *Mater*. **19**, 4071–4074.

79. Young, K. L., Scott, A. W., Hao, L. L., Mirkin, S. E., Liu, G. L. and Mirkin, C. A. (2012). *Nano Lett.* **12**, 3867–3871.

80. Mitchell, G. P., Mirkin, C. A. and Letsinger, R. L. (1999). *J. Am. Chem. Soc.* **121**, 8122–8123.

81. Giljohann, D. A., Seferos, D. S., Prigodich, A. E., Patel, P. C. and Mirkin, C. A. (2009). *J. Am. Chem. Soc.* **131**, 2072–2073.

82. Hao, L. L., Patel, P. C., Alhasan, A. H., Giljohann, D. A. and Mirkin, C. A. (2011). *Small* **7**, 3158–3162.

83. Seferos, D. S., Giljohann, D. A., Rosi, N. L. and Mirkin, C. A. (2007). *ChemBioChem* **8**, 1230–1232.

84. Zhang, K., Cutler, J. I., Zhang, J. A., Zheng, D., Auyeung, E. and Mirkin, C. A. (2010). *J. Am. Chem. Soc.* **132**, 15151–15153.

85. Cutler, J. I., Zhang, K., Zheng, D., Auyeung, E., Prigodich, A. E. and Mirkin, C. A. (2011). *J. Am. Chem. Soc.* **133**, 9254–9257.

86. Jones, M. R., Macfarlane, R. J., Lee, B., Zhang, J. A., Young, K. L., Senesi, A. J. and Mirkin, C. A. (2010). *Nat. Mater.* **9**, 913–917.

87. Millstone, J. E., Park, S., Shuford, K. L., Qin, L. D., Schatz, G. C. and Mirkin, C. A. (2005). *J. Am. Chem. Soc.* **127**, 5312–5313.

88. Lytton-Jean, A. K. R. and Mirkin, C. A. (2005). *J. Am. Chem. Soc.* **127**, 12754–12755.

89. Massich, M. D., Giljohann, D. A., Seferos, D. S., Ludlow, L. E., Horvath, C. M. and Mirkin, C. A. (2009). *Mol. Pharm.* **6**, 1934–1940.

90. Prigodich, A. E., Alhasan, A. H. and Mirkin, C. A. (2011). *J. Am. Chem. Soc.* **133**, 2120–2123.

91. Zwanikken, J. W., Guo, P. J., Mirkin, C. A. and de La Cruz, M. O. (2011). *J. Phys. Chem. C* **115**, 16368–16373.

92. Park, S. J., Lazarides, A. A., Storhoff, J. J., Pesce, L. and Mirkin, C. A. (2004). *J. Phys. Chem. B* **108**, 12375–12380.

93. Xiong, H. M., van der Lelie, D. and Gang, O. (2008). *J. Am. Chem. Soc.* **130**, 2442–2443.

94. Macfarlane, R. J., Lee, B., Hill, H. D., Senesi, A. J., Seifert, S. and Mirkin, C. A. (2009). *Proc. Natl. Acad. Sci. U.S.A.* **106**, 10493 –10498.

95. Li, T. I. N. G., Sknepnek, R., Macfarlane, R. J., Mirkin, C. A. and de La Cruz, M. O. (2012). *Nano Lett.* **12**, 2509–2514.

96. Hill, H. D., Macfarlane, R. J., Senesi, A. J., Lee, B., Park, S. Y. and Mirkin, C. A. (2008). *Nano Lett.* **8**, 2341–2344.

97. Sebba, D. S. and Lazarides, A. A. (2008). *J. Phys. Chem. C* **122**, 18331–18339.

98. Woodcock, L. V. (1997). *Nature* **385**, 141–143.

99. Auyeung, E., Cutler, J. I., Macfarlane, R. J., Jones, M. R., Wu, J. S., Liu, G., Zhang, K., Osberg, K. D. and Mirkin, C. A. (2012). *Nat. Nanotechnol.* **7**, 24–28.

100. Nie, L., Liu, S. Y., Shen, W. M., Chen, D. Y. and Jiang, M. (2007). *Angew. Chem.* **119**, 6437–6440; *Angew. Chem. Int. Ed.* **46**, 6321–6324.

101. Millstone, J. E., Georganopoulou, D. G., Xu, X. Y., Wei, W., Li, S. Y. and Mirkin, C. A. (2008). *Small* **4**, 2176–2180.

102. Rycenga, M., McLellan, J. M. and Xia, Y. N. (2008). *Adv. Mater.* **20**, 2416–2420.

103. Maye, M. M., Nykypanchuk, D., Cuisinier, M., van der Lelie, D. and Gang, O. (2009). *Nat. Mater.* **8**, 388–391.

104. Sun, D. Z., Stadler, A. L., Gurevich, M., Palma, E., Stach, E., van der Lelie, D. and Gang, O. (2012). *Nanoscale* **4**, 6722–6725.

105. Zhang, Z. L. and Glotzer, S. C. (2004). *Nano Lett.* **4**, 1407–1413.

106. Glotzer, S. C. and Solomon, M. J. (2007). *Nat. Mater.* **6**, 557–562.

107. Millstone, J. E., Hurst, S. J., Metraux, G. S., Cutler, J. I. and Mirkin, C. A. (2009). *Small* **5**, 646–664.

108. Jin, R. C., Cao, Y. W., Mirkin, C. A., Kelly, K. L., Schatz, G. C. and Zheng, J. G. (2001). *Science* **294**, 1901–1903.

109. Jin, R. C., Cao, Y. C., Hao, E. C., Metraux, G. S., Schatz, G. C. and Mirkin, C. A. (2003). *Nature* **425**, 487–490.

110. Métraux, G. S. and Mirkin, C. A. (2005). *Adv. Mater.* **17**, 412–415.

111. Xue, C. and Mirkin, C. A. (2007). *Angew. Chem.* **119**, 2082–2084; *Angew. Chem. Int. Ed.* **46**, 2036–2038.

112. Nikoobakht, B. and El-Sayed, M. A. (2003). *Chem. Mater.* **15**, 1957–1962.

113. Liu, M. Z. and Guyot-Sionnest, P. (2005). *J. Phys. Chem. B* **109**, 22192–22200.

114. Murphy, C. J., Gole, A. M., Hunyadi, S. E. and Orendorff, C. J. (2006). *Inorg. Chem.* **45**, 7544–7554.

115. Personick, M. L., Langille, M. R., Zhang, J. and Mirkin, C. A. (2011). *Nano Lett.* **11**, 3394–3398.

116. Niu, W. X., Zheng, S. L., Wang, D. W., Liu, X. Q., Li, H. J., Han, S. A., Chen, J., Tang, Z. Y. and Xu, G. B. (2009). *J. Am. Chem. Soc.* **131**, 697–703.

117. Zhang, J. A., Langille, M. R., Personick, M. L., Zhang, K., Li, S. Y. and Mirkin, C. A. (2010). *J. Am. Chem. Soc.* **132**, 14012–14014.

118. Langille, M. R., Personick, M. L., Zhang, J. and Mirkin, C. A. (2011). *J. Am. Chem. Soc.* **133**, 10414–10417.

119. Tao, A., Sinsermsuksakul, P. and Yang, P. D. (2006). *Angew. Chem.* **118**, 4713–4717; *Angew. Chem. Int. Ed.* **45**, 4597–4601.

120. Jones, M. R., Macfarlane, R. J., Prigodich, A. E., Patel, P. C. and Mirkin, C. A. (2011). *J. Am. Chem. Soc.* **133**, 18865–18869.

121. Hill, H. D., Hurst, S. J. and Mirkin, C. A. (2009). *Nano Lett.* **9**, 317 –321.

122. Hill, H. D., Millstone, J. E., Banholzer, M. J. and Mirkin, C. A. (2009). *ACS Nano* **3**, 418–424.

123. Jones, M. R. and Mirkin, C. A. (2013). *Angew. Chem.* **125**, 2958 –2963; *Angew. Chem. Int. Ed.* **52**, 2886–2891.

124. Lee, J. S., Stoeva, S. I. and Mirkin, C. A. (2006). *J. Am. Chem. Soc.* **128**, 8899–8903.

125. Lee, J. S., Seferos, D. S., Giljohann, D. A. and Mirkin, C. A. (2008). *J. Am. Chem. Soc.* **130**, 5430–5431.

126. Seo, D., Il Yoo, C., Chung, I. S., Park, S. M., Ryu, S. and Song, H. (2008). *J. Phys. Chem. C* **112**, 2469–2475.

127. Damasceno, P. F., Engel, M. and Glotzer, S. C. (2012). *Science* **337**, 453–457.

128. Sun, D. Z. and Gang, O. (2011). *J. Am. Chem. Soc.* **133**, 5252–5254.

129. Yoo, H. J., Millstone, J. E., Li, S. Z., Jang, J. W., Wei, W., Wu, J. S., Schatz, G. C. and Mirkin, C. A. (2009). *Nano Lett.* **9**, 3038–3041.

130. Auyeung, E., Macfarlane, R. J., Choi, C. H. J., Cutler, J. I. and Mirkin, C. A. (2012). *Adv. Mater.* **24**, 5181.

131. Taton, T. A., Mucic, R. C., Mirkin, C. A. and Letsinger, R. L. (2000). *J. Am. Chem. Soc.* **122**, 6305–6306.

132. Demers, L. M., Park, S. J., Taton, T. A., Li, Z. and Mirkin, C. A. (2001). *Angew. Chem.* **113**, 3161–3163; *Angew. Chem. Int. Ed.* **40**, 3071–3073.

133. Chung, S. W., Ginger, D. S., Morales, M. W., Zhang, Z. F., Chandrasekhar, V., Ratner, M. A. and Mirkin, C. A. (2005). *Small* **1**, 64–69.

134. Xiong, H. M., Sfeir, M. Y. and Gang, O. (2010). *Nano Lett.* **10**, 4456–4462.

135. Maye, M. M., Kumara, M. T., Nykypanchuk, D., Sherman, W. B. and Gang, O. (2010). *Nat. Nanotechnol.* **5**, 116–120.

136. Park, S. Y., Lee, J. S., Georganopoulou, D., Mirkin, C. A. and Schatz, G. C. (2006). *J. Phys. Chem. B* **110**, 12673–12681.

137. Barrow, S. J., Wei, X., Baldauf, J. S., Funston, A. M. and Mulvaney, P. (2013). *Nat*. *Commun*. **3**, 1275.

138. Deng, Z., Pal, S., Samanta, A., Yan, H. and Liu, Y. (2013). *Chem*. *Sci*. **4**, 2234–2240.

Chapter 6

Programmable Materials and the Nature of the DNA Bond*

Matthew R. Jones,[a,d] Nadrian C. Seeman,[b] and Chad A. Mirkin[a,c,d]
[a]*Department of Materials Science and Engineering, Northwestern University, 2220 Campus Drive, Evanston, IL 60208, USA*
[b]*Department of Chemistry, New York University, New York, NY 10003, USA*
[c]*Department of Chemistry, Northwestern University, 2145 Sheridan Road, Evanston, IL 60208, USA*
[d]*International Institute for Nanotechnology, Northwestern University, 2145 Sheridan Road, Evanston, IL 60208, USA*
chadnano@northwestern.edu; ned.seeman@nyu.edu

For over half a century, the biological roles of nucleic acids as catalytic enzymes, intracellular regulatory molecules, and the carriers of genetic information have been studied extensively. More recently, the sequence-specific binding properties of DNA have been exploited to direct the assembly of materials at the nanoscale. Integral to any methodology focused on assembling matter from

*From Jones, M. R., Seeman, N. C. and Mirkin, C. A. (2015). Programmable materials and the nature of the DNA bond, *Science* **347**(6224). Reprinted with permission from AAAS.

Spherical Nucleic Acids, Volume 1
Edited by Chad A. Mirkin

ISBN 978-981-4800-35-8 (Hardcover), 978-0-429-20015-1 (eBook)
www.jennystanford.com

smaller pieces is the idea that final structures have well-defined spacings, orientations, and stereo-relationships. This requirement can be met by using DNA-based constructs that present oriented nanoscale bonding elements from rigid core units. Here, we draw an analogy between such building blocks and the familiar chemical concepts of "bonds" and "valency" and review two distinct but related strategies that have used this design principle in constructing new configurations of matter.

6.1 Introduction

A grand challenge in the fields of chemistry and materials science is the ability to construct materials with absolute control over the placement of each component in order to tailor properties for a given application. Synthetic chemists regularly wield this degree of control over atoms by manipulating the formation of covalent bonds, and supramolecular chemists control the organization of larger molecular species through the manipulation of noncovalent interactions. A key requirement for these bonds is that their interactions be sufficiently directional so that the final arrangement and orientation of molecules may be predicted with reasonable accuracy [1, 2]. When this condition is not met—when interactions are conformationally flexible—it is difficult for a system to arrive at a singular thermodynamic product that is well-defined (for example, inherent nonuniformity found in polymer systems), and rational control over the final material is greatly diminished. The synthesis of nanomaterials and their assembly into larger well-defined architectures has conceptually similar goals. We foresee the recent advances in nanomaterials synthesis facilitated by DNA-based assembly processes as capable of one day producing a synthetic methodology that may rival, and in certain cases exceed, at the nanoscale what small-molecule chemists have achieved at the molecular scale [3, 4]. Therefore, we find it useful to explore the concepts of "valency" and the "bond" when applied to nanoscale building blocks whose interactions are governed by DNA hybridization.

Aside from their obvious role as carriers of genetic information, nucleic acids have also been used by biological systems to generate

natural nanostructures such as ribozymes [5] and Holliday junctions [6] that serve crucial roles in a variety of cellular processes. Perhaps the most salient feature of DNA that can explain its versatility in biological settings is the specificity of canonical Watson–Crick base-pairing interactions (A-T and G-C). Permutation of the nucleobase sequence of particular DNA strands, even those that are relatively short, results in an enormous library of orthogonal interactions that can direct hybridization to occur with high selectivity and specificity.

The concept of controlled valency or directional DNA bonding in programmable materials synthesis can be traced to two seminal papers [7, 8] and several patents (acknowledgements, this paper) published circa 1996 (Fig. 6.2). These examples were the first to use rigid nanoscale building materials that retained the tailorability of DNA-mediated interactions, as opposed to structures defined only by topology that were explored in early efforts to gain structural control with DNA [9]. Although rigidity of a central building block is essential to the valency control in both of these approaches, they differ in how such rigidity is attained and the types of architectures one can envision and construct. The first methodology uses branched DNA architectures (molecules containing multiple crossover junctions between double helical domains) [8], which results in constructs that lacked the flexibility seen previously with only a single crossover junction [2, 10, 11] and form much of the basis for what is called "structural DNA nanotechnology" (Fig. 6.1A) [12]. In this approach, carefully designed hybridization and intertwining of DNA strands create a rigid building block with programmable bonding characteristics and allow one to make functional architectures with well-defined geometries. Although these molecules, commonly known as DX tiles, were intriguing for a variety of fundamental reasons [13], it was the demonstration of their conformational rigidity [8] and later their assembly into large crystals [14] that proved their ability to function as two-dimensional (2D) nanoscale building blocks with programmable bonds.

The second approach introduced the concept of a programmable atom equivalent comprised of a rigid non-nucleic acid core, densely functionalized with a layer of highly oriented single strands of DNA [7]. The valency in these structures, now termed spherical nucleic acids (SNAs) [15], is dictated by both the central particle and the dense loading of oligonucleotides on the surface of the structure

(Fig. 6.1); crowding directs the oligonucleotide bonding elements and provides subnanometer control with respect to particle-particle binding events. They do not require hybridization to create a functional building block, and they permit building hybrid materials not attainable via the approaches that rely on nucleic acids to attain valency. Although the prototypical example was a spherical gold particle chemically functionalized with alkylthiol-modified DNA [7], there is now a large table of element equivalents consisting of particles that vary in size, composition, shape, and type of functionalized nucleic acid [3]. With this approach, a number of assembled structures, first with short-range order [16, 17] and ultimately with extended 3D periodicity [18, 19], demonstrated the power of this nanoparticle building block to imbue DNA with bonding properties.

Contemporaneous with these aforementioned contributions to DNA valency, a more complete fundamental understanding of the thermodynamics of DNA hybridization allowed for quantitative predictions of duplex melting temperatures that included empirically relevant conditions such as sequence and salt dependencies [20]. In addition, a number of important materials possessing only topological order were reported that used DNA to assemble proteins [21] and nanoparticles on discrete molecular templates [22]. This approach was expanded by using organic molecules or transition metal complexes whose inherently well-defined bonding geometries allow for DNA hybridization events to be somewhat oriented in space [23, 24]. Although these structures do not present rigid DNA bonds and are not useful for programming the formation of macroscopic materials, they are valuable for labeling nucleic acid architectures and building certain molecular analogs to the 3D materials that are the focus of this manuscript.

The field of nucleic acid–guided programmable materials has been bifurcated into two subdivisions that achieve the goal of rigid, directional, DNA-based bonds through different fundamental chemical interactions: (i) the use of intricately woven oligonucleotides participating in hybridization to produce rigid architectures such as tiles and scaffolds, and (ii) the use of rigid nanoparticle cores, which act to template directional interactions on the basis of the core geometry (Fig. 6.2). We will commonly differentiate these methodologies by referring to each as “hybridization-based DNA bonds” or “nanoparticle-templated DNA bonds,” respectively.

These methods represent contrasting but powerful approaches at manipulating matter at the nanoscale through DNA bonds and the principle of valency. Just as the character of different atomic bonds dictates the types of materials that can be constructed from atoms, each type of nanoscale building block presented here has distinct properties that allow access to different materials that are constructed using DNA.

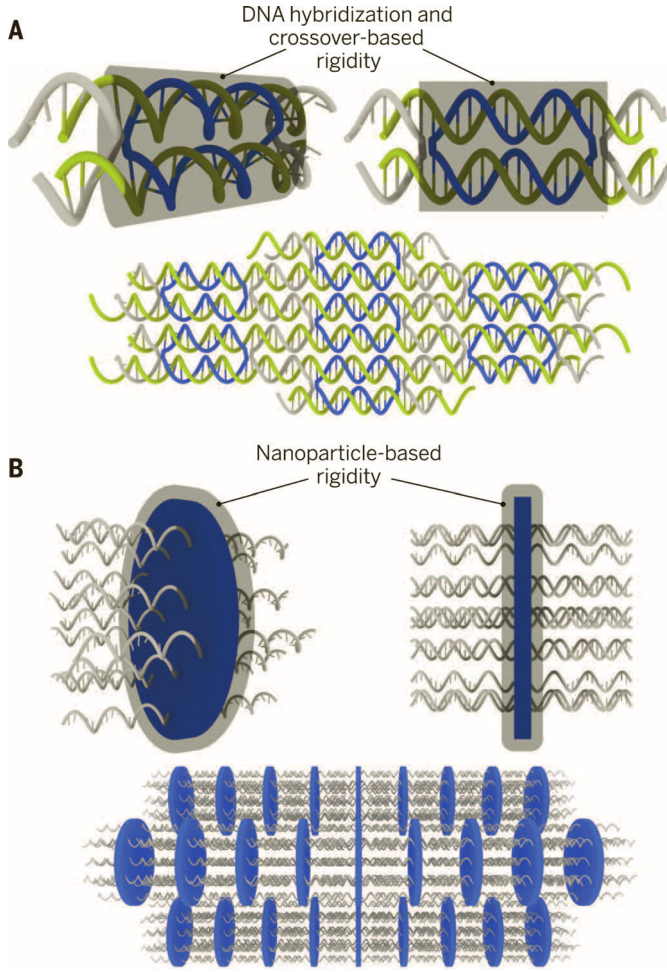

Figure 6.1 Differentiating nanoscale DNA bonds. (A) Multiple strand crossover events and DNA hybridization produce a conformationally constrained molecule with a rigid core. (B) A rigid nanoparticle acts as a scaffold for the immobilization and organization of DNA strands in a surface-normal direction.